HAW HAMBURG

Master Thesis

Master of Sciences

Investigations into The Characterization and Thioether-Based Immobilization of Antimicrobial Peptides NK-2, Arenicin and Their Derivatives

Submitted by:

Theonardho Ryvan

[redacted]

Hamburg, 06. February 2026

First Reviewer : Prof. Dr. Jörg Andrä, HAW Hamburg

Second Reviewer : Prof. Dr. Serhat Sezai Cicek, HAW Hamburg

Department Biotechnology

Hamburg University of Applied Sciences

Acknowledgements

First of all, I would like to express my deepest gratitude to God. Only by His blessing have I been able to come this far and reach this chapter of my life.

I would also like to express my sincere gratitude to Prof. Dr. Jörg Andrä for trusting me and giving me the opportunity to conduct my Master thesis in his research group. I am equally grateful to Prof. Dr. Serhat Sezai Cicek for the avaibility as the second reviewer of my thesis and for the valuable discussions throughout my Master thesis. Further, I would like to thank Frau Petra Jöpcke, Frau Nadja Schnell, Herr Andreas Graß and Frau Elke Wiechens, who were always willing to help and support me during my laboratory work.

For me, this journey has been more than an academic path to pursue a degree. As someone who came to a new country eight years ago and had to learn the language and adapt to the new environment independently and facing both good and difficult times, this experience has been a profound life journey that has shaped me into the person I am today. It was not an easy chapter, but I am deeply grateful that I was able to finish it in the best possible way.

My deepest gratitude also goes to my family, especially my parents, who have supported me endlessly since day one. I am also very thankful to my girlfriend, Vanessa, for her constant support throughout my Master studies. Finally, I would like to express my appreciation to all my friends and to my colleagues whom I met during my studies and work.

This closing chapter marks the beginning of a new and bigger chapter in my life, one that I am truly excited to enter and continue growing both personally and professionally.

List of Abbreviations

AMPs	Antimicrobial Peptides
AFPs	Antifungal Peptides
ACPs	Anticancer Peptides
RP - HPLC	Reverse Phased – High Performance Liquid Chromatography
DTT	Dithiothreitol
TCEP	Tris(2-carboxyethyl) phosphine
TFA	Trifluoroacetic acid
CD	Circular Dichroism
FTIR	Fourier transform infrared spectroscopy
NMR	Nuclear Magnetic Resonance
TFE	Trifluoroethanol
PG	Phosphatidylglycerol
PC	Phosphatidylcholine
GRAVY	Grand Average of Hydropathy
SEC	Size Exclusion Chromatography
SDS-PAGE	Sodium Dodecyl Sulfate – Polyacrylamide Gel Electrophoresis
MIC	Minimum Inhibitory Concentration
DNA	Deoxyribonucleic Acid
RNA	Ribonucleic Acid
ATP	Adenosine Triphosphate
LPS	Lipopolysaccharides
SPPS	Solid Phase Peptide Synthesis
ACN	Acetonitrile
SAMs	Self-Assembled Monolayers
PEG	Polyethyleneglycol
CV	Column Volumes
UV/VIS-Spectrophotometer	Ultraviolet-visible spectrophotometer
GHS	Global Harmonized System

Abstract

The misuse and overuse of antibiotics have led to a rise in antimicrobial resistance, which is now considered a global health emergency (Kyvik *et al.*, 2023). This problem is further worsened by the ability of bacteria to form biofilms, which make them 10–1000 times more resistant to antibiotics than planktonic bacteria (Kyvik *et al.*, 2023). Biofilm formation on medical implants such as heart valves, catheters, contact lenses, joint prostheses, intrauterine devices, and dental units can cause persistent urinary tract and bloodstream infections. In many cases, the only effective treatment is removal of the infected implant, which can be a major burden for patients (Costerton, Montanaro, and Arciola, 2005). Immobilization of antimicrobial peptides (AMPs) onto solid surfaces has therefore become a promising strategy to prevent biomaterial-associated infections, as medical implants and prosthetic devices are often colonized by biofilm-forming bacteria that are resistant to conventional antibiotic treatment (Riool *et al.*, 2017).

Prior to immobilization, the peptides were characterized using SDS-PAGE and RP-HPLC. In total, seven peptides were investigated in this study: NK-2 and its derivatives NK27, ALK-33C, and N33-ALK, as well as Ar-1 (arenicin) and its derivatives C/S-Ar-1 and R/K-Ar-1. For peptide immobilization, one core immobilization strategy was applied, which was developed and optimized based on previous Bachelor and Master theses conducted by Sara Jashari and Marina Lesniewski. In the present thesis, this immobilization approach was further expanded, and four different immobilization combinations were investigated. In addition, trypsin digestion and UV/VIS-spectrophotometry were employed as complementary analytical methods.

The results demonstrate that all seven peptides were successfully characterized using SDS-PAGE and RP-HPLC. Regarding the immobilization, two out of the four tested combinations showed progressive results compared to previous studies, with indications of successful peptide immobilization observed in both SDS-PAGE and RP-HPLC results. However, further verification is required, including microdilution assays to determine minimum inhibitory concentration (MIC) values and activity studies of the peptides before and after immobilization.

Future studies may address alternative immobilization strategies beyond the current thioether-based approach, such as Schiff base formation using AminoLink® resins (Lapetina and Gil-Henn, 2017) or covalent immobilization on gold surfaces (Wadhwani *et al.*, 2017).

Table of Contents

1. Introduction

1.1 Background and Motivation

The abuse of antibiotics and reckless usage of antibiotics has led to an increase in microorganism resistance to antibiotics, which has been classified as a global health emergency (Kyvik *et al.*, 2023). Pathogens such as *Escherichia coli*, *Staphylococcus aureus*, *Klebsiella pneumoniae*, *Streptococcus pneumoniae*, *Acinetobacter baumannii*, and *Pseudomonas aeruginosa* were responsible for 929,000 resistance-associated death cases in 2019 (Murray *et al.*, 2022). A deeper challenge occurs because bacteria form biofilms, which make them 10–1000 times more resistant to antibiotics compared with planktonic bacteria (Kyvik *et al.*, 2023). Sharma *et al*. state that approximately 80% of chronic and recurrent microbial infections in the human body are due to bacterial biofilms (Sharma, Misba and Khan, 2019). Biofilms can be formed on abiotic surfaces, especially in infections associated with indwelling medical devices and native biofilm infections of host tissue (Sharma, Misba and Khan, 2019). Biofilm formation on medical implants such as heart valves, catheters, contact lenses, joint prostheses, intrauterine devices, and dental units can lead to urinary tract and bloodstream infections. The only way to treat these infections is by removing the implants, which can be problematic for patients (Costerton, Montanaro and Arciola, 2005).

The immobilization of antimicrobial peptides (AMPs) onto solid surfaces has emerged as an innovative strategy to combat biomaterial-associated infections. Medical implants, catheters, and prosthetic devices are often colonized by bacteria forming persistent biofilms that are resistant to antibiotic treatment (Riool *et al.*, 2017). Conventional antibiotic coatings typically suffer from short-term release, leading to declining efficacy and the risk of resistance development. In contrast, the covalent immobilization of AMPs provides a non-leaching, long-term antimicrobial surface. Immobilized peptides remain attached to the substrate while retaining their ability to interact electrostatically with bacterial membranes. This approach reduces cytotoxic side effects, ensures stability under physiological conditions, and enables repeated use of peptide-functionalized materials (Costa *et al.*, 2011).

However, immobilizing AMPs onto surfaces also comes with technical and biological challenges, mainly loss of activity, safety concerns, and durability problems for real-world use cases. Yasir *et al.* showed in their research that immobilized AMPs were able to bind bacterial Lipopolysaccharide (LPS) and cause some membrane disruption, which was facilitated by the release of adenosine triphosphate (ATP) and deoxyribonucleic acid (DNA) / ribonucleic acid (RNA) from cells and was associated with bacterial death. However, the membrane disruption and killing kinetics of immobilized AMPs occurred at a slower rate compared to their soluble counterparts (Yasir *et al.*, 2020). The physical properties of synthetic AMPs, such as cationic charge and peptidic nature, can lead to host cell toxicity (Riool *et al.*, 2017). Another challenge faced in AMP immobilization is poor stability and susceptibility to proteolytic degradation, which can lead to a reduced half-life. The stability of AMPs *in vivo* is generally low because they are sensitive and easily degraded by both endogenous digestive enzymes of the host and enzymes secreted by pathogenic organisms (Zhang *et al.*, 2021).

Studies have shown that by applying sequence and structural engineering of AMPs, as well as chemical modification and conjugation, the technical and biological challenges of AMP

application can be addressed. Terminal modifications such as N-acetylation, C-amidation, or lipidation tune membrane affinity and protect against exopeptidases. Furthermore, PEGylation or attachment to polymers also reduces immunogenicity and prolongs circulation of AMPs (Bucataru and Ciobanasu, 2024). Conjugating AMPs to targeting ligands (e.g., antibodies, sugars) or antibiotics focuses activity on specific pathogens can exploit synergy, which allows dose reduction and helps limit toxicity and resistance development (Bucataru and Ciobanasu, 2024). To be able to immobilize AMPs, it is therefore important to understand their characteristics. These characteristics include amino acid sequence, charge, hydrophobicity, amphipathicity, secondary structure, physicochemical parameters, and biological activities. In this thesis, therefore, the AMPs will first be characterized using sodium dodecyl sulfate polyacrylamide gel electrophoresis (SDS-PAGE) and reversed-phase high performance liquid chromatography (RP-HPLC) and then immobilized onto the resin.

1.2 Aim of The Thesis

This thesis focuses on the approach to immobilize peptides onto a resin by chemical immobilization using covalent bonding, specifically the formation of a thioether bond between the peptide and the resin. Antimicrobial peptides (AMPs) are used as samples due to their antimicrobial ability to kill bacteria through membrane-targeting mechanisms, whereas current bacterial infections, due to bacterial aggregation forming biofilms, can lead to increased resistance against currently available antibiotics. AMPs, with their unique mechanism of action against bacteria, provide an alternative approach to address the bacterial resistance problem.

In this thesis, four experimental combinations were investigated to immobilize peptides onto the resin by utilizing thioetherbonds. The immobilization method developed is based on previous studies conducted by bachelor’s and master’s students, Sara Jashari and Marina Lesniewski, within the research group of Prof. Dr. Jörg Andrä, and the method is further expanded and optimized based on the experimental results obtained during this thesis.

Through optimization of the immobilization method and comparison of the results from the previous studies and results published in literatures, it can be evaluated whether the immobilization approach has led to an advancement and considered as successfull.

Further, characterization of the peptides was performed prior to immobilization by utilizing analytical methods such as SDS-PAGE and RP-HPLC. The aim of this characterization is to enable the selection of more suitable immobilization conditions that promote effective chemical bonding of the peptides to the resin.

2. Theoretical Background

2.1 Antimicrobial Peptides

Antimicrobial peptides (AMPs) are small peptides with a length of 20 to 40 amino acids. AMPs are divided into four major types of peptide structures, namely α-helical, β-sheet, combined α-helix and β-sheet, and linear extended peptides (Schromm *et al.*, 2021). Modified structures, such as circular structures, are also reported (Andrä *et al.*, 2008, 2009). By nature, AMPs possess strong amphiphilic characteristics, meaning they have both hydrophilic (water-attracting) and hydrophobic (water-repelling) regions. Furthermore, they typically exhibit a net cationic charge (Schromm *et al.*, 2021).

The diverse structures of AMPs and their cationic charge form the basis of their antimicrobial activity (Bucataru and Ciobanasu, 2024). AMPs are considered a promising alternative to conventional antibiotics due to their bacteriostatic and bactericidal effects, as well as their lower susceptibility to microbial resistance compared to conventional antibiotics (Li *et al.*, 2017).

2.1.1 Classification of AMPs

Antimicrobial peptides (AMPs) can be classified based on their source, structure, activity, and amino acid composition, as displayed in Figure 1 (Bucataru and Ciobanasu, 2024). In the following subchapter, each of these classifications will be thoroughly discussed.

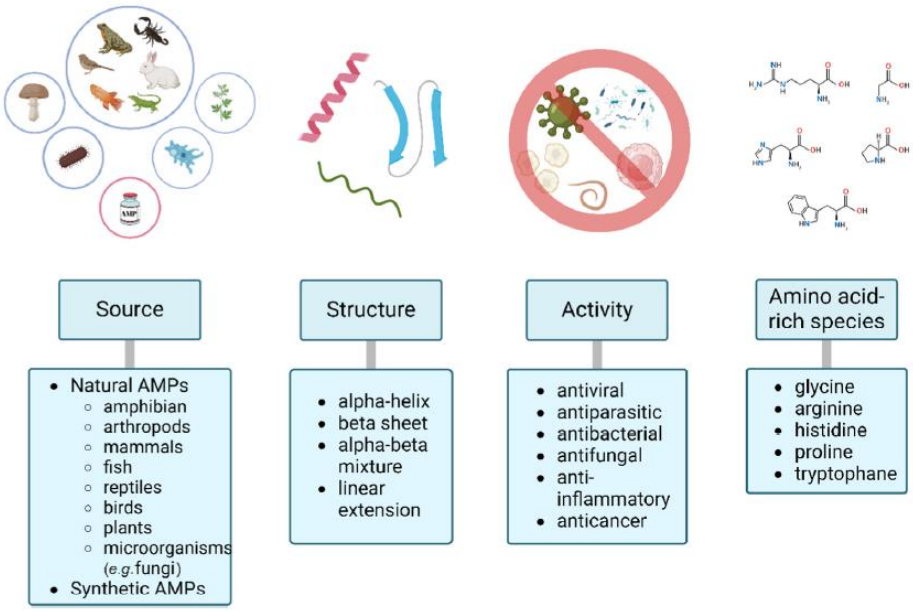

Figure 1: Classification of antimicrobial peptides. Figure shows that AMPs are classified based on their source, structure, activity and amino acid richness (Bucataru and Ciobanasu, 2024).

Classification by Origin

AMPs have two main origins, which can be classified as natural AMPs and synthetically produced AMPs. Natural AMPs can be derived from different kingdoms of life, these include microorganisms, marine arthropods, plants, fungi, mammals, and amphibians as showed in Table 1.

Table 1: Origin of natural AMPs. Listed in the table are the examples of natural AMPs and its origin (Bucataru and Ciobanasu, 2024).

Sources	Natural AMPs
Microorganisms	Bacteriocins (Darbandi *et al.*)
Marine Athropods	Penaeidins, Crustins (Saucedo-Vasquez *et al.*)
Plants	Thionins, Defensins, Haveins, Snakins (Lima *et al.*)
Fungi	Peptaibols (Duclohier *et al.*)
Mammals	Defensins, Histatins, LL-37, Indolicidin, Protegrins, Lactoferins (Dutta and Das *et al.*)
Amphibians	Esculentin, Japonicin 2, Nigrocin 2, Temporin, Dermaseptin, Maganin, Buforin II (Patocka *et al.*)

On the other hand, synthetically produced AMPs are peptides that are produced in laboratories by the scientist. Synthetically produced AMPs mainly demonstrate improved effectiveness, stability, and selectivity because scientists design and modify these peptides by exploiting specific characteristics and features of natural AMPs. Typical modifications performed by scientists include alterations in amino acid sequence, adjustments in peptide length, incorporation of non-natural amino acids, and structural modifications. Lima *et al.* described in their review article that the primary objective behind the changes and modifications of synthetically produced AMPs is to enhance antibacterial activity, selectivity, and resistance to degradation (Lima *et al.*, 2022).

Classification by (Secondary) Structure

Based on their secondary structure, AMPs can be distinguished into four groups, namely α-helical, β-sheet, α/β mixed, and peptides lacking both α-helical and β-sheet structures (Wang *et al.*, 2022; Bucataru and Ciobanasu, 2024). AMPs characterized by an α-helical structure show a distinctive and functionally significant arrangement of amino acid chains in a helical spiral shape, which imparts specific properties to these peptides and influences their interactions with microbial membranes and their overall antimicrobial efficacy (Bucataru and Ciobanasu, 2024). Magainin-2, a peptide isolated from the skin of *Xenopus laevis*, is an example of a peptide with an α-helical structure. Magainin has demonstrated broad-spectrum antimicrobial activity against bacteria, fungi, and certain viruses (Zasloff, 2002).

On the other hand, AMPs with a β-sheet structure have a folded arrangement that forms sheets of amino acid chains. This structural form is often stabilized by intramolecular disulfide bonds, which contribute significantly to the overall stability and functionality of the peptides. B-sheet AMPs display antimicrobial activity against bacteria, fungi, and viruses. Human α-defensins are examples of this class of peptides and play an important role in the innate immune system (Bucataru and Ciobanasu, 2024).

AMPs with an αβ-mixed structure show a diverse and hybrid arrangement of both α-helical and β-sheet elements within their peptide chains. Most AMPs with an αβ structure exhibit

amphipathic characteristics by possessing regions of both hydrophobic and hydrophilic amino acids. One example of a peptide from this class is LL-37, which belongs to the cathelicidin-derived peptides in humans. It also exhibits broad-spectrum antimicrobial activity and immunomodulatory effects (Sancho-Vaello *et al.*, 2020; Bucataru and Ciobanasu, 2024).

The final secondary structure classification includes AMPs with an extended or random coil structure. This structure is characterized by elongated or looped conformations, which differ from typical α-helical or β-sheet structures. Bucaratau *et al.* state that this structural diversity contributes to the versatility of these peptides in interacting with microbial membranes and maximizes their antimicrobial effects. One example of an AMP from this class is indolicidin, which is derived from the cathelicidin family. This peptide possesses an extended structure with a propensity for β-turns. Furthermore, it is known for its broad-spectrum antimicrobial activity against bacteria, fungi, and certain parasites (Koehbach and Craik, 2019; Bucataru and Ciobanasu, 2024).

Table 2: List of natural AMPs. In the table, natural AMPs are listed and classified based on the sequence, origin, structure and its activity against bacteria and fungi. Source: (Bucataru and Ciobanasu, 2024).

AMP	Sequence	Origin	Structure	Activity
Melittin	GIGAVLKVLTTGLPALISWIKRKRQQ	Bee venom	α-helix	Broad-spectrum, including bacteria, fungi, cancer
Magainin	GIGKFLHSAGKFGKAFVGEIMKS	African clawed frog Xenopus laevis	α-helix	Gram-positive and Gram-negative bacteria
Nisin	ILLSKFLRNWAILAILKWRNA	Bacteria Lactococcus lactis	Polycyclic β-sheet with loops	Gram-positive bacteria
Buforin II	TRSSRAGLQFPVGRVHRLLRK	Asian toad Bufobufogargarizans	α-helix-hinge-helix structure	Resistant bacteria and fungi
Gramicidin A	VGALAVVVWLWLWLWG	Soil bacterium Brevibacillus brevis	Linear	Gram-positive bacteria
Colistin (Polymyxin E)	CLCRFRRVCVGSRCRCVGR YKQOSKADJPQZHB-QNPLFGSASA-N	Bacterium Bacillus polymyxa	Cyclic polypeptide	Multidrug-resistant Gram-negative bacteria
Defensin (HNP-1)	ACYCRIPACIAGERRYGTCIYQGRLWAFCC	Human (Neutrophil)	β-sheet	Broad-spectrum, including bacteria, fungi, viruses (s HIV, influenza)
LL-37	LLGDFFRKSKEKIGKEFKRIVQRIKDFLRNLV PRTES	Human (Cathelicidin)	α-helix	Broad-spectrum, including bacteria, fungi and viruses
Indolicidin	ILPWKWPWWPWRR	Bovine neutrophils	Linear	Broad-spectrum, including bacteria and fungi
Lactoferricin	FKCRRWQWRM KKLGAPSITCVRRAF	Hukam (Milk, saliva, tears, and nasal secretions)	α-helix	Gram-positive and Gram-negative bacteria, fungi, viruses, cancer

Classification by Biological Activity

Another way to classify AMPs is based on their biological activity. Depending on the specific types of microorganisms they target, AMPs can be antibacterial, antiviral, antiparasitic, antifungal, anti-inflammatory, anticancer, anti-fibrotic, and others (refer to Figure 2).

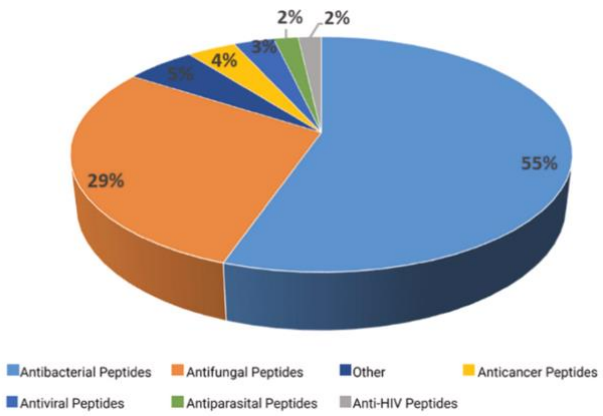

Figure 2: Classification and distribution of AMPs based on their biological activity. Pie chart shows that antibacterial peptides contribute most to the distribution with 55 %, followed by antifungal peptides on the second position with 29 %. The rest 16 % are divided by anticancer, antiviral, antiparasital, anti-HIV and others peptides. Source: (Bucataru and Ciobanasu, 2024).

Antibacterial peptides, which constitute approximately 55% of the overall AMP pool, exhibit a wide range of inhibitory effects against pathogenic bacteria in clinical medicine, including vancomycin-resistant *Enterococcus* (VRE), *Acinetobacter baumannii*, and methicillin-resistant *Staphylococcus aureus* (MRSA). Furthermore, a study by Huang *et al.* also shows that this class of AMPs has inhibitory effects on foodborne bacteria such as *Staphylococcus aureus*, *Listeria monocytogenes*, and *Escherichia coli*, as well as aquatic pathogens such as *Salmonella* and *Vibrio parahaemolyticus* (Huan *et al.*, 2020). An interesting study demonstrated by Li *et al.* in 2023 shows that a novel peptide derived from sturgeon (fish) spermary peptides possesses antibacterial properties and exhibits remarkable inhibitory activity against *E. Coli* with an inhibitory rate of 76.46%, indicating promising potential as an effective antibacterial agent (Li *et al.*, 2023).

Antifungal peptides (AFPs) represent the second largest group after antibacterial peptides, accounting for 29% of the distribution (refer to Figure 2). AFPs constitute a specific category of antimicrobial peptides with enhanced capacity to combat fungal infections characterized by increased resistance to conventional drugs. As stated by Fernández de Ullivarri *et al.* in their review article, numerous AFPs have demonstrated notable efficacy against prevalent pathogenic fungi, including *Aspergillus* and *Candida albicans*, in clinical medicine (Fernández De Ullivarri *et al.*, 2020). Furthermore, Pellisari *et al.* showed in their study that peptides derived from statherin have the capability to reduce colonization and biofilm formation of *Candida albicans*, a common and naturally occurring yeast in the human body, particularly in the gut, skin, and oral cavity (Pellissari *et al.*, 2021).

Antiviral peptides, accounting for 5% of the distribution (refer to Figure 2), possess the ability to hinder the multiplication or replication of viruses. Antiviral peptides exert their activity through diverse mechanisms, including disruption of the viral membrane, inhibition of viral entry into host cells, interference with viral replication, inhibition of viral protein synthesis, or modulation of the host immune response to viruses (Vilas Boas *et al.*, 2019). One example of an AMP with antiviral properties is Bomidin, a commercially available recombinant antimicrobial peptide derived from bovine myeloid antimicrobial peptide-27. Liu *et al.* claim that Bomidin exhibits antiviral activity against a diverse array of enveloped viruses, such as

severe acute respiratory syndrome coronavirus 2 (SARS-CoV-2), herpes simplex virus (HSV), dengue virus (DENV), and chikungunya virus (CHIKV) (Liu *et al.*, 2022).

A further classification of AMPs based on biological activity includes anti-inflammatory peptides. The mechanism of action of anti-inflammatory peptides, as emphasized by Luo and Song in their review article, involves suppression of pro-inflammatory mediators and pathways within the human body. These processes include cytokines, enzymes (such as inducible nitric oxide synthase (iNOS)), and signaling pathways (such as the nuclear factor kappa B (NF-κB) pathway). Anti-inflammatory peptides are able to modulate immunological responses and contribute to the maintenance of homeostasis between pro-inflammatory and anti-inflammatory factors (Luo and Song, 2021).

Another classification of AMPs includes anticancer peptides (ACPs). AMPs with ACP properties have been shown to possess antitumor and anticancer activity. ACPs can destroy cancer cells by inducing apoptosis, for example through membrane lysis, blocking angiogenesis (i.e., the formation of new blood vessels that support tumor growth), or modulating immune responses against cancer cells (Chinnadurai *et al.*, 2023).

Classification by Amino Acid Composition

AMPs can also be classified based on properties such as amino acid composition, charge, and hydrophobicity. AMPs are often rich in amino acids such as arginine, histidine, proline, tryptophan, or glycine. Decker *et al.*, in their review article, state that the term “rich” is used to denote the presence of specific amino acids occurring in the sequence at a minimum frequency of 25% (Decker, Mechesso and Wang, 2022). Based on net charge, AMPs are predominantly cationic (88%), with neutral peptides accounting for 6% and anionic peptides comprising the remaining 6% (Bucataru and Ciobanasu, 2024). Most AMPs are amphipathic by nature, with only rare cases in which AMPs are exclusively composed of either hydrophobic or hydrophilic amino acids (Bucataru and Ciobanasu, 2024).

2.1.2 Mode of Action and Mechanisms of AMPs

AMPs exert their effects through multiple pathways (refer to Figure 3), such as membrane lysis, inhibition of biofilm formation, regulation of intracellular targets, and modulation of the immune response. AMPs have the ability to bind to and penetrate the bacterial membrane and subsequently interact with the phospholipid components of the cytoplasmic membrane, which leads to pore formation and disruption of membrane integrity, causing leakage of cellular components and ultimately resulting in cell lysis and death (Lei *et al.*, 2019). Furthermore, AMPs can also target essential cellular mechanisms within pathogens by binding to intracellular molecules (refer to Figure 3), such as DNA, RNA, and proteins, and inhibiting their functions, ultimately leading to pathogen destruction (Scocchi *et al.*, 2015).

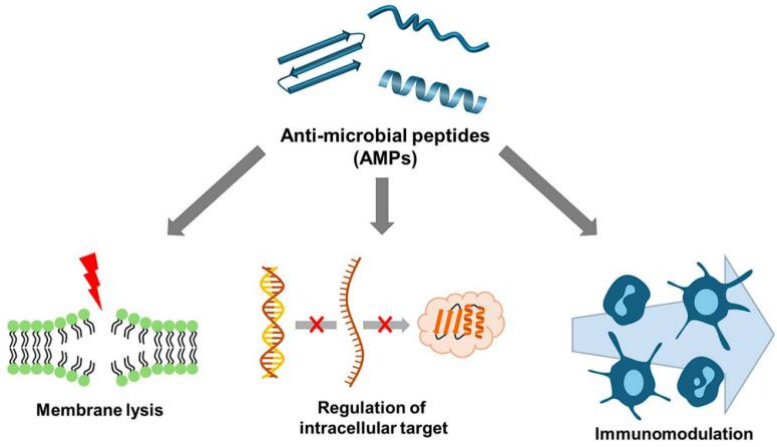

Figure 3: Mechanisms of action of AMPs. AMPs have various pathways to apply their effects, including membrane lysis, inhibition of biofilm formation, regulation of intracellular targets and modulation of the immune response. Source: (Min *et al.*, 2024).

Another remarkable mechanism of AMPs is their ability to modulate the immune response. These immunomodulatory properties enable the activation of interleukins, chemokines, and cytokines to enhance immune responses and aid in clearing pathogens from the body (Haney and Hancock, 2013). In addition to the aforementioned antimicrobial actions, AMPs can also inhibit biofilm formation by disrupting microbial adhesion and interfering with quorum sensing (i.e., the process by which bacteria communicate and coordinate with one another by sensing population density using small chemical signals called autoinducers), while also degrading the extracellular matrix of existing biofilms, thereby making them easier to treat (Luo and Song, 2021).

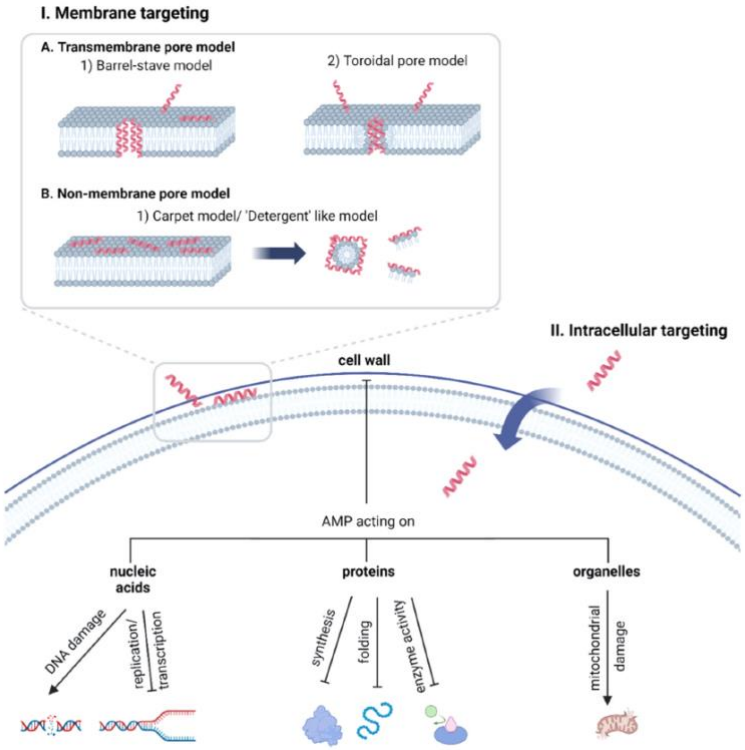

Figure 4: Antimicrobial Peptide Action Mechanisms. AMPs act through two main mechanisms: (I) membrane targeting and (II) intracellular targeting. (I) Membrane targeting includes pore formation via the barrel-stave and toroidal models, as well as the carpet model, which disrupts the membrane without forming pores. (II) Intracellular targeting occurs when AMPs enter the cell and interact with intracellular components such as nucleic acids and

proteins, which lead to cell damage or inhibition of essential processes. Blue arrows indicate AMP entry, straight arrows indicate induction, and end arrows indicate inhibition. Source: (Bucataru and Ciobanasu, 2024).

AMPs have two main mechanisms for killing bacteria, first, membrane targeting and disruption, and second, intracellular activity (refer to Figure 4), which will be thoroughly discussed in the next chapter.

Membrane Targeting

The basis of the interaction between AMPs and cell membranes is the charge difference between them. AMPs mainly possess a positive charge, whereas cell membranes exhibit little to no net charge on the outer leaflet (Figure 5) and a predominantly negative charge on the inner leaflet facing the cytoplasm, which leads to electrostatic interactions (Zasloff, 2002; Bucataru and Ciobanasu, 2024).

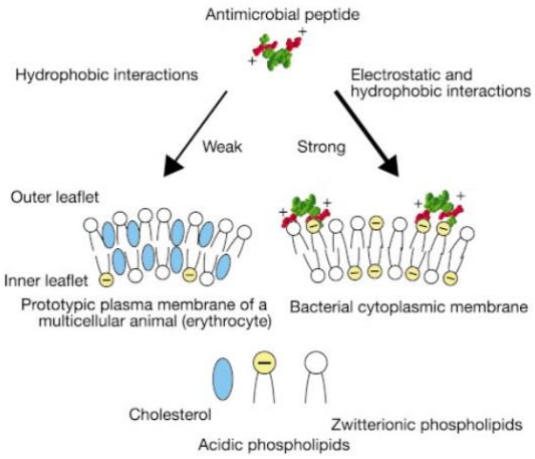

Figure 5: Basis of the interaction between AMPs and membrane of 9esirable9l9r organisms. Source: (Zasloff, 2002).

The mechanism proceeds as follows, first, the outer membrane is disrupted, subsequently, AMPs undergo a structural transition and adopt an amphipathic secondary structure. Through these amphipathic characteristics, the hydrophilic regions of the peptide interact with the charged head groups of phospholipids, while the hydrophobic segments engage with the lipid bilayer of the cytoplasmic membrane (Bucataru and Ciobanasu, 2024).

As shown in Figure 5, the presence of cholesterol in the target membrane weakens and reduces the activity of antimicrobial peptides, either due to stabilization of the lipid bilayer or through direct interactions between cholesterol and the peptide (Zasloff, 2002). On the other hand, increasing ionic strength is believed to reduce AMP activity due to weakened electrostatic interactions required for the initial binding step (Zasloff, 2002). Several models describe the modes of action of AMPs on cell membranes, including the barrel-stave model, the toroidal-pore model, and the carpet model (Zasloff, 2002; Min *et al.*, 2024).

The Barrel-Stave Model

This model belongs to the transmembrane pore models (refer to Figure 4 – I.A.1), in which AMPs form transmembrane channels by interacting and assembling with one another into oligomeric structures within the lipid bilayer. The hydrophobic regions of the AMPs interact

with lipid acyl chains, while the hydrophilic regions face the aqueous environment within the channel. This pore formation leads to a loss of membrane barrier function, resulting in unregulated passage of ions and molecules and ultimately causing cell death (Bucataru and Ciobanasu, 2024; Min *et al.*, 2024).

The Toroidal-Pore Model

This model is also categorized as a transmembrane pore model (refer to Figure 4 – I.A.2) and involves cooperative interactions between AMPs, lipids, and water molecules to form transient pores (i.e., channels formed within the membrane) in the bacterial membrane. As shown in Figure 4, lipid head groups bend inward to form a pore structure, while AMPs and water molecules are located within the pore interior. This structure maintains the continuity of the lipid bilayer while allowing the passage of ions and small molecules into the bacterial cell interior, which ultimately leads to membrane disruption and cell death (Raheem and Straus, 2019; Bucataru and Ciobanasu, 2024).

The Carpet Model

This model belongs to the non-transmembrane pore models and is also referred to as the detergent-like model (refer to Figure 4 – I.B.1). AMPs accumulate in a parallel orientation, forming a carpet-like layer on the membrane surface and interacting extensively with phospholipid head groups. The extensive surface coverage and interactions of AMPs destabilize the membrane, leading to high local peptide concentrations, subsequent membrane thinning, membrane disintegration, and increased permeability. Continuous insertion of AMPs into the membrane ultimately results in membrane destabilization and cell lysis (Bucataru and Ciobanasu, 2024; Min *et al.*, 2024).

Intracellular Targeting (Non-Membrane Targeting)

Apart from membrane-targeting mechanisms, AMPs are also able to exert intracellular activity through non-membrane-targeting mechanisms. AMPs enter cells through direct penetration or endocytosis. Once AMPs reach the intracellular environment, they can alter cellular metabolic processes, subsequently leading to inhibition of bacterial growth and other microorganisms. Within the cell, AMPs act directly on vital bacterial organelles and intracellular proteins or target nucleic acids (DNA and RNA) and protein synthesis. This results in induced damage or inhibition of replication and transcription processes, interference with protein synthesis by affecting folding steps or inhibiting specific enzymatic activities, and targeting of vital organelles, such as mitochondria, through structural damage (Le, Fang and Sekaran, 2017; Bucataru and Ciobanasu, 2024; Min *et al.*, 2024).

2.1.3 Features and Characteristics of Antimicrobial Peptides

Antimicrobial peptides share common sequence and structural characteristics despite their diverse biological origins and functions. These fundamental physicochemical properties explain their ability to selectively bind to and disrupt microbial membranes (Zasloff, 2002). Cationicity serves as a prerequisite for electrostatic attraction to negatively charged bacterial

surfaces (Zasloff, 2002). As shown in Figure 6, features of peptides with antimicrobial activity are categorized based on charge, hydrophobicity, amphipathicity, and secondary structure.

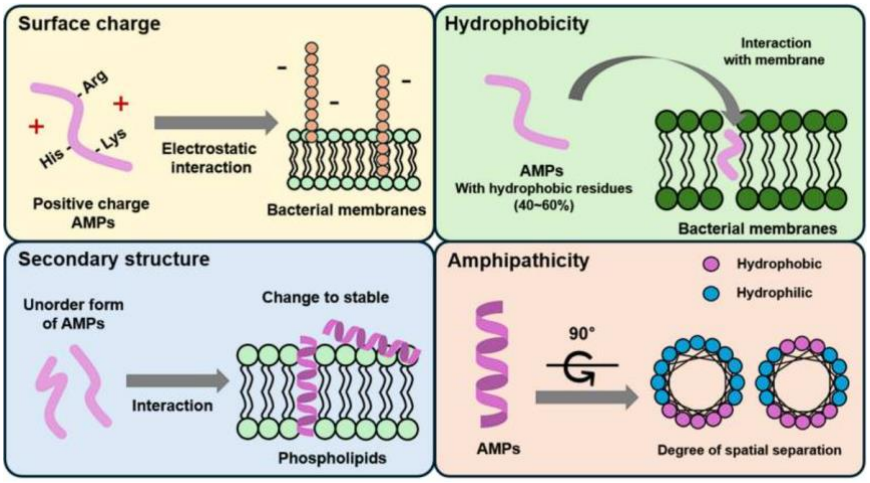

Figure 6: Key features of AMPs which allow antibacterial effects. This figures explains design principles of AMPs consists of four key categories, including positive surface charge, hydrophobicity, secondary structure and amphipaticity. Source: (Min *et al.*, 2024).

Amino Acid Sequence and Charge

Antimicrobial peptides (AMPs) share several characteristic features in their primary amino acid sequence that are essential for their biological function. One of the most defining properties is their strongly cationic nature, which arises from a high proportion of lysine and arginine residues. As described by Zasloff, most naturally occurring AMPs possess a net positive charge ranging from +2 to +11 at physiological pH, and this cationicity is a critical prerequisite for selective interaction with microbial membranes (Zasloff, 2002). The dominance of positively charged residues enables AMPs to bind strongly to the negatively charged outer leaflet of bacterial membranes, which are rich in phosphatidylglycerol (PG), cardiolipin, and in Gram-negative bacteria, lipopolysaccharides (LPS). In contrast, mammalian cell membranes are composed primarily of zwitterionic lipids such as phosphatidylcholine (PC) and sphingomyelin, providing them with a largely neutral surface charge this fundamental difference in lipid composition is the molecular basis for AMP selectivity toward bacteria (Costa *et al.*, 2011, 2021; Li *et al.*, 2017).

AMPs are composed of basic residues such as lysine (K) and arginine (R), neutral residues such as cysteine (C), as well as hydrophobic residues like leucine (L), isoleucine (I), valine (V), tryptophan (W), and phenylalanine (F). The arrangement of amino acids within the peptide sequence not only determines net charge but also influences hydrophobicity, secondary structure formation, membrane insertion, and stability. For example, hydrophobic amino acids such as leucine, isoleucine, valine, phenylalanine, and tryptophan typically cluster on one side of the peptide during folding, helping to form an amphipathic structure, whereas charged residues cluster on the opposite side. Simm *et al.* demonstrated that the interplay between hydrophobicity and charge is crucial for classifying peptides into functional groups and for predicting their structural transitions upon membrane contact (Simm *et al.*, 2016). Their analysis of 98 hydrophobicity scales revealed that peptides with balanced hydrophobic and cationic residues are most capable of forming membrane-active structures such as α-helices or β-sheets (Simm *et al.*, 2016). Thus, even small changes in sequence, such as substituting

a single hydrophobic residue or relocating a positively charged residue, can markedly influence a peptide's physicochemical behavior and antimicrobial potency.

Another important sequence-dependent feature is the presence of cysteine (Cys) residues. Cysteines can form intramolecular or intermolecular disulfide bonds, which may alter peptide conformation, stability, or oligomerization state. In the context of AMPs used in biomedical applications, cysteines play a crucial role in covalent immobilization strategies. For example, thiol-containing peptides can be specifically coupled to functionalized surfaces (e.g., iodoacetyl-activated resins) via thioether linkages, enabling oriented attachment. This principle is described by Prabhakar *et al.*, who reviewed cysteine-driven immobilization chemistry and highlighted how sequence design (e.g., addition of a terminal cysteine) allows precise control over peptide orientation and activity on biomaterial surfaces (Prabhakar *et al.*, 2025). Structural studies on NK-2 further confirm the functional impact of cysteine. Andrä *et al.* (2024) showed that the oxidation state of the cysteine residue in NK-2 influences peptide folding and membrane association, which demonstrated that sequence composition directly affects biophysical behavior (Andrä *et al.*, 2024).

Taken together, the primary amino acid sequence of an AMP determines far more than its chemical identity. It defines the peptide's net charge, topological distribution of residues, folding tendency, membrane affinity, and biological activity.

Hydrophobicity and Amphipathicity

AMPs contain between 30–60% hydrophobic amino acids, which are essential for their ability to interact with and insert into lipid bilayers. Hydrophobic residues such as leucine (L), isoleucine (I), valine (V), phenylalanine (F), and tryptophan (W) promote partitioning of the peptide into the acyl-chain region of membranes, a region composed of long hydrocarbon chains in lipids such as phospholipids and triacylglycerols, which facilitates initial anchoring and subsequent membrane destabilization. Simm *et al.* claimed that hydrophobicity is not only crucial for membrane affinity but also directly influences a peptide's ability to adopt secondary structures in lipid environments. The formation of α-helices or β-sheets is strongly dependent on the surrounding hydrophobic milieu, indicating that hydrophobic interactions are a primary driving force for peptide folding and membrane engagement (Simm *et al.*, 2016).

Beyond overall hydrophobic content, the structural hallmark of most AMPs is amphipathicity. Amphipathicity refers to the spatial segregation of hydrophobic and hydrophilic (often cationic) residues into distinct structural domains upon peptide folding, typically into α-helices or β-sheets. This results in a molecular architecture with one hydrophobic face capable of penetrating the lipid core, while the oppositely oriented hydrophilic face interacts with the negatively charged membrane surface (Li *et al.*, 2017).

The structural duality of hydrophobic and cationic regions is not merely a passive feature but a functional determinant of antimicrobial activity, as emphasized by Costa *et al.*, amphipathicity is one of the most powerful predictors of peptide efficacy, particularly when AMPs are used in surface immobilization or coating strategies for biomaterials (Costa *et al.*, 2011). Costa *et al.*'s review shows that peptides with high amphipathic moments exhibit stronger membrane-disruptive effects, improved antibacterial potency, and more robust performance on biomedical implant surfaces. Furthermore, a balanced combination of hydrophobicity and cationicity improves AMP selectivity, whereas peptides with excessive hydrophobicity may disrupt

mammalian membranes and become cytotoxic, while peptides with insufficient hydrophobicity may fail to penetrate bacterial membranes (Costa *et al.*, 2011).

The intersection between hydrophobicity and amphipathicity therefore forms the biophysical foundation of AMP function, contributing to membrane binding, folding, insertion depth, destabilization mechanisms, and ultimately antibacterial potency.

Secondary Structure

A characteristic feature of many antimicrobial peptides (AMPs) is their structural flexibility in aqueous environments. In solution, AMPs often exist in a disordered or random-coil conformation because the polar environment does not provide the hydrophobic or electrostatic cues required to stabilize a folded structure. This behavior is well documented across multiple AMP classes, including α-helical peptides such as magainins, cathelicidins, NK-lysin derivatives, and numerous synthetic analogues. The absence of stable secondary structure in water is not a functional limitation, rather, it is considered an adaptive advantage because it minimizes nonspecific interactions and cytotoxicity before the peptide reaches its biological target as discussed broadly by Li *et al.* (Li *et al.*, 2017).

The transition from an unstructured state to a folded conformation occurs when AMPs encounter negatively charged membranes or membrane-mimicking environments (e.g., SDS micelles, trifluoroethanol (TFE), or PG-rich lipid bilayers). This phenomenon, known as induced folding, which is driven by a combination of electrostatic attraction (between cationic residues and anionic lipids) and hydrophobic partitioning (of nonpolar residues into the lipid interface). As the peptide approaches the membrane, hydrophobic residues are buried within the acyl-chain region, while polar and charged residues remain solvent-accessible, allowing the peptide to adopt energetically favorable α-helical or β-sheet conformations. Such membrane-induced conformational switching is a core principle of AMP biophysics and has been confirmed by numerous structural studies using circular dichroism (CD), Fourier-transform infrared spectroscopy (FTIR) and nuclear magnetic resonance (NMR), as summarized in Costa *et al*. (Costa *et al.*, 2021).

For NK-2–type peptides specifically, Andrä *et al.* provided detailed biophysical evidence demonstrating the strict lipid dependence of AMP folding. Using CD spectroscopy, they showed that NK-2 remains largely unstructured in buffer but undergoes a pronounced random-coil-to-α-helix transition when interacting with membranes containing at least 50 mol% phosphatidylglycerol (PG). Below this threshold, only partial or unstable α-helical structures were detected. This demonstrates that anionic charge density of the membrane is a decisive factor in promoting stable secondary structure formation. Complementary solid-state NMR measurements in the same study further revealed that the resulting α-helix adopts a well-defined orientation relative to the membrane plane, reinforcing the concept that membrane composition directly dictates both helical stability and topological alignment (Andrä *et al.*, 2024).

The orientation of helical AMPs at the membrane interface, represents another crucial mechanistic aspect, rather than deep membrane insertion. As explained by Li *et al.*, most α-helical AMPs, including NK-2, LL-37, and synthetic helix-forming peptides, lie parallel to the membrane surface in an interfacial binding mode. This orientation maximizes electrostatic contact with negatively charged headgroups while allowing hydrophobic residues to partially

insert into the lipid acyl chains. Such a surface-parallel orientation supports models such as the carpet and interfacial activity mechanisms, in which membrane disruption results from lipid packing perturbation, curvature strain, and membrane thinning rather than formation of stable, well-defined transmembrane pores. Li *et al.* emphasize that deeply inserted barrel-stave pores are rare among natural AMPs and are largely restricted to specialized peptides (e.g., alamethicin), whereas broad-spectrum host-defense peptides typically operate at the membrane interface (Li *et al.*, 2017).

These principles of induced folding, lipid-dependent secondary structure formation, and surface-parallel orientation also apply broadly to modern synthetic AMPs, as supported by the structural analyses reviewed in Costa *et al.* Their work emphasizes that many rationally designed AMPs mimic the behavior of natural peptides as they remain disordered in solution, fold into amphipathic helices upon encountering microbial membranes, and exert their antimicrobial effects through interfacial membrane interactions rather than forming stable, classical pores. This shared behavior across natural and synthetic peptides underline the fundamental role of environment-dependent structural plasticity in AMP function. (Costa *et al.*, 2021).

2.1.4 Design of Peptide NK-2, Arenicin and Derivatives

NK-2 and Derivatives

NK-2 is an α-helical fragment derived from mammalian NK-lysin. It exhibits broad-spectrum activity against both Gram-negative and Gram-positive bacteria while remaining non-toxic to human cells (Andrä and Goldman 2011). NK-2 has a linear structure and possesses an overall net positive charge resulting from the presence of four arginine (R) and six lysine (K) residues.

In this thesis, three modifications of the peptide NK-2 were applied. NK-27 is a modified variant of NK-2 in which the non-functional cysteine (C) residue at position 7 is substituted with serine (S). This substitution is intended to reduce the sensitivity of the peptide to oxidation while maintaining its overall structural and physicochemical properties (Andrä *et al.*, 2007). ALK-33C and N33-ALK are modifications in which cysteine (C) at position 7 was replaced by alanine (A). The cysteine residue is not involved in the formation of disulfide bonds. Therefore, this replacement has no effect on the stability of the α-helical structure (Andrä, Montreal, 2007). Furthermore, at position 11, the amino acid methionine (M) was replaced by leucine (L). Both replacements lead to a reduced sensitivity to oxidative reactions (Andrä *et al.*, 2007). Another replacement occurs at position 21, where the negatively charged aspartic acid (D) was replaced by the strongly positively charged lysine (K), resulting in an increase in net positive charge from +10 to +11 (refer to Table 5). Andrä and Monreal reported that the net charge is correlated with the activity of antimicrobial peptides (AMPs) (Andrä *et al.*, 2007). In addition, a linker was added to the sequence of ALK-33C at the C-terminus and to N33-ALK at the N-terminus.

Table 3: Amino acid sequence of NK-2 and derivatives. In the table, the amino acid sequence of NK-2 and its modifications are presented. The modified sequence are highlighted as yellow.

Peptide		Amino Acid Sequence							
Stem	**NK-2**		KILRG	VCKKI	MRTFL	RRISK	DILTG	KK	
Derivate	**NK-27**		KILRG	VSKKI	MRTFL	RRISK	DILTG	KK	
	ALK-33C		KILRG	VAKKI	LRTFL	RRISK	KILTG	KK	GSGSG C
	N33-ALK	C GSGSG	KILRG	VAKKI	LRTFL	RRISK	KILTG	KK	

Arenicin Ar-1 and Derivatives

Arenicin (Ar-1) is a β-sheet antimicrobial peptide isolated from the coelomocytes of the marine polychaete lugworm *Arenicola marina* (Andrä *et al.*, 2009). It exhibits broad-spectrum activity against Gram-negative and Gram-positive bacteria as well as fungi. Ar-1 is a cyclic peptide with an overall net positive charge resulting from six arginine (R) residues (Andrä *et al.*, 2009).

Ar-1 possesses a cysteine-bridged cyclic structure (yellow bridge, refer to Figure 7), and its arginine residues are essential for biological activity and interaction with biomembranes. The first Ar-1 modification, C/S-Ar-1 (S008), is a linear peptide in which the two cysteine (C) residues are exchanged for serine (S) residues. The second Ar-1 modification, R/K-Ar-1 (K009), is a cyclic peptide in which all arginine (R) residues are replaced by lysine (K) residues. Jörg Andrä *et al.* reported that the linear peptide appears significantly more hydrophobic on a reversed-phase HPLC column compared to the two cyclic peptides (Andrä *et al.*, 2009).

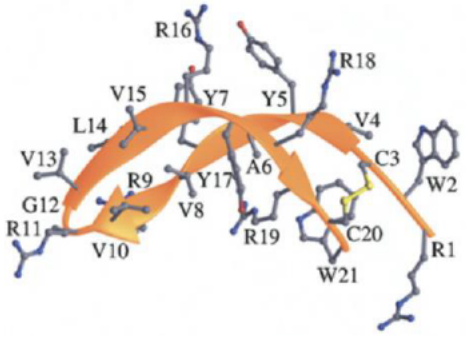

Figure 7: Three dimentional structure of Arenicin. β-sheeted AMPs with cysteine-bridged cyclic structure (yellow) and six arginine residues. Source: (Andrä *et al.*, 2008).

Table 4: Amino acid sequence of Ar-1 and derivatives. In the table, the amino acid 15esirabl of peptide Ar-1 and its modifications are presented. The modified sequence are highlighted as yellow.

Peptide			Amino Acid Sequence				
Stem	**Ar-1**		RWCVY	AYVRV	RGVLV	RYRRC	W
Derivate	**C/S-Ar-1**		RWSVY	AYVRV	RGVLV	RYRRS	W
	R/K-Ar-1		KWCVY	AYVKV	KGVLV	KYKKC	W

Table 5: Characteristics of the applied peptides. In the table, the sequenz and number of amino acids, number of positively and negatively charged residues, GRAVY value and structure of the AMPs are listed. GRAVY value represents the average hydropathy of all amino acids in a peptide. Positive GRAVY value indicates a highly hydrophobic peptide and negative value indicates a hydrophilic peptide. Source: Expassy ProtParam.

Peptide	Number of Amino Acids	Positively Charged Residues (Arg + Lys)	Negatively Charged Residues (Asp + Glu)	GRAVY Value	Structure
NK-2	27	10	1	-0.263	Linear
NK27 (C7S)	27	10	1	-0.385	Linear
ALK-33C	33	11	0	-0.200	Linear
N33-ALK (CK-33)	33	11	0	-0.200	Linear
Ar-1 (R007)	21	6	0	-0.071	Cyclic
C/S-Ar-1 (S008)	21	6	0	-0.386	Linear
R/K-Ar-1(K009)	21	6	0	0.100	Cyclic

2.2 Strategies of Peptide Immobilization

One effective approach to harness the antimicrobial activity of peptides on materials is through their immobilization onto solid surfaces such as resins, implants, catheters, or membranes. This allows the peptides to remain structurally intact while forming stable interactions with the surface, thereby preventing their removal by washing or exposure to physiological fluids. The immobilization of antimicrobial peptides (AMPs) onto solid supports is a key strategy for creating bioactive surfaces that inhibit microbial adhesion and biofilm formation on medical and industrial biomaterials.

AMP immobilization can be broadly categorized into two main strategies, as outlined by Nicolas *et al.*, physical methods (e.g., adsorption or Layer-by-Layer (LbL) assembly) and chemical methods (e.g., covalent bonding or the use of Self-Assembled Monolayers (SAMs)). Studies have shown that covalent immobilization provides several advantages, including enhanced stability, sustained antimicrobial efficacy, reduced toxicity, and limited diffusion of the AMP into surrounding tissues (Nicolas *et al.*, 2021). A crucial consideration in these systems is that only low surface concentrations of AMPs are required to achieve high antimicrobial efficacy.

Additional insights from Bagheri *et al.* highlight the importance of linker design in immobilization. Their findings show that peptides attached to resin surfaces via polyethylene glycol (PEG) spacers exhibit decreased antimicrobial activity as spacer length increases. This loss of activity cannot be compensated for by increasing the surface density of the peptide, underscoring the importance of maintaining an optimal spatial configuration.

Recent studies have demonstrated the successful functionalization of various solid substrates for AMP immobilization, including polymers, titanium, gold, stainless steel, and glass. Several critical factors influence the antimicrobial performance of immobilized peptides, such as surface coverage or density, peptide orientation, distance from the surface, and lateral mobility (Bagheri, Beyermann and Dathe, 2009; Nicolas *et al.*, 2021). The following subchapters will provide a detailed discussion of the immobilization strategies.

2.2.1 Covalent Immobilization

Covalent immobilization strategies exploit the functional groups of antimicrobial peptides (AMPs), such as amine, carboxyl, thiol, and hydroxyl groups to form stable, mostly irreversible covalent bonds with reactive groups on material surfaces (Soyhan *et al.*, 2024). These covalent interactions ensure strong attachment of the peptide to the substrate, minimizing desorption under physiological conditions and enhancing long-term stability.

Several factors significantly influence the biological activity and biocompatibility of covalently immobilized peptides. These include the tether length (i.e., the distance between the peptide and the surface), orientation (which determines the exposure of active sites), and surface density (which affects both antimicrobial potency and potential cytotoxicity). Optimizing these parameters is essential for designing effective and safe antimicrobial surfaces.

Orientation of Attachment (N- or C-Terminus)

Peptides possess two directional ends, the N-terminus (amino terminus) and the C-terminus (carboxyl terminus). The N-terminus contains a free amino group ($–NH_2$ or $–NH_3^+$), while the C-terminus carries a free carboxyl group ($–COO^-$ or –COOH). By convention, peptides are both written and synthesized from the N-terminus (left) to the C-terminus (right).

The orientation of peptide attachment, either via the N- or C-terminus, plays a significant role in determining antimicrobial activity. This is primarily due to the impact of terminal exposure on the peptide's overall charge distribution and interaction with microbial membranes. As demonstrated by Bagheri *et al.*, N-terminal immobilization can lead to enhanced antimicrobial activity for certain peptide sequences. The N-terminus typically carries a positive charge, contributing to the overall cationic nature of AMPs. This positive charge is essential for electrostatic interactions with negatively charged bacterial membranes, because it facilitates the initial membrane binding (Bagheri, Beyermann and Dathe, 2009).

In contrast, the C-terminus is naturally negatively charged, which may result in electrostatic repulsion during the initial contact with bacterial membranes, potentially reducing antimicrobial efficacy. To mitigate this effect, researchers have employed C-terminal amidation, which involves converting the terminal carboxyl group into a neutral amide group ($–CONH_2$). This modification removes the negative charge and increases the net positive charge of the peptide, thereby enhancing its affinity for bacterial membranes and improving antimicrobial performance (Bagheri, Beyermann and Dathe, 2009; Nicolas *et al.*, 2021; Soyhan *et al.*, 2024).

Spacer (or Linker) Length and Flexibility

The length and flexibility of spacer molecules are critical parameters that influence the biological performance of covalently immobilized antimicrobial peptides (AMPs). Spacers function by creating distance between the peptide and the material surface. Without a spacer, AMPs may be positioned too close to the surface and behaves more like an inert coating rather than an active, membrane-disruptive molecule. This close proximity can result in strong steric hindrance, which limits the peptide's conformational freedom, impairs the formation of amphipathic α-helices, and weakens electrostatic interactions with bacterial membranes. Collectively, these effects lead to reduced antimicrobial activity.

Incorporating long and flexible spacers, such as polyethylene glycol (PEG) chains (10–30 Å) or elastin-like linkers can enhance peptide mobility and improve accessibility to bacterial membranes. These flexible linkers allow the peptide to adopt favorable conformations and orientations required for effective interaction with microbial surfaces. Conversely, very short or rigid spacers may restrict peptide movement and orientation, increase steric hindrance, and ultimately lower antimicrobial efficacy (Bagheri, Beyermann and Dathe, 2009; Hasan *et al.*, 2020; Zare *et al.*, 2025).

Surface Density

Surface density refers to the number of peptide molecules immobilized per unit area of a surface. Achieving an optimal peptide density is critical, as both excessively high and overly low surface densities can negatively impact antimicrobial performance.

Very high surface densities of covalently immobilized AMPs can lead to steric crowding, which restricts the peptide conformational flexibility and reduces their accessibility to bacterial membranes. These effects ultimately result in diminished antimicrobial activity. In contrast, moderate surface densities with adequate intermolecular spacing promote favorable peptide orientation and allow the formation of amphipathic structures, thereby enhancing antimicrobial efficacy.

Surface density can be regulated by diluting reactive functional groups on the surface with inert molecules. This is commonly achieved through the use of mixed self-assembled monolayers (SAMs) or co-grafted polymers, which help optimize peptide spacing and preserve their biological function (Hasan *et al.*, 2020; Nicolas *et al.*, 2021; Skerlavaj and Boix-Lemonche, 2023).

2.2.2 Physical Immobilization

Physical immobilization of antimicrobial peptides (AMPs) involves non-covalent interactions such as electrostatic attraction, hydrophobic interactions, hydrogen bonding, or physical entrapment within polymeric matrices to retain peptides on material surfaces (Riool *et al.*, 2017; Costa *et al.*, 2021). These strategies preserve the native chemical structure of the peptides and enable straightforward surface functionalization without requiring chemical coupling reactions (Glinel *et al.*, 2012). However, the non-covalent nature of these interactions often results in limited binding strength, poor control over peptide orientation, and susceptibility to desorption under physiological conditions, particularly in the presence of salts or serum proteins (Humblot *et al.*, 2009). Consequently, the observed antimicrobial activity may, in part, result from peptide release into the surrounding environment rather than direct surface-bound action (Gabriel *et al.*, 2006). While physical immobilization may be appropriate for short-term antimicrobial coatings or controlled-release applications, it generally offers lower stability and less mechanistic control compared to covalent immobilization. As such, covalent strategies are typically favored for long-term antimicrobial surfaces and implant-associated applications (Riool *et al.*, 2017; Costa *et al.*, 2021).

2.3 Coupling Chemistry

2.3.1 SulfoLink® - Thioether Bond

The basis of thioether bond formation is the reaction between a free sulfhydryl group (–SH) and an iodoacetyl group on the resin. The resin itself consists of agarose beads with a 12-atom spacer arm and an iodoacetyl group located at the end of the spacer. The 12-atom spacer arm minimizes steric hindrance and ensures efficient binding interaction with the coupled molecule.

The sulfhydryl group of the peptide must be reduced to generate a free sulfhydryl group, only then can the reaction between the iodoacetyl group and the sulfhydryl group occur to form a thioether bond. Reducing agents cleave disulfide bonds, thereby making sulfhydryl groups available for coupling. However, the presence of reducing agents can hinder immobilization, as they compete with the peptide for reaction with the iodoacetyl group. Therefore, reducing agents must be removed prior to immobilization, for example by RP-HPLC purification or

desalting (e.g. with Size Exclusion Chromatography (SEC)). The binding capacity of the resin is approximately 1 mg of sulfhydryl-containing peptide per 1 mL of settled resin.

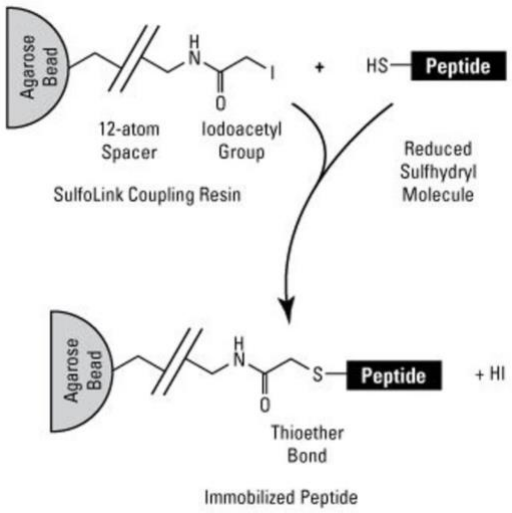

Figure 8: Immobilization chemistry between peptide and SulfoLink® resin. Figure shows thioether bond as the basis of the reaction between the free sulfhydryl group of the peptide and iodoacetyl group of the resin. Source: ThermoFischer Scientific – SulfoLink® Product Catalog.

The thioether-based immobilization strategy applied in this thesis builds upon previous thesis conducted by Marina Lesniewski (Master's thesis, 2022) and Sara Jashari (Bachelor's thesis, 2024). Marina Lesniewski developed an initial immobilization protocol, which is presented in Figure 12 of her thesis. Her method included a buffer exchange using SEC prior to immobilization, as well as a quenching step following immobilization, accompanied by additional washing procedures. However, in the discussion section of her thesis, she concluded that the method did not successfully result in peptide immobilization on the resin (Marina Lesniewski, 2022).

Sara Jashari further developed the method by testing four different experimental conditions for covalent immobilization via thioether bonds. In one of these conditions, referred to as Condition B, she extended the incubation time and reported partial immobilization of the peptide (Sara Jashari, 2024). Based on the findings of both previous studies, one core immobilization scheme and four experimental conditions, named as combination A, B, C and D, were tested in this thesis. The details of the method are described in Chapter 3.6.2 – "Immobilization Strategies and The Verification".

2.3.2 AminoLink® – Schiff Base Bond

AminoLink® Coupling Resin is a 4% crosslinked agarose bead matrix with surface-bound aldehyde groups (R–CHO). It is intended for covalent immobilization of proteins, such as antibodies, through their primary amines (e.g., lysine residues). This approach of immobilization utilizes the free lysine at the N-terminus of an amino acid on the AMP, which has affinity for the free aldehyde group of the coupling resin. The basis of the immobilization is the covalent bond between the aldehyde groups and primary amines, which form a reversible Schiff base bond. The Schiff base bond is then reduced using a mild reductant, such as cyanoborohydride, to form a stable secondary amine bond. The Schiff base-bonded peptide

must be incubated for 4 to 6 hours in a simple, non-amine buffer such as phosphate buffered saline (PBS) to allow the reductive amination coupling reaction.

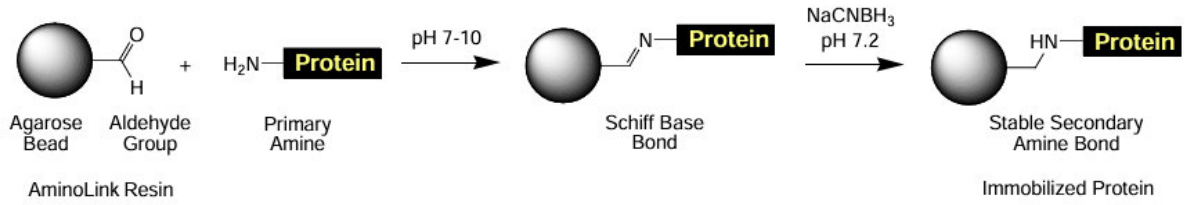

Figure 9: Immobilization chemistry between peptide and AminoLink® resin. Figure shows 20esira-base bond as the basis of the reaction between the free lysin at N-terminus of the peptide and aldehyde group of the resin. Source: AminoLink® User Manual - ThermoFischer Scientific.

In experiments using AminoLink® aldehyde-activated agarose beads, covalent immobilization of biomolecules via primary amines resulted in highly stable and reproducible surface attachment with minimal ligand leakage. The immobilization proceeds through Schiff base formation between bead-bound aldehyde groups and N-terminal or lysine amines of the coupled molecule, followed by reductive stabilization to yield a permanent secondary amine bond. Lapetina and Gil-Henn demonstrated that this chemistry enables near-quantitative coupling efficiencies and produces immobilized bait molecules that remain stably attached during extensive washing and downstream assays (Lapetina and Gil-Henn, 2017). Importantly, blocking of remaining reactive sites effectively suppressed nonspecific binding, allowing reliable separation of bound and unbound interaction partners. The immobilized molecules retained their functional binding capability, enabling quantitative analysis of interactions without detectable loss of activity or significant batch-to-batch variability. These results highlight AminoLink® immobilization as a robust and chemically stable strategy for covalent surface functionalization, providing a well-defined and reproducible platform suitable for downstream biochemical and biofunctional studies (Lapetina and Gil-Henn, 2017).

2.3.3 Gold Surface – Covalent bond between Thiol group and Au

Antimicrobial peptides can be immobilized on gold (Au) surfaces by exploiting the strong and highly specific interaction between thiol groups and gold atoms. The two most common modes of attaching a peptide to gold. First, a labile Au–N bond (as in lysine, allowing easy release of the drug), and second, a relatively stable covalent Au–S bond (for surface functionalization). A research group from the Karlsruhe Institute of Technology in Germany, Wadhwani *et al.*, developed an approach utilizing the Au–S bond (refer to Figure 10), which is also combined with strict control over peptide orientation and flexibility. In the experiment, each AMP was modified to carry a single cysteine residue at the N-terminus, separated from the active sequence by a flexible glycine spacer, while all other side chains (especially lysine residues) were temporarily protected (Wadhwani *et al.*, 2017). This AMP design ensures site-selective, single-point anchoring of the peptide to the gold surface, which prevents non-specific interactions between positively charged lysine side chains and gold. As a result, the immobilized AMPs remain conformationally flexible and are not forced into an inactive, flattened conformation. Conceptually, gold nanoparticles thus serve not only as inert carriers but also as well-defined scaffolds that allow AMPs to remain unstructured in aqueous solution and to fold into their biologically active and amphiphilic α-helical conformation once the AMPs

come into contact with bacterial membranes, which is essential for antimicrobial function (Wadhwani *et al.*, 2017).

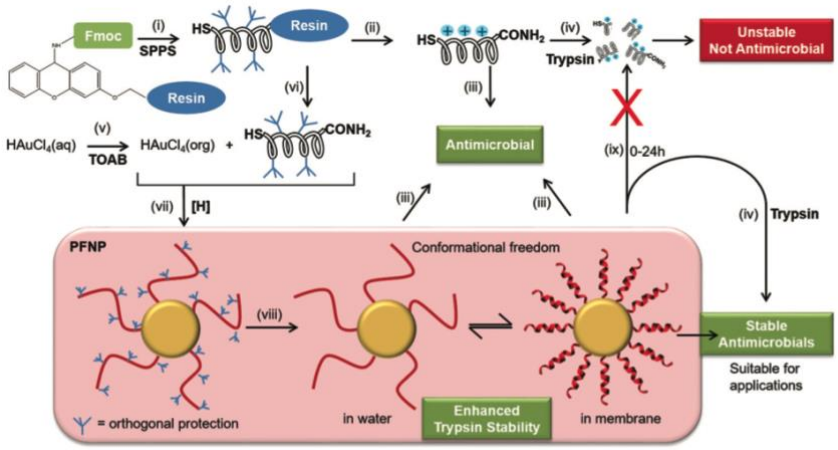

Figure 10: Schematic illustration of the site-selective immobilization of antimicrobial peptides (AMPs) on gold nanoparticles. Peptides are synthesized with an N-terminal cysteine and attached to gold via a strong Au–S bond, ensuring single-point anchoring and preserving conformational flexibility. Free peptides are rapidly degraded by trypsin, whereas gold-tethered peptides remain stable and biologically active. After immobilization and deprotection, the peptides retain their ability to fold into amphiphilic α-helices in membrane-like environments and exhibit antimicrobial activity comparable to that of free peptides, while showing enhanced resistance to proteolytic degradation. Source: (Wadhwani *et al.*, 2017)

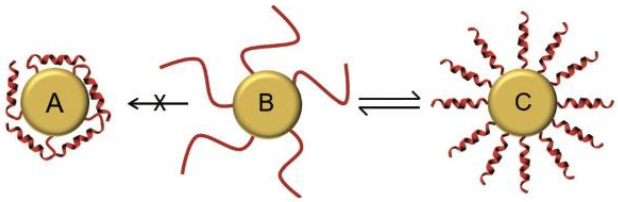

Figure 11: Schematic illustration of peptides tethered to the gold nanoparticle. The gold (Au)-nanoparticle are represented by (A), (B) and (C). The desired configuration is shown in (C), where peptides adopt functional amphiphilic helical structures upon interaction with bacterial membranes. In contrast, configuration (A) is unfavorable, as interactions between lysine side-chain amino groups and the gold surface can restrict peptide conformation and impair biological activity. (B) represents an intermediate and less 21esirable ordered state. Source: (Wadhwani *et al.*, 2017)

Using a one-pot synthesis based on a modified Brust–Schiffrin method, the authors successfully prepared peptide-functionalized gold nanoparticles with homogeneous size (≈5–7 nm) and high peptide surface coverage. Circular dichroism spectroscopy was used to investigate the secondary structure of AMPs tethered to gold nanoparticles. The results in Figure 11 demonstrated that the gold-tethered AMPs were largely disordered in aqueous buffer but adopted a clear α-helical structure in membrane-mimicking environments, comparable to their free counterparts (Wadhwani *et al.*, 2017).

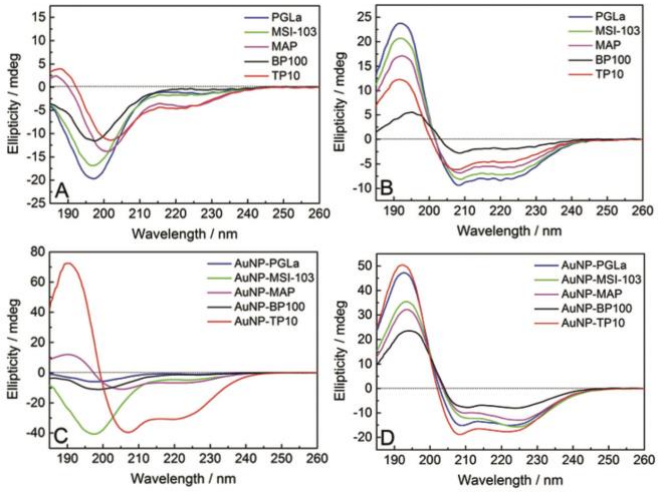

Figure 12: CD spectra of the free peptides (A, B) and when tethered to gold nanoparticles (C, D). In aqueous buffer (A,C), the peptides are largely disordered, with the exception of AuNP-TP10. In the presence of lipid vesicles composed of DMPC/DMPG (B, D), both free and tethered peptides adopt a pronounced α-helical structure. DMPC is 1,2-dimyristoyl-sn-glycero-3-phosphocholine, a zwitterionic (neutral) phospholipid. DMPG is 1,2-dimyristoyl-sn-glycero-3-phosphoglycerol, a negatively charged phospholipid. Source: (Wadhwani *et al.*, 2017).

Importantly, antimicrobial assays showed that the immobilized peptides retained essentially the same antibacterial activity as free peptides against both Gram-positive and Gram-negative bacteria. A further important result was the dramatic increase in proteolytic stability, whereas free AMPs were rapidly degraded by trypsin within minutes, gold-bound AMPs remained largely intact and biologically active for many hours, even up to 24 h. This enhanced stability was attributed to steric hindrance and high surface density on the gold nanoparticles, which limit protease access. Overall, the study demonstrates that site-selective immobilization of AMPs on gold nanoparticles preserves antimicrobial activity while improving peptide stability, which highlight gold as a powerful platform for functional and durable AMP immobilization (Wadhwani *et al.*, 2017).

3. Materials and Methods

3.1 Equipment

Table 6: List of equipment used.

Equipment	Manufacturer
Aluminium Foil	Toppits
Centrifuge Minispin	Eppendorf
HPLC Glass Vials (300 μL) with 1.5 μL inlet	ThermoScientific / VWR
HPLC Guard Column LiChrospher® 100 RP-18, 5 μm	Merck
HPLC Column Vydac® 218 TP C18, 250 x 4 mm, 5 μm	Avantor
HPLC Instrument – Primaide	Hitachi
Magnetic Stirrer	Komet
pH – Meter	Knick
Precision Balances	KERN
Pipette 10, 100 and 1000 μL	Eppendorf
Rocker 2D basic	IKA
SDS-PAGE Equipment	BioRad
Thermomixer	Eppendorf
Vortexer	Heidolph
UV/VIS Spectrometer Libra S22	biochrom
Quartz Cuvette Suprasil	HellmaAnalytic
Hei-PLATE Magnetic Stirrer with Heating	Heidolph

3.2 Chemicals

Table 7: List of chemicals used.

Chemicals	Manufacturer	Lot Number
Acetic Acid	Roth	193334687
Acetonitrile	Roth	-
Acryl / Bisacrylamid (40%)	Roth	481317897
Ammonium Peroxodisulfate (APS)	Roth	410162406
Boric Acid	Roth	313335383
Ethanol	Roth	-
Glutardialdehyd	Roth	199283500
Glycerol	Roth	048266863
Orange G	Sigma Aldrich	-
Roti Blue – Coomassie (5x)	Roth	411315733
Sodium Dodecyl Sulfate (SDS)	Roth	6291236
SulfoLink™ Coupling Resin	Thermo Scientific	YC364883
TEMED	Roth	264355771
Tricine	Roth	385231585
Tris	Roth	222324515
Trifluoroacetic Acid (TFA)	Sigma Aldrich	BCBC3517V

3.3 Antimicrobial Peptides

In Table 8 and 9, the peptides used in this thesis are listed. All peptides used in this thesis were synthesized by solid phase peptide synthesis (SPPS) with an amidated C-terminus and were provided in a RP-HPLC purified form. The peptides ALK-33C and N33-ALK were purchased from Proteogenix.

Table 8: Origin of the sample NK-2 and its derivatives.

Peptide Name	NK-2	NK-27 (C7S)	ALK-33C	N33-ALK
Concentration	1 mM	1 mM	1 mM	1 mM
Lyophil weight	1.6 mg	2.9 mg	1.81 mg	1.81 mg
Molecular Mass	3202.1 g/mol	3186 g/mol	3614 g/mol	3614 g/mol
Solvent	in 0.01 % TFA	in 0.01 % TFA	in 0.01 % TFA	in 0.01 % TFA
Date of Origin	-	09.03.2011	27.10.2025	27.10.2025
Abbreviation	-	-	Try	Try
Manufacturer	Research Center Borstel	Research Center Borstel	Proteogenix	Proteogenix

Table 9: Origin of the sample Ar-1 and its derivatives.

Peptide Name	Ar-1 (R007)	C/S-Ar-1 (S008)	R/K-Ar-1 (K009)
Concentration	1 mM	1 mM	1 mM
Lyophil weight	1.32 mg	1.26 mg	1.59 mg
Molecular Mass	2758.3 g/mol	2728.2 g/mol	2590 g/mol
Solvent	in 0.01 % TFA	in 0.01 % TFA	in 0.01 % TFA
Date of Origin	21.09.2011	10.06.2025	10.06.2025
Abbreviation	-	Try	Try
Manufacturer	Research Center Borstel	Research Center Borstel	Research Center Borstel

3.4 Analytical Methods

3.4.1 Tricine SDS – PAGE

Sodium dodecyl sulfate–polyacrylamide gel electrophoresis (SDS-PAGE) is an analytical method used to separate proteins according to their size and can therefore be applied to determine protein purity and molecular mass (Schägger and Von Jagow, 1987). The gel is composed of cross-linked polyacrylamide, which can be visualized as a molecular mesh. When an electric field is applied, negatively charged molecules migrate through the gel matrix toward the positive electrode, which is located at the lower part of the gel chamber where the anode buffer is present (Figure 13). Due to the sieving properties of the gel matrix, proteins of different sizes migrate at different rates, with smaller molecules migrating faster than larger ones (Schägger and Von Jagow, 1987). In this thesis, Tricine-SDS-PAGE was applied to characterize and verify the molecular weight of peptides, as this method is particularly suitable for the detection of low-molecular-weight peptides (Schägger and Von Jagow, 1987). Furthermore, Tricine-SDS-PAGE enables analysis under both reducing and non-reducing conditions. Reducing agents such as dithiothreitol (DTT) and tris(2-carboxyethyl) phosphine

(TCEP) are suitable for use in this analytical method. Using Tricine-SDS-PAGE, the molecular weight of peptides can be verified by comparison with a standard molecular weight marker.

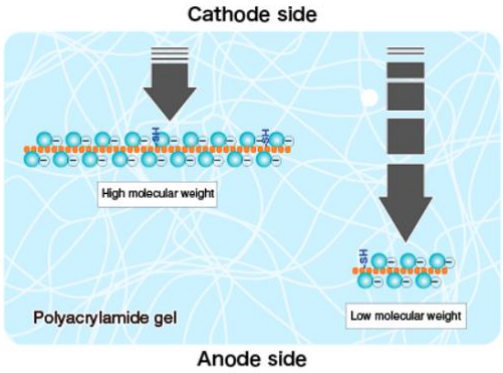

Figure 13: Principle of SDS-PAGE. Figure shows protein migration from cathode to anode. Smaller protein migrates further to the lower molecular weight range, while bigger protein stays at the higher molecular weight range. Source: https://www.mblbio.com/bio/g/support/method/sds-page.html

To perform Tricine-SDS-PAGE, the stacking, spacer, and separation gels must first be prepared. The composition of each gel is listed in Table 10. The gels were prepared by assembling glass plates in the Bio-Rad gel casting apparatus. The prepared gel solutions were pipetted into the space between the glass plates, and a comb was inserted at the top. Polymerization was initiated by the addition of ammonium persulfate (APS). After approximately 30 minutes, the gels were fully polymerized and the comb was removed. At this stage, the gels were ready for sample loading; however, the protein samples had to be prepared beforehand.

Protein samples were prepared in two forms, reduced and unreduced. Unreduced samples were mixed directly in a 1:1 ratio with 2x-sample buffer. Reduced samples were first treated with either DTT or TCEP as reducing agents and subsequently mixed 1:1 with 2x-sample buffer. The addition of reducing agents breaks disulfide bonds within the peptides, converting oligomeric or dimeric species into monomeric forms. After preparation, samples were heated at 95 °C for 5 minutes prior to loading onto the gel. For each well, 20 µL of peptide sample was loaded. Molecular weight marker peptides were prepared by mixing 1.25 µL of marker solution with 98.75 µL of 1x marker buffer and heating at 62 °C for 2 minutes. Empty wells were filled with a 1:1 mixture of 0.01% trifluoroacetic acid (TFA) and 2x sample buffer. After all samples were loaded, cathode buffer was added to the space between the glass plates, and anode buffer was added to the outer chamber of the electrophoresis unit. Electrophoresis was performed at a constant current of 20 mA per gel. After approximately 1.5–2 hours, the protein bands reached the lower part of the gel, indicating completion of the run. The gel was then removed from the glass plates and placed in fixation solution for 30 minutes. Subsequently, the gel was washed three times with demineralized water before staining overnight with ROTI® Quant Blue. Finally, the gel was destained using a destaining solution and washed three times with demineralized water. In Table 10 to 19, the composition of SDS-Gel, buffers, fixating solution, staining and destaining solutions are listed.

Table 10: Composition of separation, spacer and stacking gel.

Component	Concentration	Separation gel (6 mL) (15%)	Spacer gel (2 mL) (9%)	Stacking gel (3 mL) (4%)
Acryl-/Bisacrylamid	30 %	3.0 mL	0.6 mL	0.45 mL
Gel buffer	3x	2.0 mL	0.65 mL	0.925 mL
Glycerol	87 %	1.0 mL	0.2 mL	-
Aqua dem.	100 %	-	0.55 mL	1.505 mL
TEMED	100 %	6 μL	2 μL	3 μL
APS	20 %	15 μL	5 μL	7.5 μL
Cast volume / gel		2.8 mL	0.4 mL	1 mL

Table 11: Composition of Gel buffer (3x).

Component	Amount
Tris Base (3 M)	36.3 g
SDS	0.3 g
Adjust pH to 8.45 and fill up to 100 mL with aqua dem.	

Table 12: Composition of Anode buffer (10x).

Component	Amount
Tris Base (2 M)	24.2 g
Adjust pH to 8.9 and fill up to 100 mL with aqua dem., dilute to 1x buffer before use	

Table 13: Composition of Cathode buffer (10x).

Component	Amount
Tris Base (1 M)	6.2368 g
Tricine (1 M)	8.98 g
SDS (1 %)	0.5 g
Adjust pH to 8.25 and fill up to 50 mL with aqua dem., dilute to 1x before use	

Table 14: Composition of Buffer S.

Component	Amount
Tris Base	6.1 g
SDS	0.4 g
Adjust pH to 6.8, fill up to 100 mL with aqua dem.	

Table 15: Composition of Sample buffer.

Component	Amount
Buffer S	2.5 mL
SDS	2 g
Orange G	40 mg
Glycerol (87 %)	20 mL
Fill up to 100 mL with aqua dem.	

Table 16: Composition of gel fixating solution (with boric acid).

Component	Amount
Boric Acid	12.37 g
Glutardialdehyd (25 %)	25 mL
Add 300 μL aqua dem., adjust to pH 8.5, fill up to 500 mL with aqua dem	

Table 17: Composition of gel fixating solution (with sodium carbonate).

Component	Amount
Sodium Carbonat (400 mM)	21.20 g
Glutardialdehyd (25 %)	25 mL
Add 300 μL aqua dem., adjust to pH 8.5, fill up to 500 mL with aqua dem	

Table 18: Composition of Coomassie-staining solution.

Component	Amount
Roti-Blue (Coomassie 5x)	100 mL
Ethanol (100%)	100 mL
Aqua dem.	300 mL

Table 19: Composition of destaining solution.

Component	Amount
Acetic acid (100%)	50 mL
Ethanol (100 %)	50 mL
Aqua dem.	400 mL

3.4.2 Reversed Phase – High Performance Liquid Chromatography (RP – HPLC)

In this thesis, RP-HPLC was applied to characterize and compare reduced and unreduced antimicrobial peptides. Using RP-HPLC, peptide purity, aggregation state (monomer or dimer), and relative hydrophobicity can be assessed. The basis of this method is the hydrophobic interaction between analytes and a non-polar stationary phase, which is composed of octadecylsilane (C18)-bonded silica particles, in combination with a polar mobile phase consisting of mixtures of water and organic solvents such as trifluoroacetic acid (TFA) and acetonitrile (ACN) (Lee, 2011). In RP-HPLC, molecules are retained based on their hydrophobicity. Compounds with higher hydrophobicity interact more strongly with the stationary phase and therefore elute later than less hydrophobic compounds.

Elution is achieved by applying a linearly increasing solvent gradient during the chromatographic run. A typical linear gradient starts at 5% organic solvent and increases up to 95%. As the organic solvent concentration increases, peptides elute from the column and can be detected by a UV detector in the form of absorbance (AU). Detection is typically performed at 214 nm for peptide bonds or at 280 nm for aromatic amino acids (Lee, 2011)(Liang, Qiao and Lian, 2017).

The RP-HPLC analyses were performed using a Hitachi Primaide HPLC system (refer to Figure 14A). This system is equipped with a pump, autosampler, column oven, degasser, leak sensor, and UV detector. Peptide separation was carried out on a Vydac® 218TP C18 column (4.6 × 250 mm, 5 µm particle size).

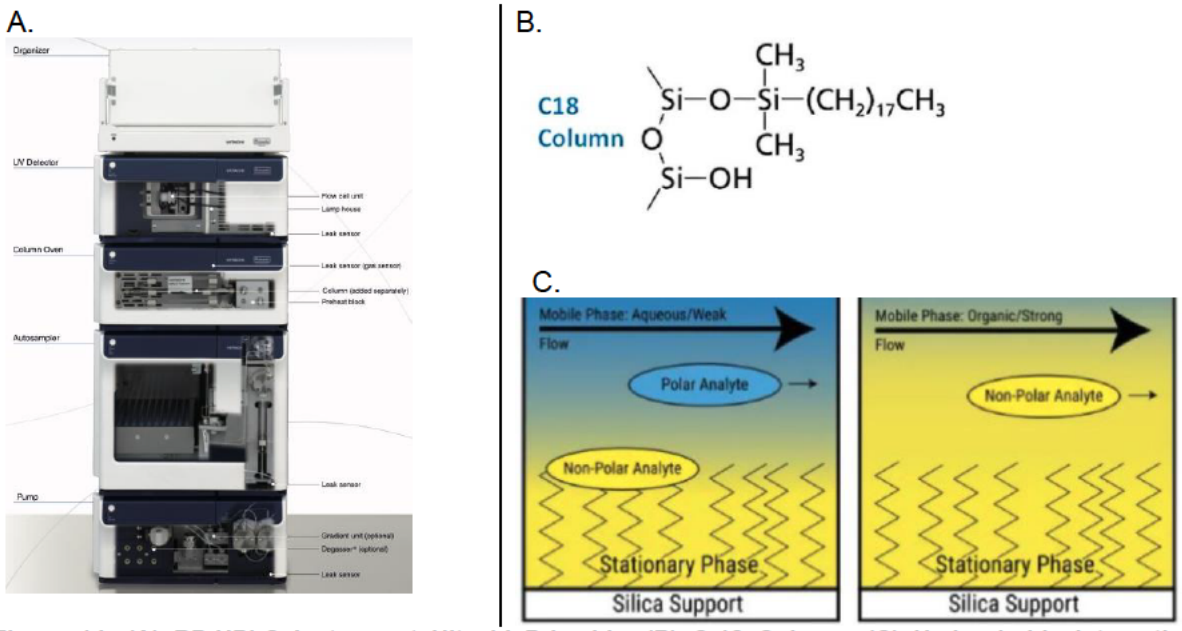

Figure 14: (A) RP-HPLC Instrument Hitachi Primaide. (B) C-18 Column. (C) Hydrophobic interaction between non polar analyte and and the non polar stationary phase. Source: Hitachi Primaide Manual and uHPLC®

Two eluents were used for the chromatographic runs:

- Eluent A: 0.1% (v/v) trifluoroacetic acid (TFA) in VE water
- Eluent B: 80% (v/v) acetonitrile and 0.05% (v/v) TFA in VE water

Detection was performed at a wavelength of 214 nm, and the flow rate was set to 1.0 mL/min. The injection volume ranged from 10 to 50 μL, depending on the desired injected peptide mass.

C18 Column

The column used in this thesis was a Vydac® 218TP C18 HPLC column, purchased from Vydac, with dimensions of 250 × 4.6 mm and diameter of 5 µm.

The C18 column contains a stationary phase consists of polar silica (SiO_2) particles bonded with non-polar 18-carbon alkyl chains (octadecylsilane or ODS). This column design gives rise to the characteristic properties of a reversed-phase system, in which the stationary phase presents a hydrophobic surface that interacts strongly with non-polar analytes, while more polar analytes are less strongly retained and elute earlier due to weaker hydrophobic interactions (Figure 14C). The column specifications are listed below.

Table 20: Specification of Vydac® 218TP C18 column.

Phase	218TP C18
Pore Size (Å)	300
Surface Area (m^2/g)	60-110
Carbon Load (%)	8
Chromatographic Properties	First generation polymeric C18 media with unique selectivity
Application/Benefit	Small polypeptides 4-5k MW, enzymatic digest fragments, natural and synthethic peptides, multiring-compounds

Column Preparation and Conditioning

Prior to peptide analysis, the column must be washed with a mixture of water and organic solvents to remove the storage buffer present inside the column. Subsequently, the column must be tested for its ability to deliver consistent results over multiple runs, referred to as robustness. This preparation step also helps to condition the silica–C18 stationary phase, thereby increasing its affinity for binding small peptide molecules.

The column can be conditioned by repeated injections of a polypeptide until the chromatographic characteristics remain constant. The manufacturer recommends injecting approximately 100 μg of polypeptide for a 4.6 mm (inner diameter) × 250 mm column, followed by elution using a typical acetonitrile gradient containing 0.1% TFA.

The HPLC Standard is a standard mixture containing peptides such follows:

Table 21: Composition of the HPLC standard peptide mixtures.

Peptides	Amino Acid Composition	Molecular Weight [g/mol]	Mass in each Vials [mg]
G 3502	GLY-TYR	238.2	0.5
V 8376	VAL-TYR-VAL	379.5	0.5
M 6638 (Methionine Enkephalin Acetate)	TYR-GLY-GLY-PHE-MET	573.7	0.5
L 9133 (Leucine Enkephalin)	TYR-GLY-GLY-PHE-LEU	555.6	0.5
A 9525 (Angiotensin II Acetate)	ASP-ARG-VAL-TYR-ILE-HIS-PRO-PHE	1046.2	0.5

Each vial contains 2.5 mg of total peptide. According to the product instruction manual, a concentration of 2 mg sample per 1 mL of diluting solution is recommended. Therefore, the 2.5 mg peptide standard mixture was dissolved in 1.25 mL of 0.01% TFA, resulting in a concentration of 2 $\mu g/\mu L$.

After injection of the standard, at least one blank run using a demineralized water should be performed. In the subsequent run, the HPLC standard mixture, and peptide samples can then be injected. An overview of the column preparation and conditioning procedure is provided in Table 22.

Table 22: In the table, the step by step to perform C18 – column conditioning is described.

	Samples	Injection Volume [μL]	Elution Gradient	Objective
Step 1	dem. H_2O	10 – 20	Constant at 5 % ACN	To get rid of the storage buffer
Step 2	HPLC Standard Mixture	10 – 20	As showed in Figure 15 and Table 23	Conditioning of the silica 18 – carbon chain
Step 3	dem. H_2O	10 – 20	As showed in Figure 15 and Table 23	Neutralize column before injecting it with another peptide sample
Step 4	Real Peptide	10 – 20	As showed in Figure 15 and Table 23	Conditioning of the silica 18 – carbon chain

The steps described in Table 22 are recommended to be performed weekly or once every two weeks to recalibrate column performance and, if possible, whenever new peptide samples that differ from previous samples are injected.

Storage (Idle) Condition of Column and HPLC Instrument

Prior to leaving the HPLC instrument in idle condition for an extended period, the manufacturer recommends purging the system by pumping an adequate volume of solvent, typically more than 10 mL, through the instrument. This is performed using an organic solvent mixture consisting of 50% acetonitrile (ACN) and 50% demineralized water (v/v).

For column storage, the column should also be washed with the same solvent mixture for 10–15 column volumes (CV). The Vydac 218TP C18 column has a column volume of approximately 4.15 mL, therefore, a minimum of 42 mL of the 50% organic solvent mixture should be passed through the column. The flow rate used for this procedure was 1.0 mL/min. After washing, the column should be sealed with the plastic plugs originally supplied by the manufacturer.

Elution Technique

Elution was initiated with 5% Eluent B for the first 10 minutes. Subsequently, a linear gradient was applied, increasing Eluent B from 5% to 95% between 10 and 30 minutes. The concentration of Eluent B was then maintained at 95% for 5 minutes, from 30 to 35 minutes. Finally, Eluent B was decreased back to 5% and maintained at this level until the end of the run at 45 minutes. The complete elution profile from the start of the run (0 minutes) to the end (45 minutes) is shown in Figure 15.

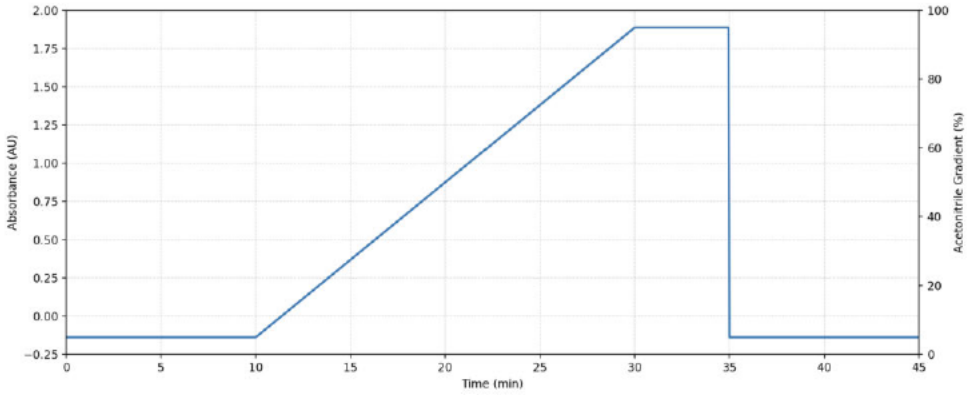

Figure 15: Gradient course of acetonitrile gradient for the elution process.

Table 23: Overview of the elution process from 0 to 45 min.

Time [min]	Elution B / Acetonitrile Gradient [%]
0 – 10	5
10 – 30	5 – 95 (linear increase)
30 – 35	95
35 – 45	5

Sample Preparation Prior to RP-HPLC Run

Prior to the RP-HPLC run, samples must be prepared using specific procedures to ensure that no dust or impurities are present, as these can lead to column clogging and consequently shorten column lifetime.

First, glass vials and vial inserts were washed with ethanol and dried in a drying cabinet. Subsequently, the samples were centrifuged for 10 minutes at 12.100 x g. After centrifugation, at least 20% of the total volume was left as pellet, and only the upper 80% of the solution was collected. This step ensures that only the clear supernatant is taken as the sample, while dust and impurities remain in the lower fraction (pellet). Finally, the supernatant was transferred into the dried glass vials and was ready for injection into the RP-HPLC system.

Cleaning Methods

The HPLC system must be cleaned and maintained regularly to ensure precise and reliable analytical performance. Common problems that may occur include ghost peaks and persistent, non-eluting peaks that appear even when no sample is injected into the column. In this thesis, a standard operating procedure (SOP) for cleaning the HPLC column was established. The cleaning method was developed based on recommendations from the VWR team and the user instructions provided by VWR.

The cleaning procedures are as follows:

1. Replace the guard column regularly (approximately once every two months).
2. Perform column cleaning in both the normal flow direction and the reverse flow direction.
3. To remove adsorbed or clogged peptide residues, use Eluent A (0.1% TFA) and Eluent B (80% ACN). Apply a gradient from 10% to 90% organic solvent and run the column for 10–20 column volumes (CV).

Methanol can also be used for column cleaning and is recommended by the manufacturer; however, since peptide samples typically do not cause severe clogging, the use of TFA and ACN was sufficient in this thesis. Furthermore, methanol was not preferred for use in the Instrumental Analytics Laboratory at HAW Hamburg Bergedorf.

After completion of the cleaning procedure, the column must be prepared and conditioned again using the HPLC standard mixture and the peptide samples to be analyzed. For details on column preparation and conditioning, refer to the previous subchapter “Column Preparation and Conditioning.”

3.4.3 UV/VIS-Spectrophotometer

In this experiment, UV/VIS spectrophotometer was used to measure the absorbance of antimicrobial peptides at 214 nm. The instrument used was a UV–VIS spectrophotometer Libra S22 from Biochrom Ltd, which is equipped with a xenon lamp. The device has a measuring range of 190–1100 nm and is coupled with PC software called “Acquire” for the management and analysis of measurement data.

Table 24: List of materials used for UV/VIS-Spectrophotometer.

Material	Manufacturer
UV/VIS-Spectrophotometer Libra S22	Biochrom Ltd
High Precision Cell Quartz Cuvette	Hellma Analytics

3.4.4 Fumigation and Vaporization with Nitrogen

Nitrogen was used in this experiment to fumigate and vaporize the acetonitrile in the peptide fractions collected after RP-HPLC separation. Acetonitrile can interfere with the immobilization of the peptide onto the resin and therefore needs to be removed. The nitrogen gas was obtained from the organic chemistry laboratory at HAW Hamburg. The materials used are listed in Table 25.

Table 25: List of the material used for fumigation and vaporization with nitrogen.

Material	Manufacturer
Laboratory Jack	SwissBoy
Eppendorf Tubes 1.5 mL	Eppendorf
Test Tube	ROTH
Test Tube stander	-

3.4.5 Trypsin Digestion

Trypsin is one of the most widely used proteases due to its high cleavage specificity and its ability to generate peptides with positively charged N- and C-terminal amino acid residues, which are well suited for RP-HPLC separation (Mansuri *et al.*, 2024). It cleaves proteins into fragments with an average size of 700–1500 Da, which is an ideal range for coupled liquid chromatography (RP-LC) and tandem mass spectrometry (MS/MS) analyses (Laskay *et al.*, 2013). Trypsin specifically cleaves peptide bonds at the carboxyl side of arginine (R) and lysine (K) residues, which results in small peptide fragments.

In this experiment, trypsin digestion was applied to cleave immobilized peptides from the resin. Through proteolysis, peptide fragments are expected to be released into the supernatant. The presence of fragmented peptides in the supernatant serves as an indication that immobilization was successful, therefore, trypsin digestion represents a suitable analytical method to verify immobilization yield. The supernatant containing the cleaved peptide fragments was subsequently analyzed using Tricine SDS-PAGE in order to detect the fragments as bands on the gel. Further, RP-HPLC were also used to detect the peaks of the fragments.

Table 26: List of the chemicals and materials used for trypsin digestion.

Chemicals	Manufacturer	Lot Number
Trypsin, Bovine Pancreas (MW 23281 Da)	EMD Milipore USA	3851198
Acetic Acid (100%)	ROTH	383337674
Materials	**Manufacturer**	**Lot Number**
Hei-PLATE Magnetic Stirrer with Heating	Heidolph	-
Magic Touch Icewares	Fischer Scientific	-

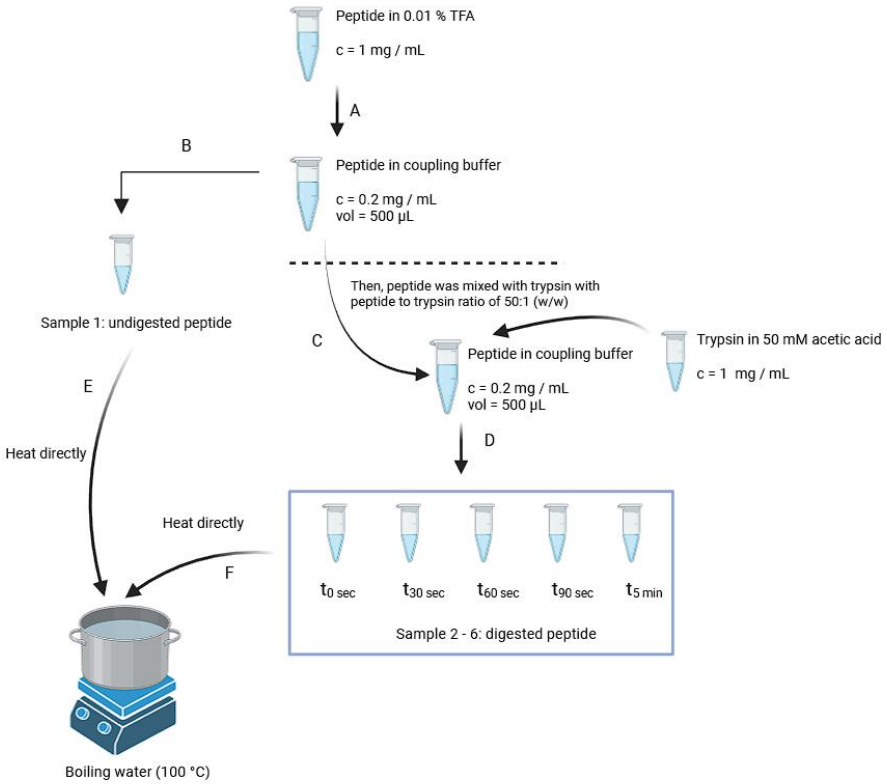

Figure 16: Trypsin digestion of peptides. Figure shows the method to perform trypsin digestion of peptide. **(A)** Peptide was diluted in coupling buffer (c = 0.2 mg/mL; 500 μL) from the stock solution of 1 mg/mL peptide in 0.01 % TFA. **(B)** 20 μL of sample was withdrawn as representative for undigested peptide. **(C)** Peptide was then mixed with trypsin with peptide to trypsin ration of 50:1 (w/w). **(D)** Peptide was taken as samples each 30 seconds until 90 seconds and lastly after 5 minutes. **(E)** Sample 1 was heated directly after withdrawn. **(F)** All samples 2 – 6 were each heated directly after withdrawn. Figure created with BioRender.

For trypsin digestion, a stock solution of trypsin (1 mg/mL) was prepared in 50 mM acetic acid. On the other hand, 1 mg/mL of peptide were prepared in 0.01 % TFA. Then, the peptide was further diluted in coupling buffer (refer to Table 28) to a final concentration of 0.2 mg/mL (total volume of 500 µL). To obtain an undigested reference sample (peptide without trypsin), 20 µL of peptide solution were withdrawn prior to the addition of trypsin, immediately heated for 5 min in a boiling water bath (~100 °C). For the digestion reaction, a peptide-to-trypsin ratio of 50:1 (w/w) was applied. The digestion reaction was initiated by adding 2 µL of the trypsin stock solution to the peptide solution. After addition, the mixture was briefly vortexed to ensure homogeneous distribution of the enzyme and uniform initiation of digestion. Immediately thereafter, the first aliquot corresponding to time point t_0 (20 µL) was withdrawn and directly placed in a boiling water bath (~100 °C) for 5 min to quench the reaction by denaturing the trypsin. Additional aliquots of 20 µL were collected at defined time points (30, 60, 90, and 120 seconds, and 5 min) and treated identically. All samples (Samples 2–6) were stored for subsequent analysis by Tricine SDS-PAGE.

3.5 Peptide Characterization

Peptides were characterized using SDS-PAGE and RP-HPLC. For SDS-PAGE, each peptide was applied to the gel in unreduced and reduced states, as described in Chapter 3.4.1 – "Tricine SDS-PAGE". Each peptide was loaded in an increasing concentration gradient ranging from 0.1 to 1 μg.

For RP-HPLC, the peptides were applied in increasing peptide masses of 1, 3, and 5 μg. Prior to the RP-HPLC run, the samples were prepared as described in Chapter 3.4.2 - "Sample Preparation Prior to RP-HPLC Run".

For reduced peptides, the peptides were heated for 5 min at 95°C after DTT was added, then prepared as described in Chapter 3.4.2 - "Sample Preparation Prior to RP-HPLC Run".

3.6 Peptide Immobilization on Resin

In this Thesis, the immobilization was performed with AminoLink® coupling resin from ThermoFischer Scientific (refer to Table 27). ThermoFischer claimed that 1 ml of resin or 2 ml of resin suspension could binds 1 mg of sulfhydryl-containing peptide (-SH). Prior to immobilization, the resin was first washed. The washing procedure is as described in Chapter 3.6.1 – "Washing the Resin Prior to Immobilization".

Table 27: Resin used for peptide immobilization.

Chemicals	Manufacturer	Lot Number
AminoLink® Coupling Resin	ThermoFischer Scientific	YC364724

3.6.1 Washing the Resin Prior to Immoblization

Prior to application, the resin was washed. Washing was performed to remove the storage buffer of the resin, which allows a buffer exchange. The storage buffer was replaced with the coupling buffer. The purpose of this step is to maximize the binding efficiency of the antimicrobial peptides to the resin by providing optimal environmental conditions for peptide coupling. The composition of the coupling buffer is listed in Table 28.

Table 28: Composition of coupling buffer.

Component	Amount
EDTA – Na_2Dihydrat	0.1861 g
Tris Base	0.6057 g
Adjust pH to 8.5 and fill up to 100 mL with demineralized Water	

The procedure used to wash the resin is illustrated in Figure 17. This procedure was developed as suggested by Prof. Dr. Jörg Andrä. It consists of four steps. First, the storage buffer was removed after centrifugation and replaced with coupling buffer. Subsequently, 1 mL of coupling buffer was added to the resin, and the mixture was horizontally shaked prior to centrifugation. This step was repeated three times. At the end of the washing process, the 1 mL of coupling buffer was removed, and 300 μL of coupling buffer was added to the washed resin. It is important to balance the resin volume, meaning that the final resin volume should be the same as the initial volume, namely 500 μL.

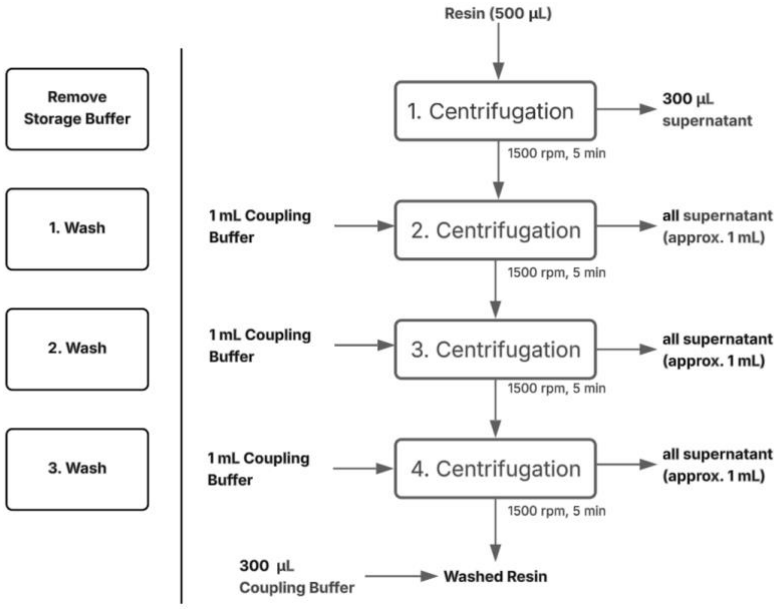

Figure 17: Procedure for washing the resin. First, $500\ \mu L$ of resin was centrifuged and $300\ \mu L$ of storage buffer in the supernatant was removed. For each washing step, 1 mL of coupling buffer was given to allow buffer exchange. At the end of the steps, $300\ \mu L$ of coupling buffer is given back to make the end volume same as the initial volume. The end volume must be 500 μL.

3.6.2 Immobilization Strategies and The Verification

In this thesis, the immobilization conditions were designed and developed based on previous studies conducted by bachelor and master student, Sara Jashari and Marina Lesniewski, as well as discussions with Prof. Dr. Jörg Andrä. Figure 18 represents the core immobilization scheme, which has been optimized based on the development of the experimental results from this thesis. Based on the core immobilization scheme in Figure 18, further four combinations as listed in Table 29 were applied in this thesis. Each combination represents a change in the experimental parameters which is deciding for the immobilization. Combination A and B were varied in the reducing agent. In Combination C, an additional step of separation between peptide and DTT using RP-HPLC were added, the detail for the additional procedures is described below in “Additional Procedures for Combination C”. In Combination D, two new NK-2 derivatives with added linker N- and C-terminus of the peptides were used as sample and two different incubation time were experimented.

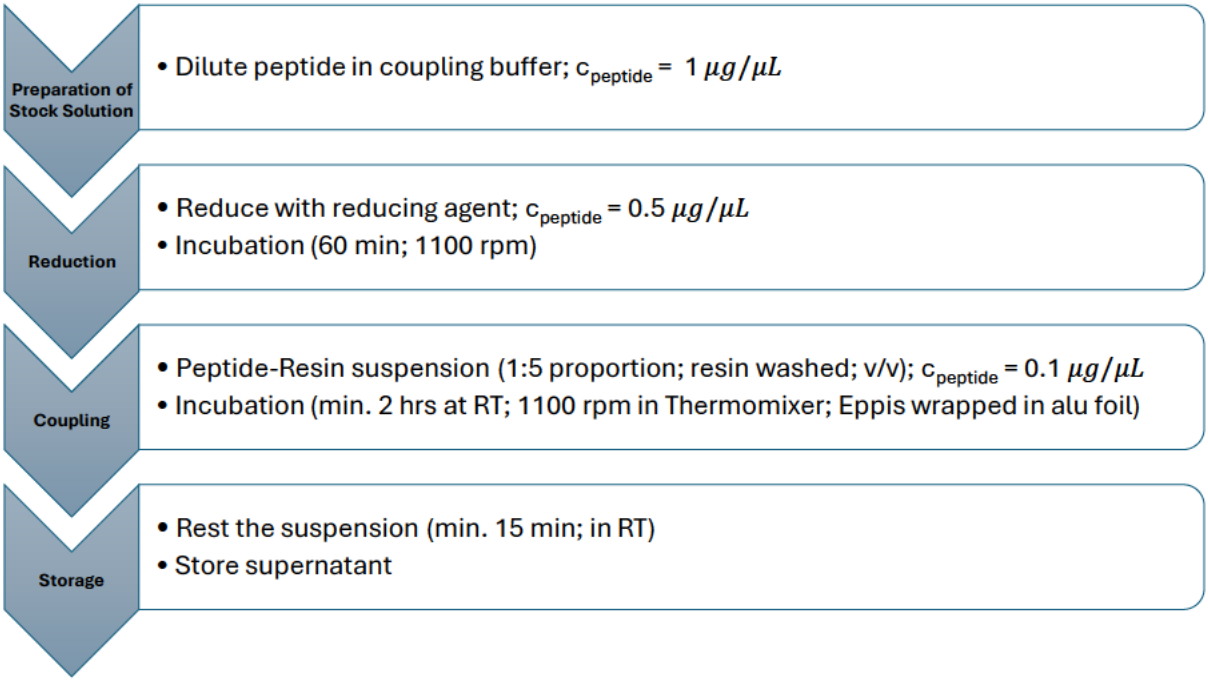

Figure 18: Core immobilization scheme. The immobilization scheme consists of four main step, where first peptide with concentration of 1 $\mu g/\mu L$ need to be prepared in coupling buffer. Coupling buffer were used as medium to provide optimal conditions for the immobilization. Second, the peptide was further diluted in coupling buffer and reduced with reducing agent, end concentration of peptide in this step was 0.5 $\mu g/\mu L$. For the reduction, the peptide was incubated for 60 min at room temperature with shaking at 1100 rpm in a thermomixer. During the coupling step, the reduced peptide solution was mixed with the washed resin in a ratio of 1:5 (v/v), resulting in a final peptide concentration of 0.1 $\mu g/\mu L$. The Eppendorf tubes were wrapped in aluminum foil to prevent iodine-induced reactions that may be triggered by light exposure. The immobilization incubation was carried out for 2 h at room temperature with shaking at 1100 rpm in a thermomixer. After coupling, the suspension was allowed to rest at room temperature for a minimum of 15 min to enable separation of the supernatant from the resin. After this resting period, two distinct phases could be observed in the tubes, the supernatant in upper phase and pellets in lower phase. The supernatant was then collected and stored for subsequent analytical procedures.

Table 29: Combination A, B, C and D of immobilization scheme.

Combination	Peptide	Reducing Agent	RP-HPLC Separation	Incubation Time
A	NK-2 and Ar-1	TCEP (0.2 M)	×	2 hrs
B	NK-2	DTT (0.1 M)	×	2 hrs
C	NK-2 and R007	DTT (0.1 M)	√	2 hrs
D	ALK-33C and N33-ALK	-	×	2 and 24 hrs

Additional Procedures for Combination C

Prior to RP-HPLC, the peptide was reduced with DTT. During the reduction, the peptide was also heated in a thermomixer at 95°C for 5 min. The reduced peptide was then injected into the RP-HPLC at a mass of 50 μg.

The collected fractions from RP-HPLC were first measured using a UV/VIS-spectrophotometer to determine which fraction showed the highest absorption value at 214 nm and to identify the peaks in which the peptide was eluted. For each measurement, the blank value was measured first. Then, 100 μL of the peptide fraction solution was transferred into a quartz cuvette. After each measurement, the peptide solution was returned, and the quartz cuvette was rinsed with water before the next measurement.

Based on the UV/VIS-spectrophotometer results, only the peptide fractions with the highest absorption values were gassed with nitrogen. If more than one fraction showed high absorption values and was close to the retention time of the peaks, the fractions could be pooled prior to nitrogen gassing. Preferably, no more than two fractions should be pooled, as pooling can dilute the peptide and thus lower its concentration.

Next, the pooled fractions were pipetted into Eppendorf tubes. The Eppendorf tubes were then placed into test tubes. Care was taken to ensure that the Eppendorf tubes fit securely in the test tubes to prevent tipping. The solution was gassed with nitrogen for approximately 30 min or until the acetonitrile was completely removed. The amount of acetonitrile present in the solution depends on the gradient elution of acetonitrile during RP-HPLC.

Verification and Analysis of Immobilization Results

To verify and evaluate whether the immobilization was successful, the supernatant and pellet of the immobilized peptide were further analyzed by SDS-PAGE, RP-HPLC and trypsin digestion, as shown in Figure 19.

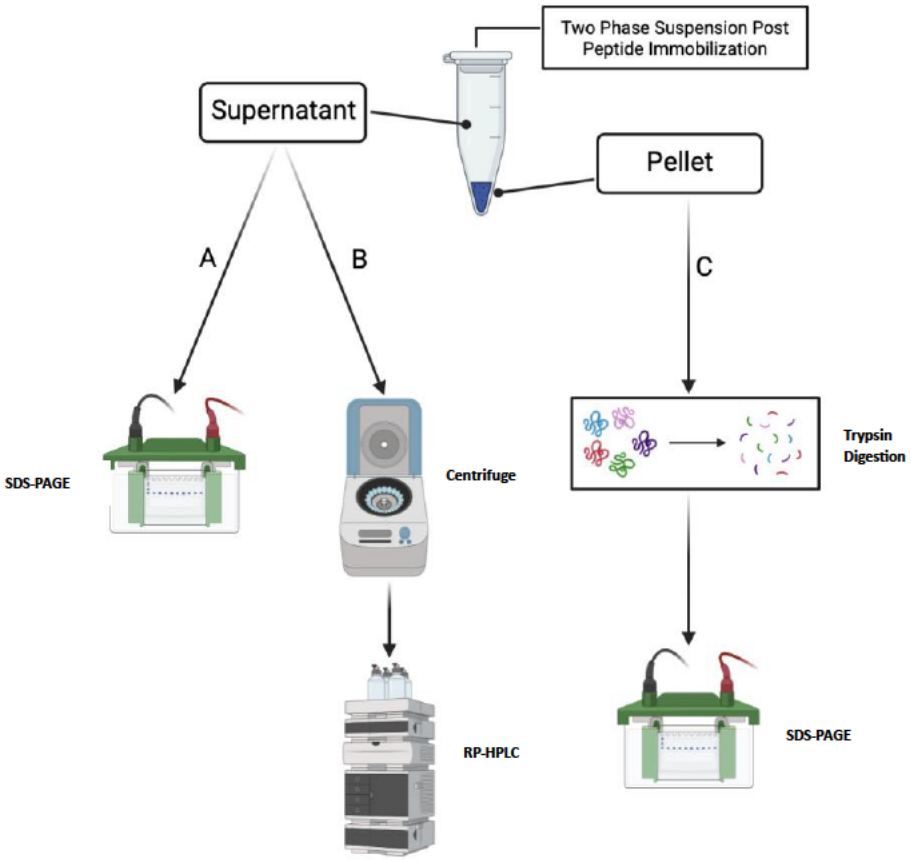

Figure 19: Verification and evaluation of immobilization results. Figure shows post immobilization where two phase suspension consists of upper and lower phase were formed. The supernatant in **(A)** was analyzed with SDS-PAGE and in **(B)** was centrifuged before further analyzed with RP-HPLC. In **(C)** the pellets were first treated with trypsin digestion and then further analyzed with SDS-PAGE. Figure created with BioRender.

For the verification and analysis of the supernatant, SDS-PAGE was applied, as shown in Figure 19A. The supertanant was treated under the conditions described in Table 30.

Table 30: Listed are the conditions applied for the supernatant of immobilized peptide for the SDS-PAGE.

Condition	Treatment
1	Peptide reduced, immobilized in resin
2	Peptide reduced, immobilized in coupling buffer (resin replaced by coupling buffer)
3	Peptide not reduced, immobilized in resin
4	Peptide not reduced, immobilized in coupling buffer (resin replaced by coupling buffer)
5	Peptide reduced, not immobilized

Figure 19B shows the verification and analysis of the supertanant with RP-HPLC. The samples were prepared as described in chapter 3.4.2 – "Sample Preparation Prior to RP-HPLC Run". However, when working with supernatants of immobilized peptides in which agarose resin is present, the samples must be centrifuged and only the supernatant collected after centrifugation. For example, if the total sample volume is 50 μL, only the upper 10-15 μL should be taken, while the remaining volume is considered the pellet containing the resin. The presence of resin can lead to clogging of the chromatographic column and reduce its lifespan.

Figure 19C shows the verification and analysis of the pellet using trypsin digestion. The following experimental procedure was applied. The pellet obtained after immobilization was filled with coupling buffer to a final volume of 500 μL and gently shaken horizontally. The suspension was allowed to rest for approximately 10 to 15 min at room temperature until two phases formed. Then, 50 μL of the pellet supernatant was taken as the initial solution without trypsin. Subsequently, 2 μL of trypsin (1 mg/mL) was added to the pellet supernatant and vortexed. Samples of 50 μL were taken at time points t_0, t_{30} and t_{60}. All samples were prepared following the same procedure described in Chapter 3.4.5 – "Trypsin Digestion". The prepared samples were then further analyzed by SDS-PAGE.

4. Results

In this Chapter, the results from the experiment are presented.

4.1 Development and Optimization of Experimental Procedures

Prior to the experiment, few parameters were tested to perform a preliminary investigation.

4.1.1 Optimization of SDS-PAGE

Comparison of DTT and TCEP as Reducing Agent

Figure 20 shows the results of peptide NK-2 and Ar-1 (R007) from the preliminary investigation, in which both peptides were prepared in unreduced and reduced forms. DTT and TCEP were used as reducing agents. For DTT, a concentration of 0.1 M was applied, while for TCEP, concentrations of 0.2 M and 0.4 M were applied. All peptides loaded on the gels were prepared at a mass of 0.5 μg. The results show that DTT has a significant stronger reducing effect than TCEP.

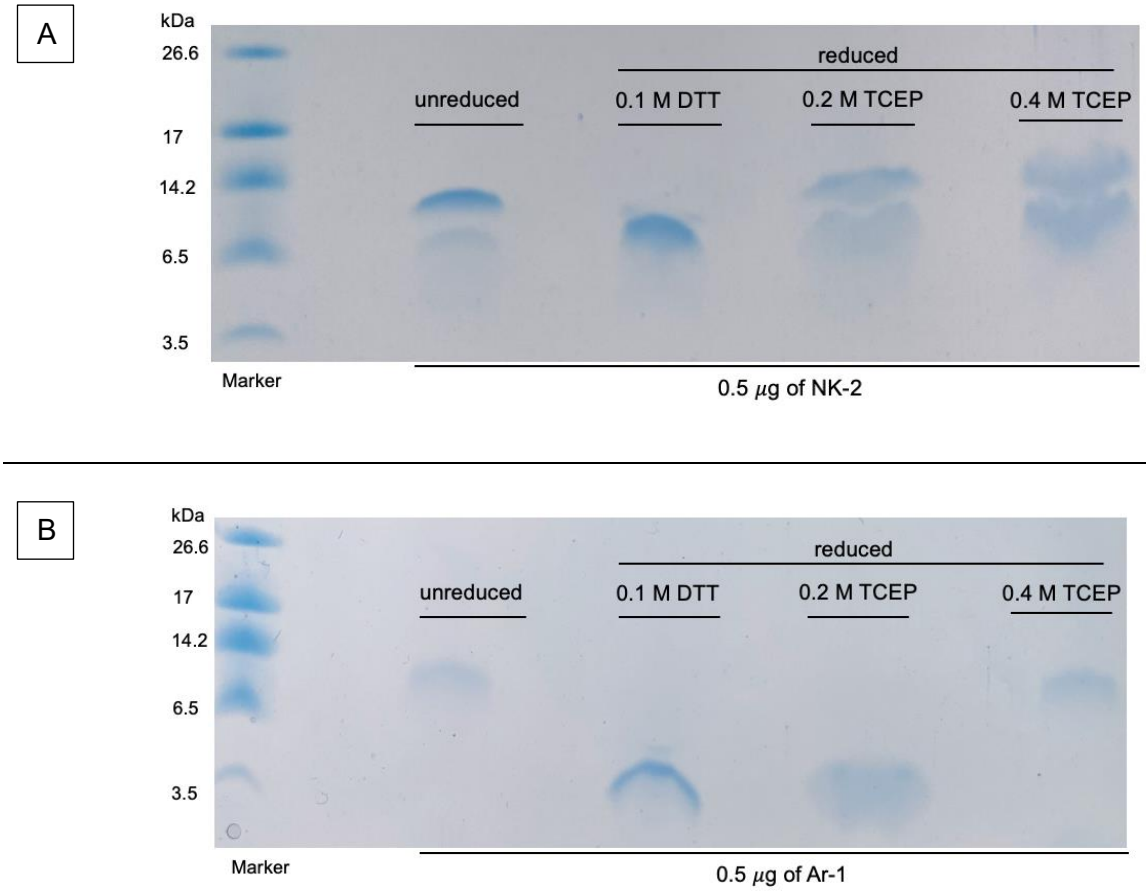

Figure 20: Comparison of DTT and TCEP as reducing agent. (A) Peptide NK-2 as sample. **(B)** Peptide Ar-1 as sample. Each gel lane was loaded with 0.5 μg of peptide. DTT was added with concentration of 0.1 M. TCEP was added with concentration of 0.2 M and 0.4 M.

Comparison of Boric Acid and Sodium Carbonat as Fixative Solution for SDS-PAGE

Figure 21 shows the results of Tricine-SDS-PAGE for 1 μg of NK-2 and Ar-1 (R007), in which the gels were fixed using two different fixative solutions. Boric acid and sodium carbonate were applied as fixative solutions. Both peptides were prepared under reduced conditions using DTT and TCEP as reducing agents. The concentrations of both reducing agents ranged from 10 mM to 50 mM. Compared to boric acid, the gels fixated with sodium carbonate show bolder bands with less artefacts.

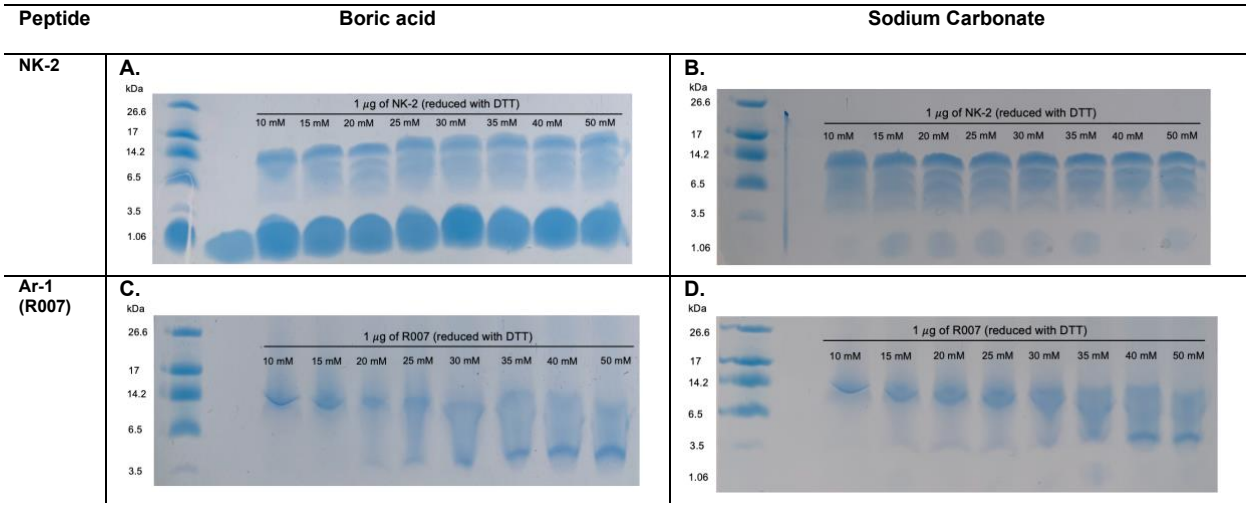

Figure 21: Comparison of boric acid and sodium carbonate as fixative solution. Peptide NK-2 and Ar-1 were used as samples. (A) and (C) were fixed with boric acid. (B) and (D) were fixed with sodium carbonate.All peptides were reduced with increasing DTT concentration, ranging from 10 mM to 50 mM. The peptide mass in each gel lane was 1 μg.

4.1.2 Preparation and Conditioning of RP-HPLC Column

Conditioning of New Chromatography Column

Prior to use, the C18 chromatographic column was prepared and conditioned. The four-step method was applied as described in Chapter 3.4.2 in Subchapter “Column Preparation and Conditioning”. Figure 22 presents the results of the preparation and conditioning of the chromatographic column. The results in Figure 22 shows that the column has been successfully conditioned and prepared with the four steps method.

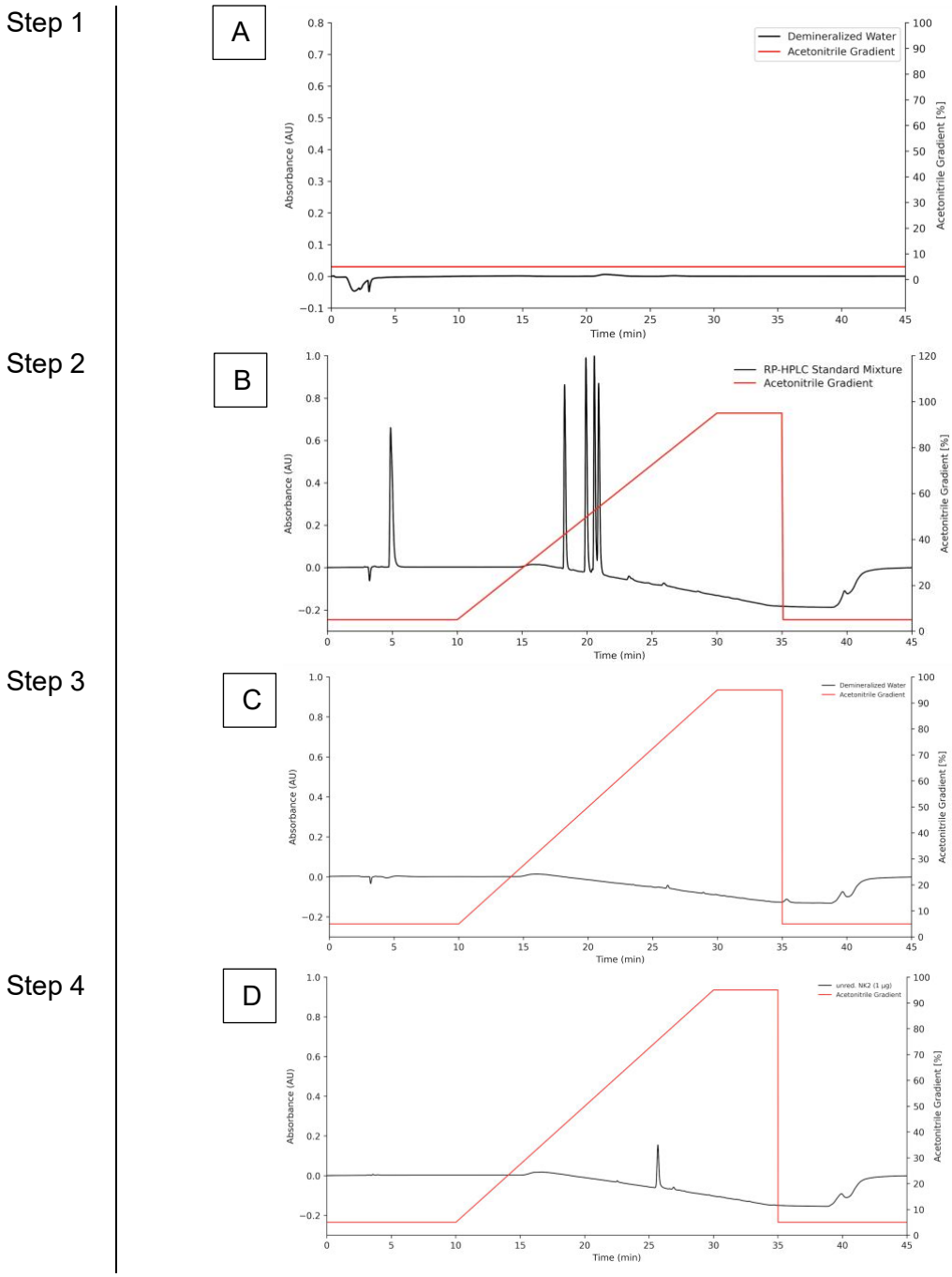

Figure 22: Conditioning of new chromatography column. Figure shows that the chromatographic column was prepared with four step methods. **(A)** In Step 1, dem. Water was injected and a flat line absorption line was observed. **(B)** In Step 2, the RP-HPLC standard mixture was injected, four peaks were detected in the chromatogram. **(C)** In Step 3, dem. Water was injected again and a flat line was also observed. **(D)** In Step 4, the unreduced NK-2 was injected and one peak was detected.

Before and After Idle Condition

Figure 23 presents the chromatograms of the column condition before and after 3.5 weeks of idle time. The column was injected with an HPLC standard at a concentration of 2 $\mu g/\mu L$. The procedure used was as described in Chapter 3.4.2 in Subchapter “Column Preparation and Conditioning”. It was expected that the column would deliver comparable results before and after the idle period.

Figure 23A shows the chromatogram obtained before 3.5 weeks of idle time, in which a total of five peaks were detected. Figures 23B and 23C represent the chromatograms obtained after 3.5 weeks of idle time, performed with injection volumes of 20 μL and 40 μL, respectively. The retention times of the detected peaks are listed in Table 31. The results shows that the column delivered the same results before and after idle condition.

Before Idle

A

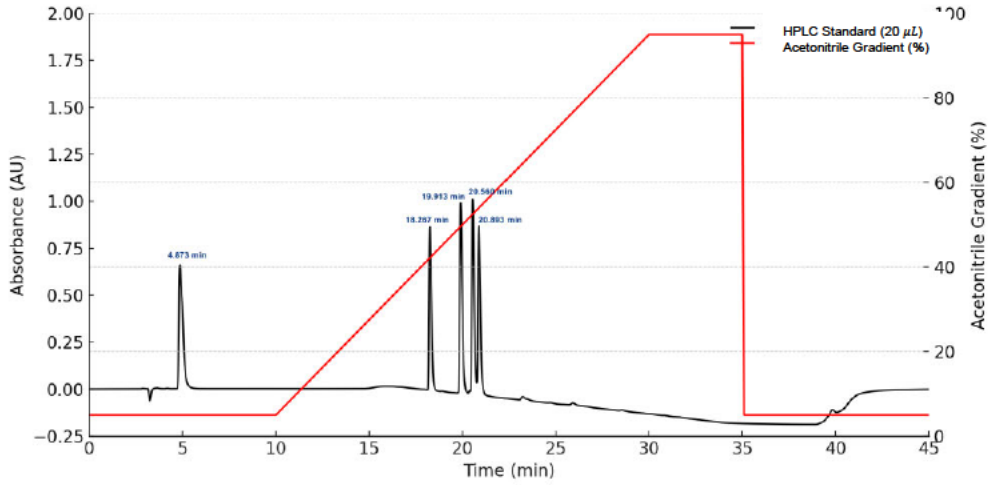

After Idle

B

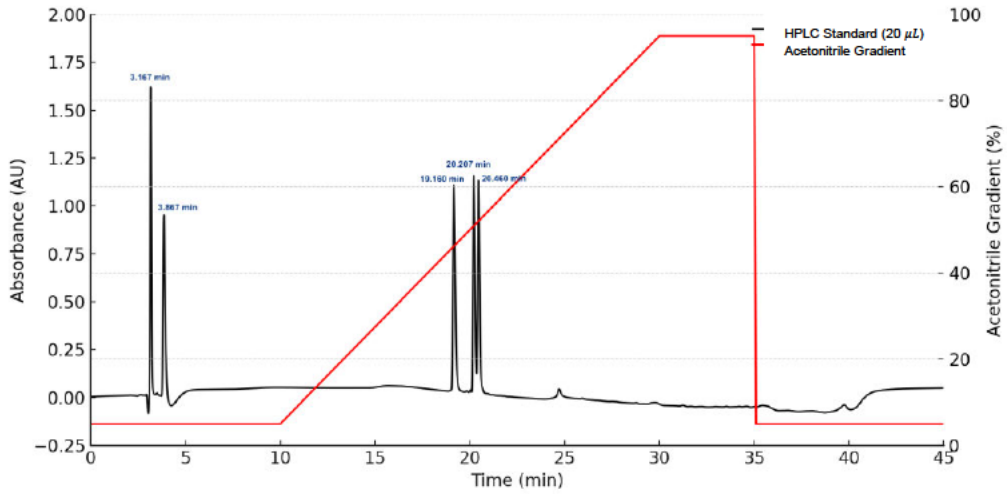

C

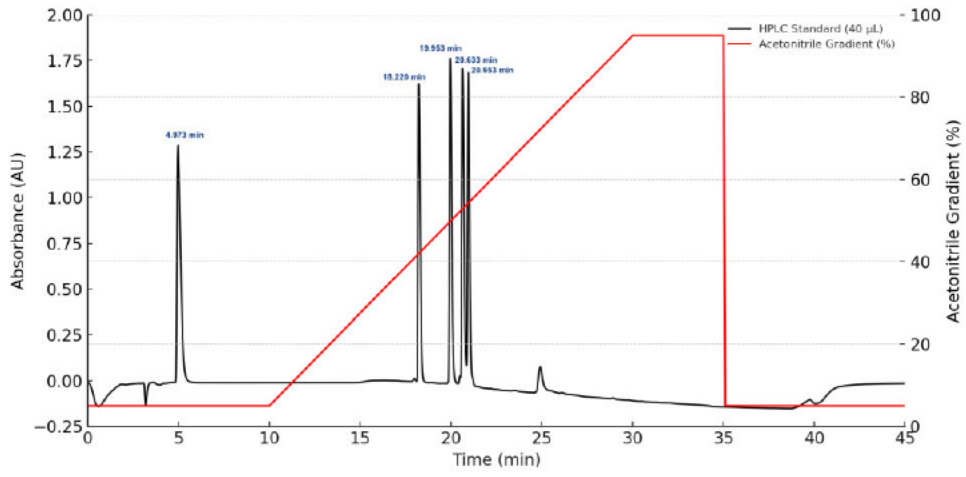

Figure 23: RP-HPLC Chromatogram of HPLC standard mixture. (A) The chromatogram was taken before 3.5 weeks idle with injection volume of 20 µL. **(B)** and **(C)** The chromatogram was taken after 3.5 weeks idle. The injection volume used was 20 and 40 µL. The HPLC standard has prepared with concentration of 2 $\mu g/\mu L$.

Table 31: Retention Time of HPLC Standard mixture.

RP-HPLC Run	Injection Volume [µL]	Retention Time [min]				
		First Peak	Second Peak	Third Peak	Fourth Peak	Fifth Peak
Before Idle	20	4.873	18.267	19.913	20.560	20.893
After Idle	20	3.167	3.867	19.160	20.207	20.460
	40	4.973	18.220	19.953	20.633	20.953

4.1.3 Trypsin Digestion

Investigation of Peptide-to-Trypsin Ratio

An investigation to determine the optimal peptide-to-trypsin ratio was performed prior to trypsin digestion. The results are presented in Figure 24, in which peptides ALK-33C and N33-ALK were used as samples and peptide-to-trypsin ratios of 50:1, 100:1 and 500:1 (w/w) were investigated. The method applied was as described in Chapter 3.4.5 – "Trypsin Digestion". The peptide to trypsin ration of 50:1 shows the boldest bands of peptides fragments compared to the other.

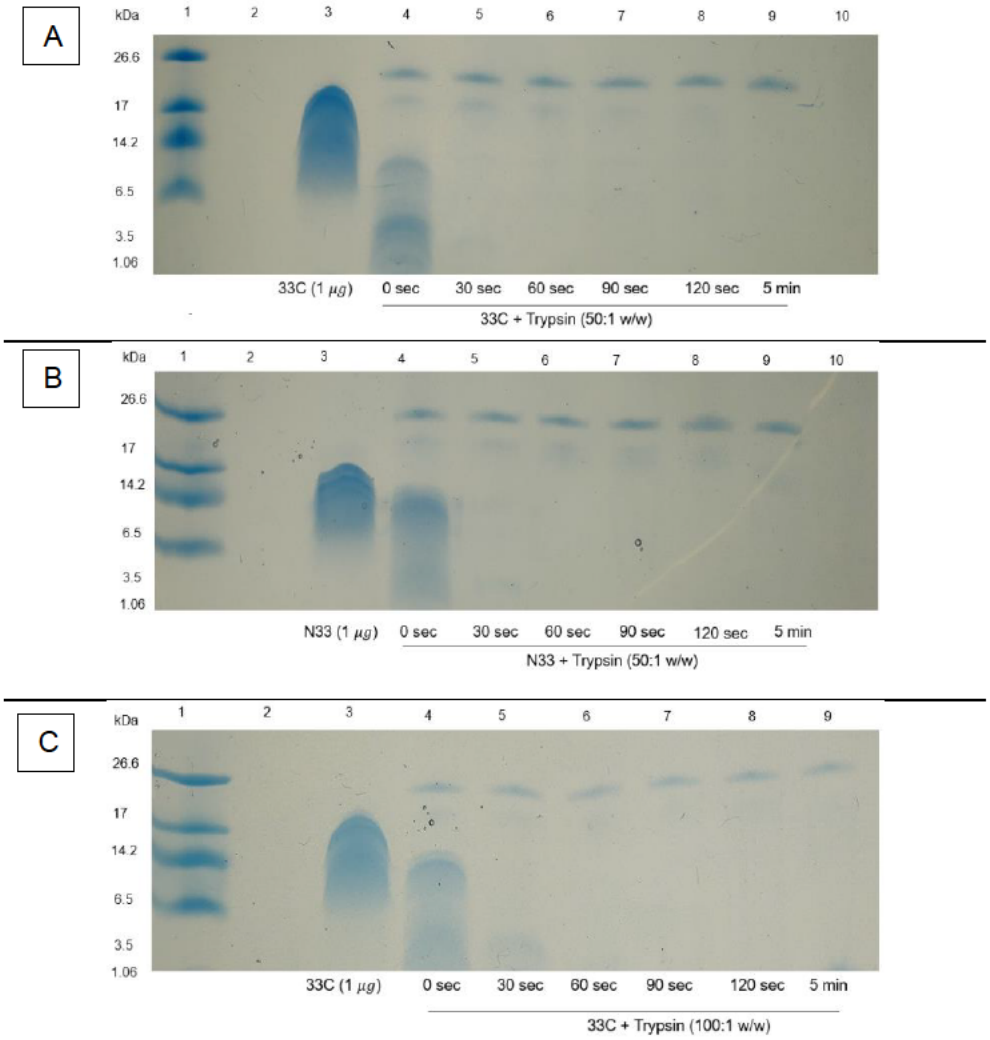

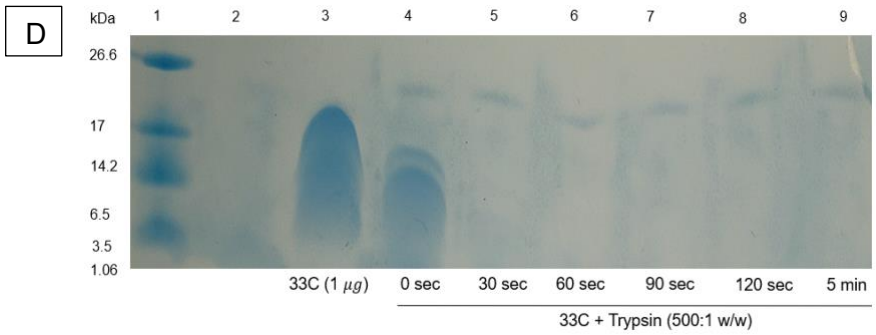

Figure 24: Investigation of peptide-to-trypsin ratio. Figures 24A to 24D show results of SDS-PAGE gels of peptides ALK-33C and N33-ALK at peptide-to-trypsin ratio of 50:1, 100:1 and 500:1 (w/w). In gel pocket 3, 1 μg of each peptide was loaded. In gel pocket 4 to 9, the digested peptides are shown with increasing digestion time ranging from 0 second to 5 minutes.

4.2 Peptide Characterization

In the following section, the results from SDS-PAGE gels and chromatograms of peptide characterization are presented. The results are divided into two subchapters, the first Subchapter 4.2.1 – "NK-2 and Derivatives" presents results from NK-2 and its derivatives, and the second Subchapter 4.2.2 – "Ar-1 and Derivatives" presents results from Ar-1 and its derivatives.

4.2.1NK-2 and Derivatives

Peptide NK-2

Figure 25 shows the results of the characterization of peptide NK-2. Figure 25A represents unreduced NK2 and Figure 25B represents reduced NK-2 (with 0.1 M DTT). In comparison to the chromatogram of unreduced NK-2 shown in Figure 25C, which displays two peaks at retention times of 22.453 min at a 60% acetonitrile gradient and 25.573 min at 70% acetonitrile gradient, only one peaks was detected in the chromatogram of reduced NK-2 (Figure 25D). This peak eluted at 22.3 min with an acetonitrile gradient of 60%.

As shown in Figures 25E and 25F, the absorbance of the quantity-dependent peak increased after reduction of NK-2, while the second peak at retention time of approximately 25 min was no longer detected in Figure 25F. It can therefore be assumed that the reduction of NK-2 led to a conformational change from dimer into monomer. Overall, the characterization of NK-2 has been successfully performed. Different characteristic of unreduced and reduced NK-2 was observed in the experiment results.

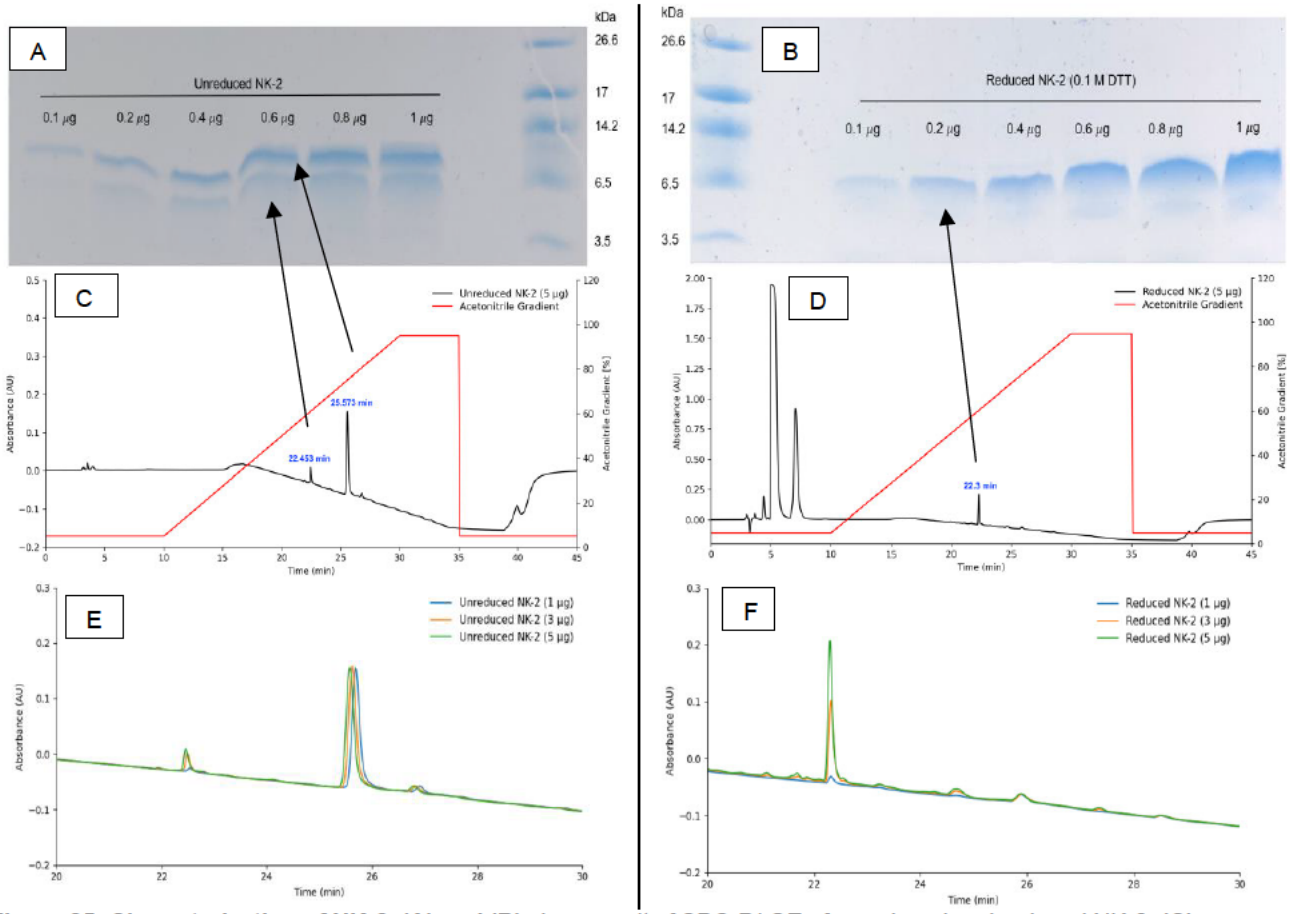

Figure 25: Characterization of NK-2. (A) and (B) show result of SDS-PAGE of unreduced and reduced NK-2. **(C)** and **(D)** show RP-HPLC chromatogram of unreduced and reduced NK-2, peptide mass injected was 5 μg. **(E)** and **(F)** shows the chromatogram of unreduced and reduced NK-2 which are plotted in increasing peptide mass of 1, 3 and 5 μg ($C_{peptides}$ = 0.1 $\mu g/\mu L$; injection volume 10, 30 and 50 μL).

Table 32: Overview of retention time for unreduced and reduced NK-2.

Peptide Mass of Unreduced NK-2 [µg]	Retention Time – First Peak [min]	Retention Time – Second Peak [min]	Peptide Mass of Reduced NK-2 [µg]	Retention Time [min]
1	22.533	25.687	**1**	22.32
3	22.487	25.620	**3**	22.32
5	22.453	25.573	**5**	22.30

Peptide NK27 (C7S)

Figure 26 shows the results of the characterization of NK27. The unreduced NK27 displays two bands at 14.2 kDa and 6.5 kDa (Figure 26A), whereas the reduced NK27 (Figure 26B) shows a band at 1.06 kDa and an additional upper band at 3.5 kDa, which is weaker than the lower band detected at peptide masses of 0.6 to 1 μg of peptide mass. It was observed that, upon reduction of the peptide, the bands shifted towards a lower molecular weight range.

The RP-HPLC chromatograms of both unreduced and reduced NK27 showed similar chromatographic profiles, with two peaks detected at retention times of approximately 22.8 min and 25.3 min retention time (Figure 26C and 26D). The first peak eluted at 60% acetonitrile gradient, while the second peak eluted at a 75% acetonitrile gradient. As shown in Figures 26E and 26F, the first peak exhibited quantity-dependent behavior, with higher peptide masses resulting in higher absorbance value. Overall, peptide NK27 has been successfully characterized. Different characteristics were observed from the unreduced and reduced Ar-1.

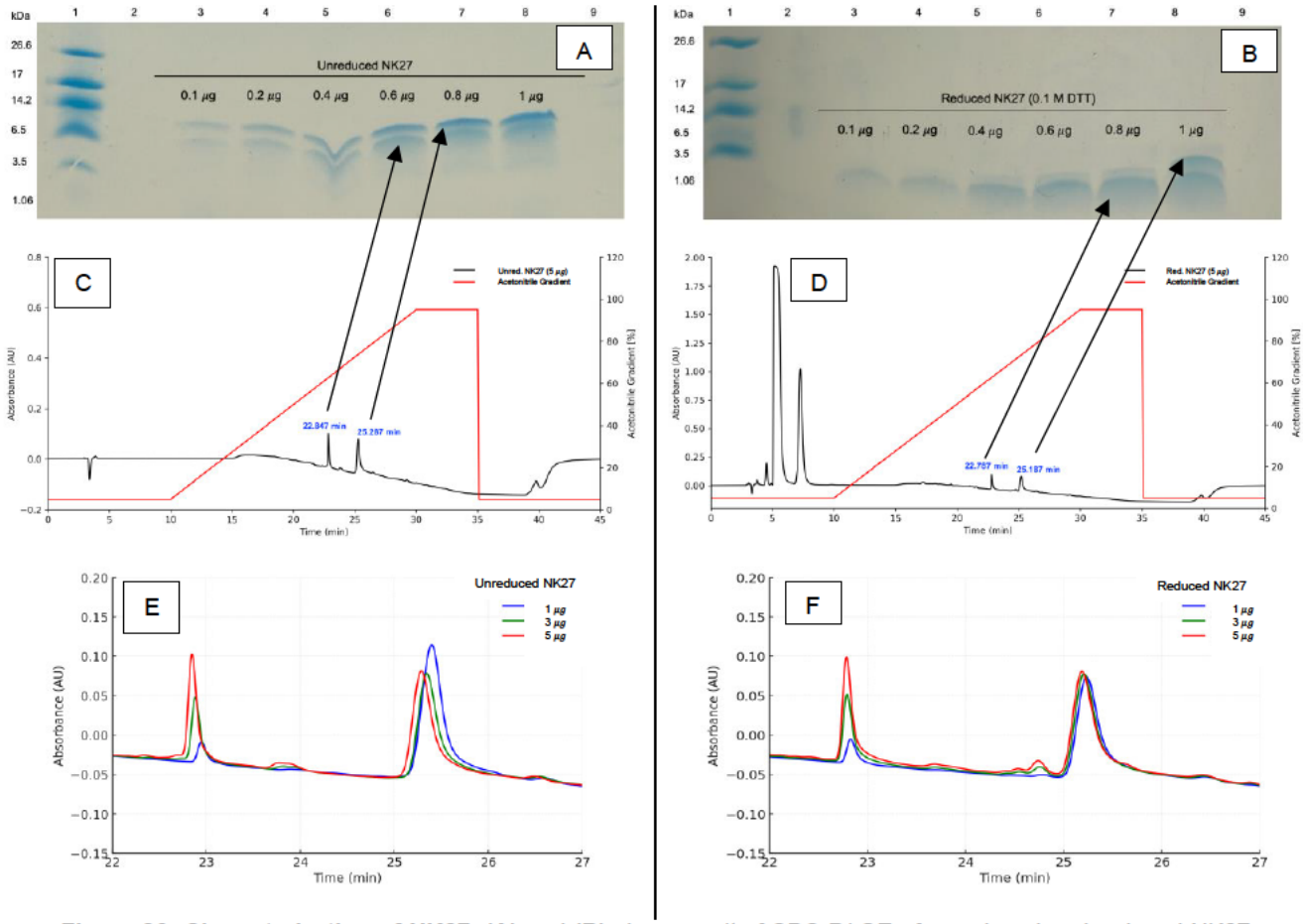

Figure 26: Characterization of NK27. (A) and **(B)** show result of SDS-PAGE of unreduced and reduced NK27. **(C)** and **(D)** show RP-HPLC chromatogram of unreduced and reduced NK27, peptide mass injected was 5 μg. **(E)** and **(F)** shows the chromatogram of unreduced and reduced NK27 which are plotted in increasing peptide mass of 1, 3 and 5 μg ($C_{peptides}$ = 0.1 $\mu g/\mu L$; injection volume 10, 30 and 50 μL).

Table 33: Overview of retention time for unreduced and reduced NK27.

Peptide Mass of Unreduced NK27 [µg]	Retention Time – First Peak [min]	Retention Time – Second Peak [min]	Peptide Mass of Reduced NK27 [µg]	Retention Time – First Peak [min]	Retention Time – Second Peak [min]
1	22.947	25.393	**1**	22.827	25.233
3	22.887	25.340	**3**	22.793	25.207
5	22.847	25.287	**5**	22.787	25.187

Peptide ALK-33C

Figure 27 presents the results of the characterization of ALK-33C. The SDS-PAGE results of both unreduced and reduced 33C show a single band at 14.2 kDa (Figure 27A). The chromatograms shown in Figure 27B and 27C also display similar chromatographic profiles, with only one peak detected at a retention time of approximately 25.7 min. Furthermore, the peaks do not exhibit quantity-dependent behavior (Figures 27D and 27E), as all peaks show absorbance value of approximately 0.4 AU despite increasing peptide mass. It can therefore be concluded that the addition of a reducing agent did not have an observable effect on the conformation of the peptide ALK-33C. The overview of the retention time is presented in Table 34. Overall, the peptide ALK-33C has been successfully characterized. Similar characteristics were observed in both unreduced and reduced ALK-33C.

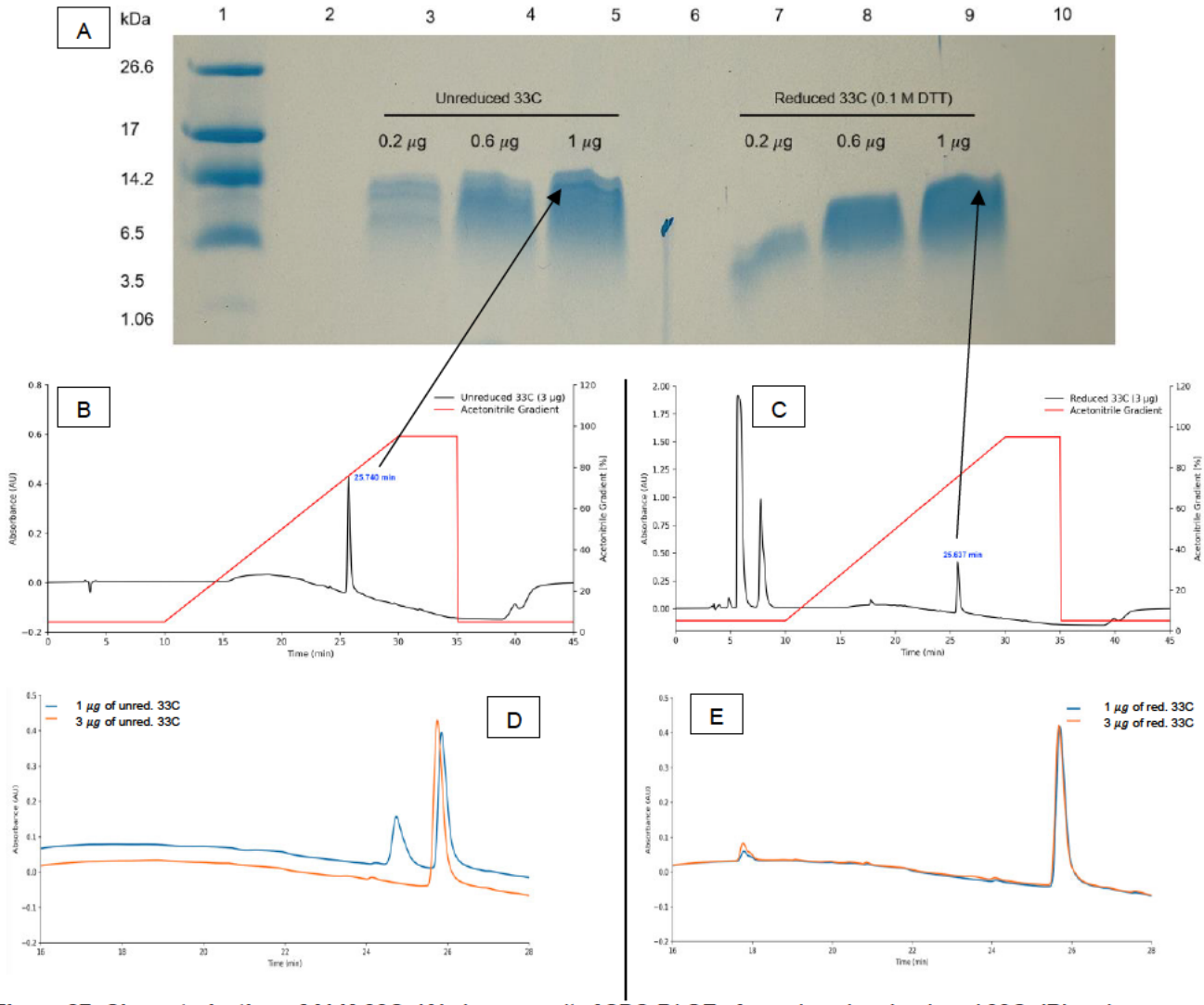

Figure 27: Characterization of ALK-33C. (A) shows result of SDS-PAGE of unreduced and reduced 33C. **(B)** and **(C)** show RP-HPLC chromatogram of unreduced and reduced 33C, peptide mass injected was 3 μg. **(D)** and **(E)** shows the chromatogram of unreduced and reduced NK-2 which are plotted in increasing peptide mass of 1 and 3 μg ($C_{peptides}$ = 0.1 $\mu g/\mu L$; injection volume 10 and 30 μL).

Table 34: Overview of retention time for unreduced and reduced ALK-33C.

Peptide Mass of Unreduced 33C [µg]	Retention Time [min]	Peptide Mass of Reduced 33C [µg]	Retention Time [min]
1	25.840	**1**	25.700
3	25.740	**3**	25.637

Peptide N33-ALK

Figure 28 shows the results of the characterization of N33-ALK. The SDS-PAGE results of unreduced and reduced N33-ALK are presented in Figure 28A. The unreduced N33-ALK shows one bands at a peptide mass of 0.2 μg. However, the bands at 0.6 and 1 μg peptide mass were smeared and therefore not realiable for analysis. The reduced N33-ALK also shows a single band at 6.5 kDa across the tested peptide mass.

Figures 28B and 28C show the RP-HPLC chromatograms of unreduced and reduced N33-ALK. In both chromatograms, only one peak was detected, which eluted after 25 min at 70% acetonitrile gradient. Figures 28D and 28E illustrate the quantity-dependent behavior of unreduced N33-ALK and non-quantity-dependent behavior of reduced N33-ALK. Both peptide masses of 1 and 3 μg showed a similar retention times with slight deviations (Table 35). Overall, the peptide N33-ALK has been successfully characterized. Similar characteristics were shown by both unreduced and reduced N33-ALK.

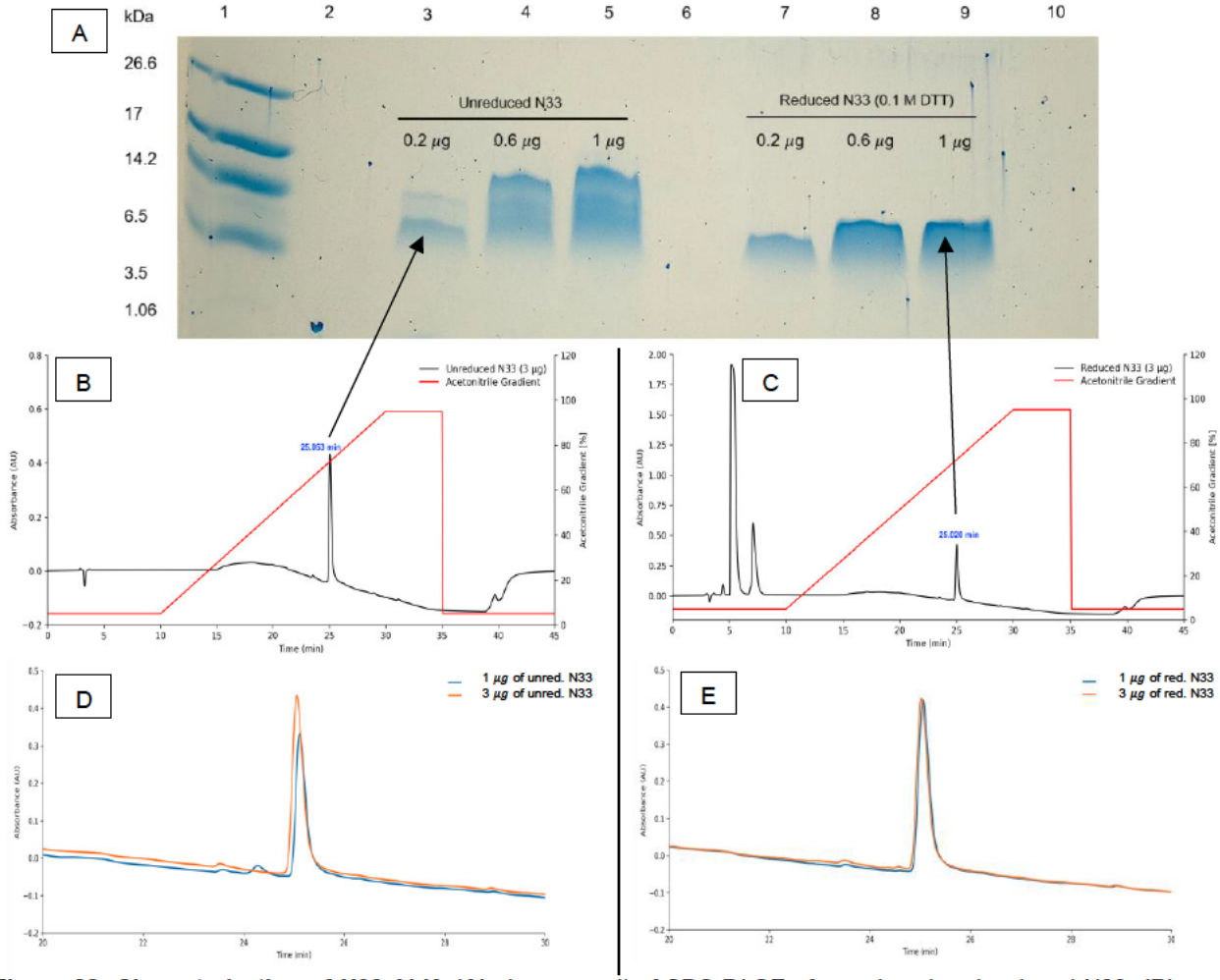

Figure 28: Characterization of N33-ALK. (A) shows result of SDS-PAGE of unreduced and reduced N33. **(B)** and **(C)** show RP-HPLC chromatogram of unreduced and reduced N33, peptide mass injected was 3 μg. **(D)** and **(E)** shows the chromatogram of unreduced and reduced NK-2 which are plotted in increasing peptide mass of 1 and 3 μg ($C_{peptides}$ = 0.1 $\mu g/\mu L$; injection volume 10 and 30 μL).

Table 35: Overview of retention time for unreduced and reduced N33-ALK.

Peptide Mass of Unreduced. N33 [µg]	Retention Time [min]	Peptide Mass of Reduced N33 [µg]	Retention Time [min]
1	25.113	**1**	25.053
3	25.053	**3**	25.020

4.2.2 Ar-1 and Derivatives

Peptide Ar-1

Figure 29 presents the results of the characterization of peptide Ar-1. The SDS-PAGE gels of unreduced and reduced Ar-1 each show one band at 14.2 kDa and 3.5 kDa, respectively (Figures 29A and 29B). Upon reduction of Ar-1 with 0.1 M DTT, the bands shifted toward a lower molecular weight range.

The RP-HPLC results show retention times of 20.793 min at 55% CAN and 25.0 min at 70% ACN for unreduced Ar-1 (Figure 29C), and elution times of 21.110 min at 57% ACN and 22.350 min at 60% ACN for reduced Ar-1 (Figure 29D). Following reduction of Ar-1, the first peak of unreduced Ar-1 eluted later, while the second peak eluted earlier. All peaks exhibited quantity-dependent behavior, except for the second peak of unreduced Ar-1 (see Figures 29E and 29F). The overview of the retention time is presented in Table 36. Overall, peptide Ar-1 has been successfully characterized. Different characteristics of unreduced and reduced Ar-1 was observed in the experiment results.

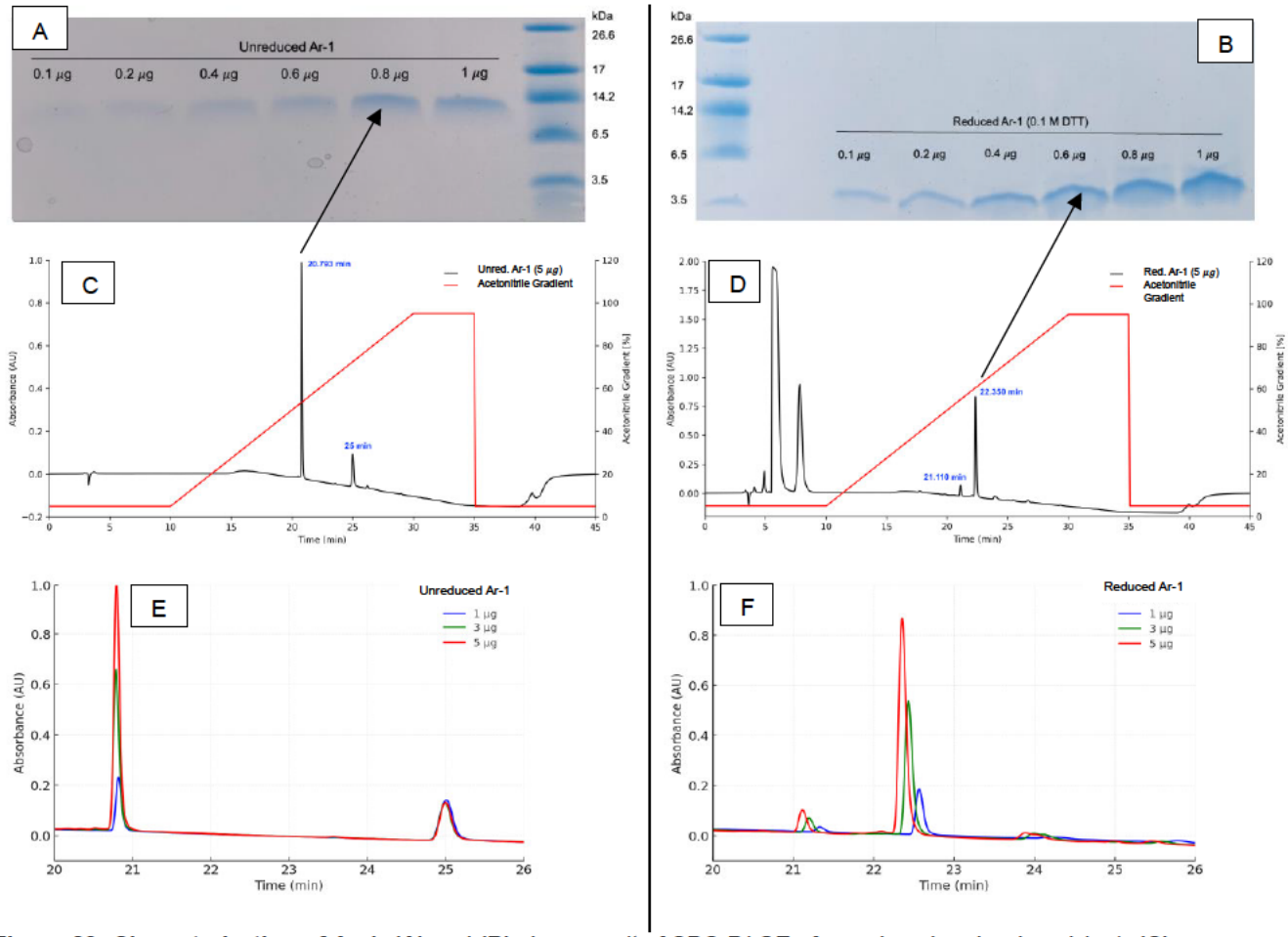

Figure 29: Characterization of Ar-1. (A) and **(B)** show result of SDS-PAGE of unreduced and reduced Ar-1. **(C)** and **(D)** show RP-HPLC chromatogram of unreduced and reduced Ar-1, peptide mass injected was 5 μg. **(E)** and **(F)** shows the chromatogram of unreduced and reduced Ar-1 which are plotted in increasing peptide mass of 1, 3 and 5 μg ($C_{peptides}$ = 0.1 $\mu g/\mu L$; injection volume 10, 30 and 50 μL).

Table 36: Overview of retention time for unreduced and reduced Ar-1.

Peptide Mass of Unred. Ar-1 [µg]	Retention Time – First Peak [min]	Retention Time – Second Peak [min]	Peptide Mass of Red. Ar-1 [µg]	Retention Time – First Peak [min]	Retention Time – Second Peak [min]
1	20.820	25.007	**1**	21.33	22.56
3	20.787	24.993	**3**	21.19	22.43
5	20.793	25.000	**5**	21.11	22.35

Peptide C/S-Ar-1 (S008)

Figure 30 presents the results of SDS-PAGE and RP-HPLC chromatograms for the characterization of peptide C/S-Ar-1 (S008). The SDS-PAGE results of both unreduced and reduced C/S-Ar-1 show similar profiles, with only one band detected at 3.5 kDa (Figures 30A and 30B). The RP-HPLC chromatograms of unreduced and reduced C/S-Ar-1 show a single peak eluting at 21.533 min at 57% acetonitrile (ACN) (Figure 30C) and at 21.827 min at 60% ACN, respectively. Both detected peaks exhibited quantity-dependent behavior (Figures 30D and 30E). The overview of the retention time are presented in Table 37.

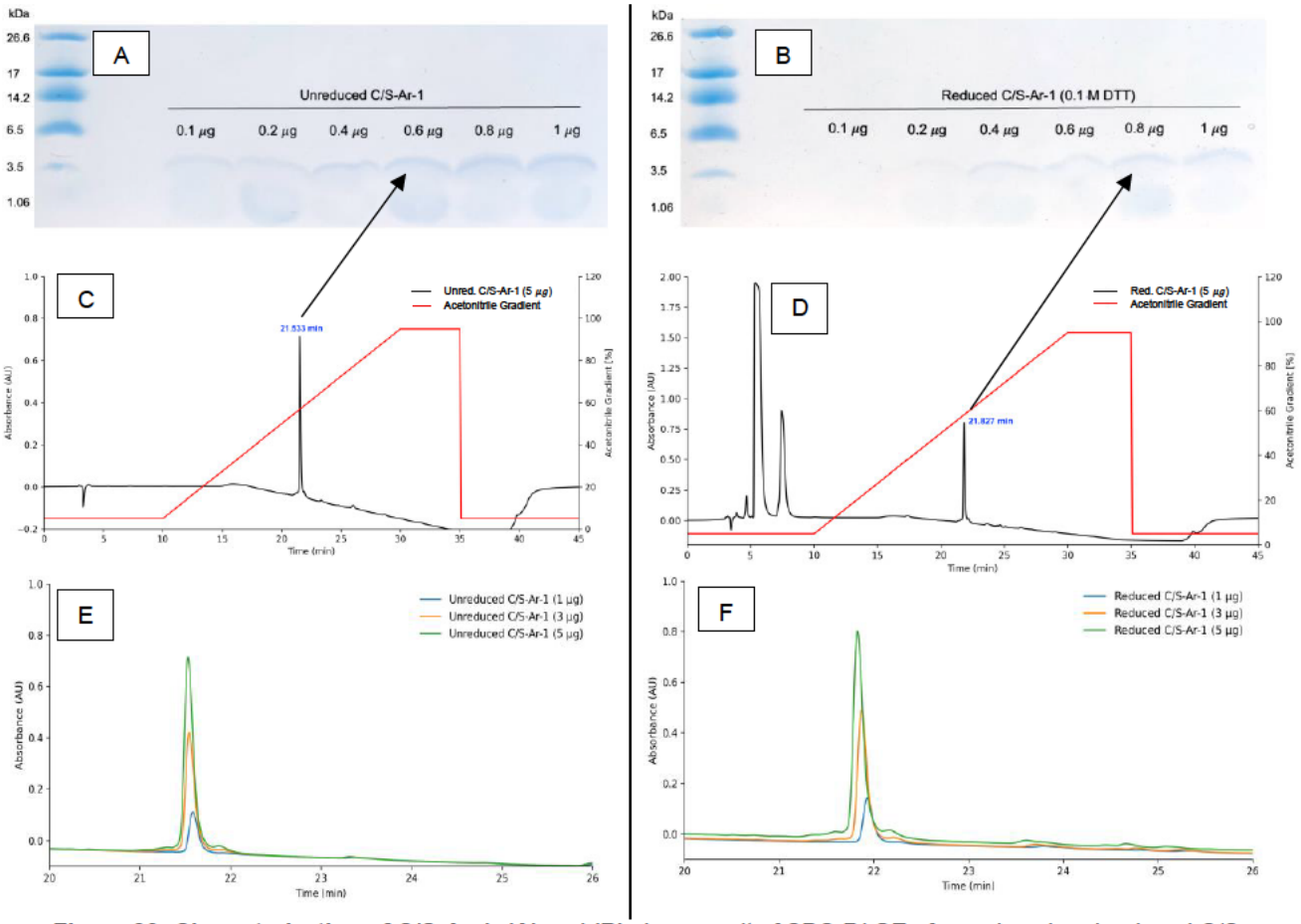

Figure 30: Characterization of C/S-Ar-1. (A) and **(B)** show result of SDS-PAGE of unreduced and reduced C/S-Ar-1. **(C)** and **(D)** show RP-HPLC chromatogram of unreduced and reduced C/S-Ar-1, peptide mass injected was 5 μg. **(E)** and **(F)** shows the chromatogram of unreduced and reduced NK-2 which are plotted in increasing peptide mass of 1, 3 and 5 μg ($C_{peptides}$ = 0.1 $\mu g/\mu L$; injection volume 10, 30 and 50 μL).

Table 37: Overview of retention time for unreduced and reduced C/S-Ar-1.

Peptide Mass of Unreduced C/S-Ar-1 [µg]	Retention Time [min]	Peptide Mass of Red. C/S-Ar-1 [µg]	Retention Time [min]
1	21.587	**1**	21.933
3	21.547	**3**	21.873
5	21.533	**5**	21.827

Peptide R/K-Ar-1 (K009)

Figure 31 presents the results of the characterization of peptide R/K-Ar-1 (K009). The SDS-PAGE gels of unreduced and reduced R/K-Ar-1 show bands at 6.5 kDa and 3.5 kDa,

respectively (Figures 31A and 31B). Upon reduction of R/K-Ar-1 with 0.1 M DTT, the bands shifted toward a lower molecular weight range.

The RP-HPLC results show retention times of 20.693 min at 55% ACN and 25.072 min at 77% ACN for unreduced R/K-Ar-1 (Figure 31C), and elution times of 20.527 min at 57% ACN and 21.647 min at 60% ACN for reduced R/K-Ar-1 (Figure 31D). Following reduction of R/K-Ar-1, the first peak at approximately 20.6 min showed a decreased absorbance value in the chromatogram of reduced R/K-Ar-1, while a new peak appeared at 21.647 min. The second peak of unreduced R/K-Ar-1 at approximately 25 min was no longer detected in the chromatogram of reduced R/K-Ar-1. All peaks exhibited quantity-dependent behavior (Figures 31E and 31F), except for the peak at approximately 25 min in the unreduced R/K-Ar-1 chromatogram (Figure 31C). The overview of the retention time is presented in Table 38. Overall, the peptide R/K-Ar-1 has been successfully characterized. Different characteristics were observed in the unreduced and reduced R/K-Ar-1.

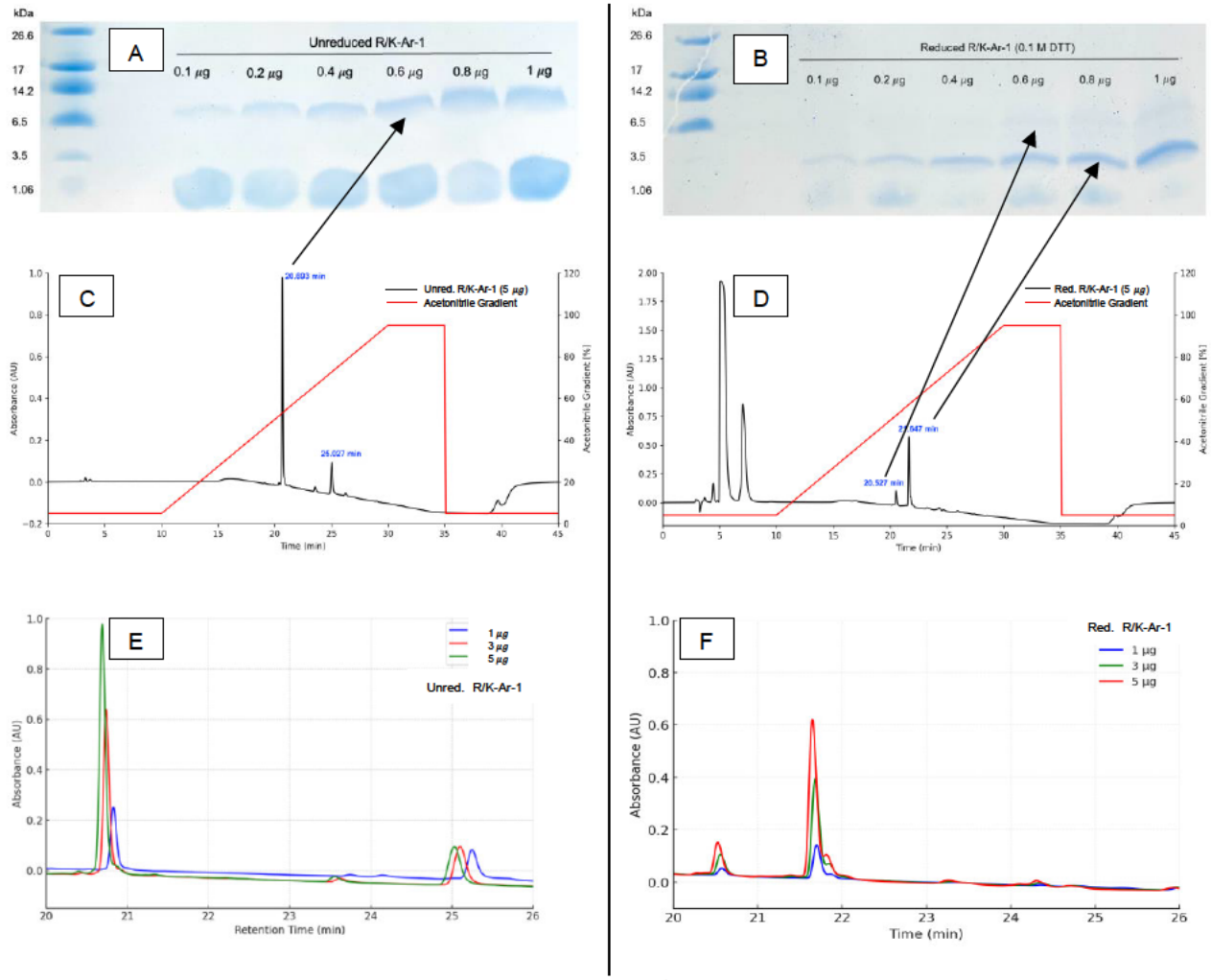

Figure 31: Characterization of R/K-Ar-1. (A) and **(B)** show result of SDS-PAGE of unreduced and reduced R/K-Ar-1. **(C)** and **(D)** show RP-HPLC chromatogram of unreduced and reduced R/K-Ar-1, peptide mass injected was 5 μg. **(E)** and **(F)** shows the chromatogram of unreduced and reduced NK-2 which are plotted in increasing peptide mass of 1, 3 and 5 μg ($C_{peptides}$ = 0.1 $\mu g/\mu L$; injection volume 10, 30 and 50 μL).

Table 38: Overview of retention time for unreduced and reduced R/K-Ar-1.

Peptide Mass of Unred. R/K-Ar-1 [µg]	Retention Time – First Peak [min]	Retention Time – Second Peak [min]	Peptide Mass of Red. R/K-Ar-1 [µg]	Retention Time – First Peak [min]	Retention Time – Second Peak [min]
1	20.827	25.247	**1**	20.573	21.700
3	20.740	25.100	**3**	20.560	21.680
5	20.693	25.027	**5**	20.527	21.647

4.3 Peptide Immobilization

In this chapter, the results of peptide immobilization are presented. The immobilization was performed using Combinations A, B, C and D and the peptides were treated for SDS-PAGE under conditions 1,2,3 and 4, as described in Chapter 3.6.2 – “Immobilization Strategies and The Verification”.

4.3.1 Combination A – TCEP as Reducing Agent

Figures 32A and 32B show peptide immobilization of NK-2 and Ar-1 using Combination A, in which TCEP was applied as the reducing agent. The results indicate that no immobilization was observed for either peptide, as peptide bands in all gel lanes showed similar intensity regardless of the condition applied. In Figure 32A, gel lanes 5 and 6 show less intense bands, which is assumed to be due to a dilution effect caused by the coupling buffer, as these samples were treated under Condition 2, in which the resin was replaced by coupling buffer. In Figure 32B, no bands were detected in gel lanes 9 and 10, which is assumed to be due to a pipetting error. Overall, the results indicate that immobilization of the peptides NK-2 and Ar-1 with Combination A was unsuccessful.

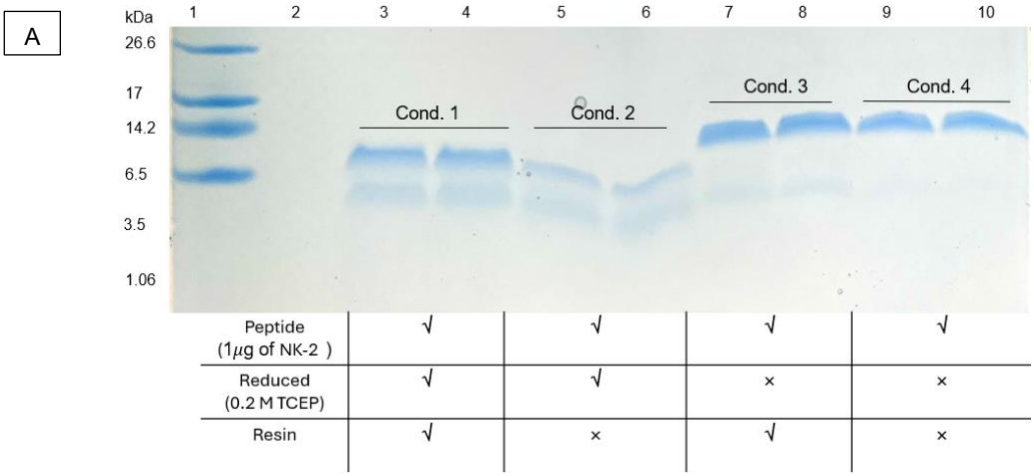

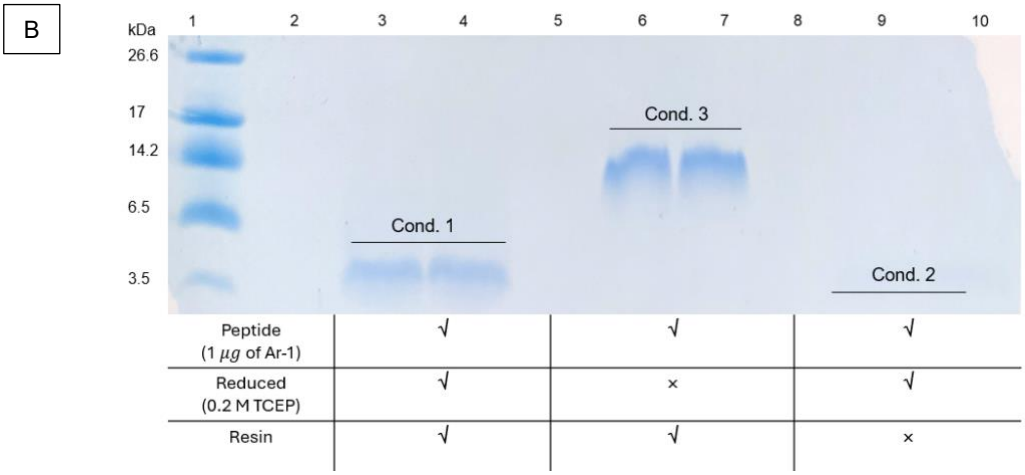

Figure 32: SDS-PAGE results of peptide immobilization using Combination A. The supernatants of immobilized **(A)** NK-2 and **(B)** Ar-1 were applied to the SDS-PAGE gel. For immobilization, the samples were treated under conditions 1 to 4 as described in Table 30. Each sample was applied to the gel in duplicate.

4.3.2 Combination B – DTT as Reducing Agent

Figure 33 shows peptide immobilization of NK-2 using Combination B, in which DTT was applied as the reducing agent. Similar to the immobilization results obtained with Combination A, as shown in the previous chapter, no differences in peptide band intensity were observed among the samples, regardless of the treatment conditions. Furthermore, artefacts in the molecular weight range of approximately 1.06 kDa were detected in all gel lanes. These artefacts may have been caused by salt contamination, sample overloading, or premature termination of the SDS-PAGE run before the protein bands reached the bottom of the gel. Overall, the results indicate that immobilization of the peptide NK-2 using Combination B was unsuccessful.

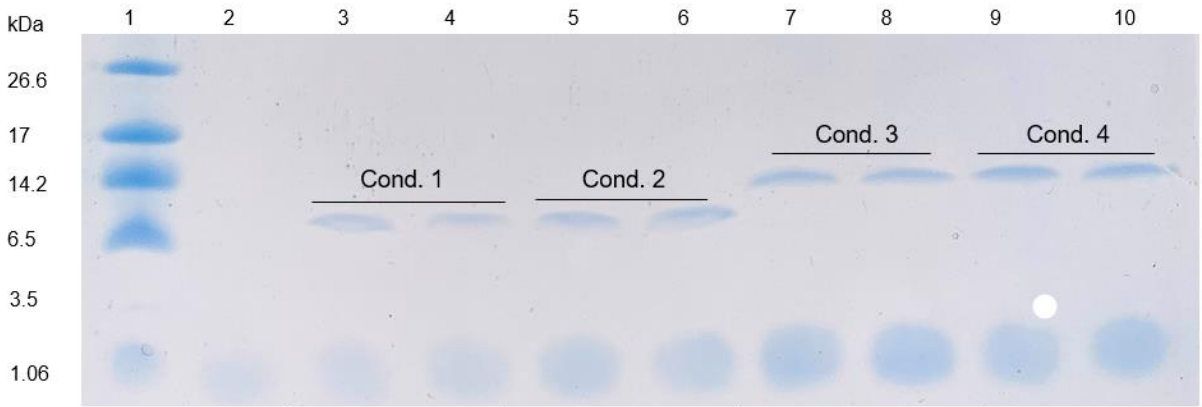

Peptide (1 μg of NK-2)	√	√	√	√
Reduced (0.1 M DTT)	√	√	×	×
Resin	√	×	√	×

Figure 33: SDS-PAGE results of peptide immobilization using Combination B. The supernatants of immobilized NK-2 were applied to SDS-PAGE gel. For the immobilization, the samples were treated under conditions 1 to 4. Each sample was applied to the gel in duplicate.

4.3.3 Combination C – Additional RP-HPLC Separation

Figure 34 and 35 shows the results of the immobilization of NK-2 and Ar-1 using Combination C, in which an additional RP-HPLC separation was applied. Both results are presented in a logical sequence following the experimental procedures.

First, Figures 34A and 35A present the chromatograms of the separation between the peptide and DTT. Figures 34B and 35B show the UV/VIS-Spectrophotometer results of the collected fractions. Subsequently, Figures 34C and 35C present the SDS-PAGE analysis of the supernatants of the immobilized peptides. Finally, Figures 34D and 35D show the chromatograms of the supernatants of the immobilized peptides. The retention times of each chromatogram are listed in Tables 39 and 40.

The immobilization results obtained with Combination C, as shown in Figures 34 and 35, demonstrated progress compared to the previous applied Combinations A and B. In Figure 34C, a less intense band was observed for the supernatant of immobilized NK-2. Similarly, in Figure 35C, no bands were detected in gel lanes 3 and 4, which represent the supernatant of immobilized Ar-1. Overall, the results from Combination C showed improved immobilization compared to the previously applied combinations.

Table 39: Overview of retention times in RP-HPLC Chromatogram from Immobilization of NK-2 with Combination C.

	Retention Time – First Peak [min]	Retention Time – Second Peak [min]
Figure 34A: RP-HPLC Separation	22.713	25.113
Figure 34D: Red. NK-2 immobilized in Resin (Cond. 1)	n. a	25.060
Figure 34D: Red. NK-2 immobilized in Coupling Buffer (Cond. 2)	n. a	25.020

Table 40: Overview of retention times in RP-HPLC Chromatogram from Immobilization of Ar-1 with Combination C.

	Retention Time – First Peak [min]	Retention Time – Second Peak [min]
Figure 35A: RP-HPLC Separation	20.887	22.173
Figure 35D: Red. R007 immobilized in Resin (Cond. 1)	24.053	25.660
Figure 35D: Red. R007 immobilized in Coupling Buffer (Cond. 2)	24.013	25.627

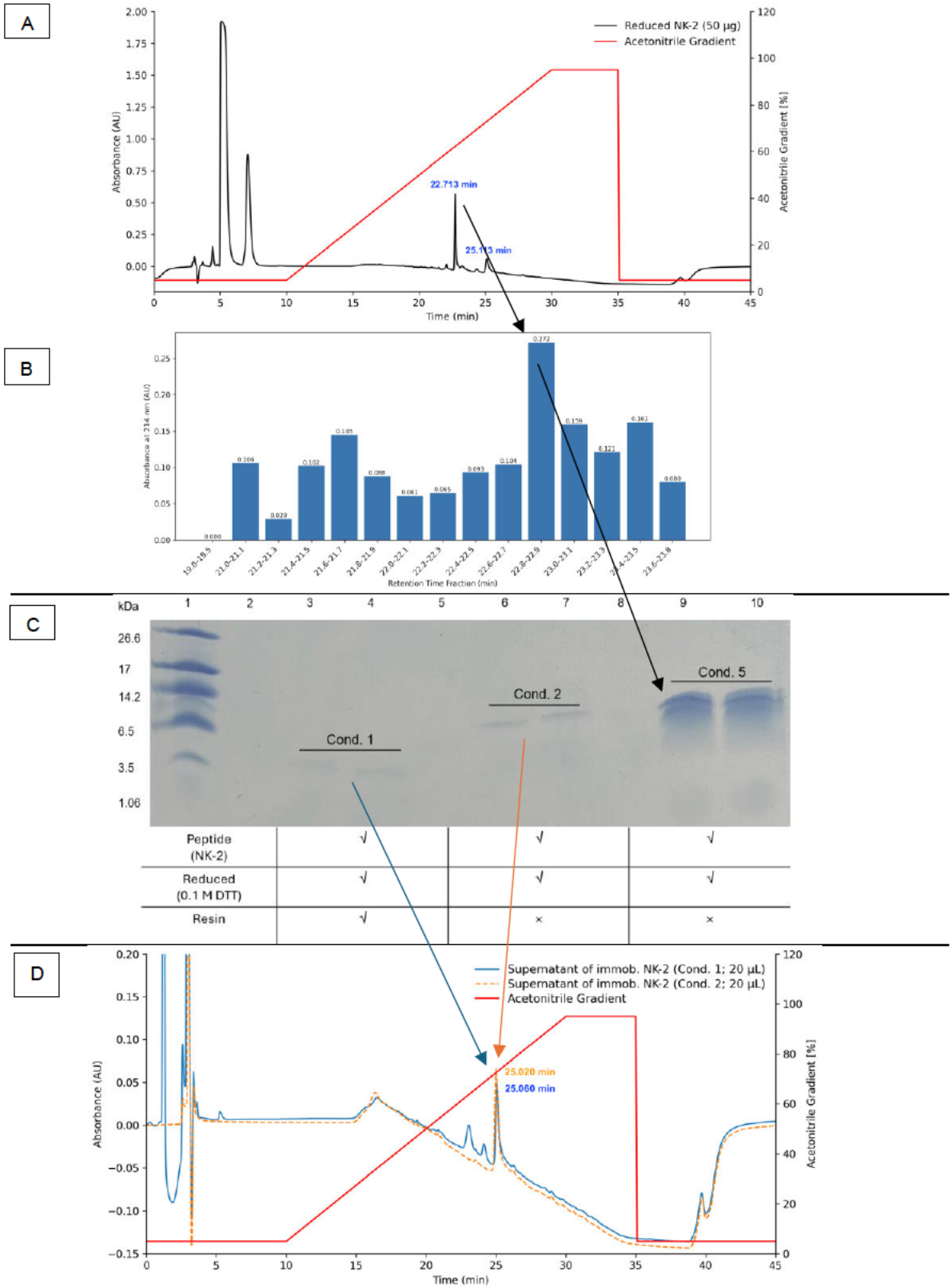

Figure 34: Immobilization of NK-2 using Combination C. (A) RP-HPLC separation of NK-2 and DTT. **(B)** Absorbance of the reduced NK-2 fraction collected from 21 to 23.8 min. **(C)** SDS-PAGE of the peptide treated under conditions 1,2 and 5. **(D)** RP-HPLC chromatogram of the peptide treated under conditions 1 and 2. The black arrow represents the peptide treated under condition 5, from which the fractions were collected, measured for absorbance and applied to the SDS-PAGE gel. The blue and yellow arrows represent peptides treated under conditions 1 and 2, respectively.

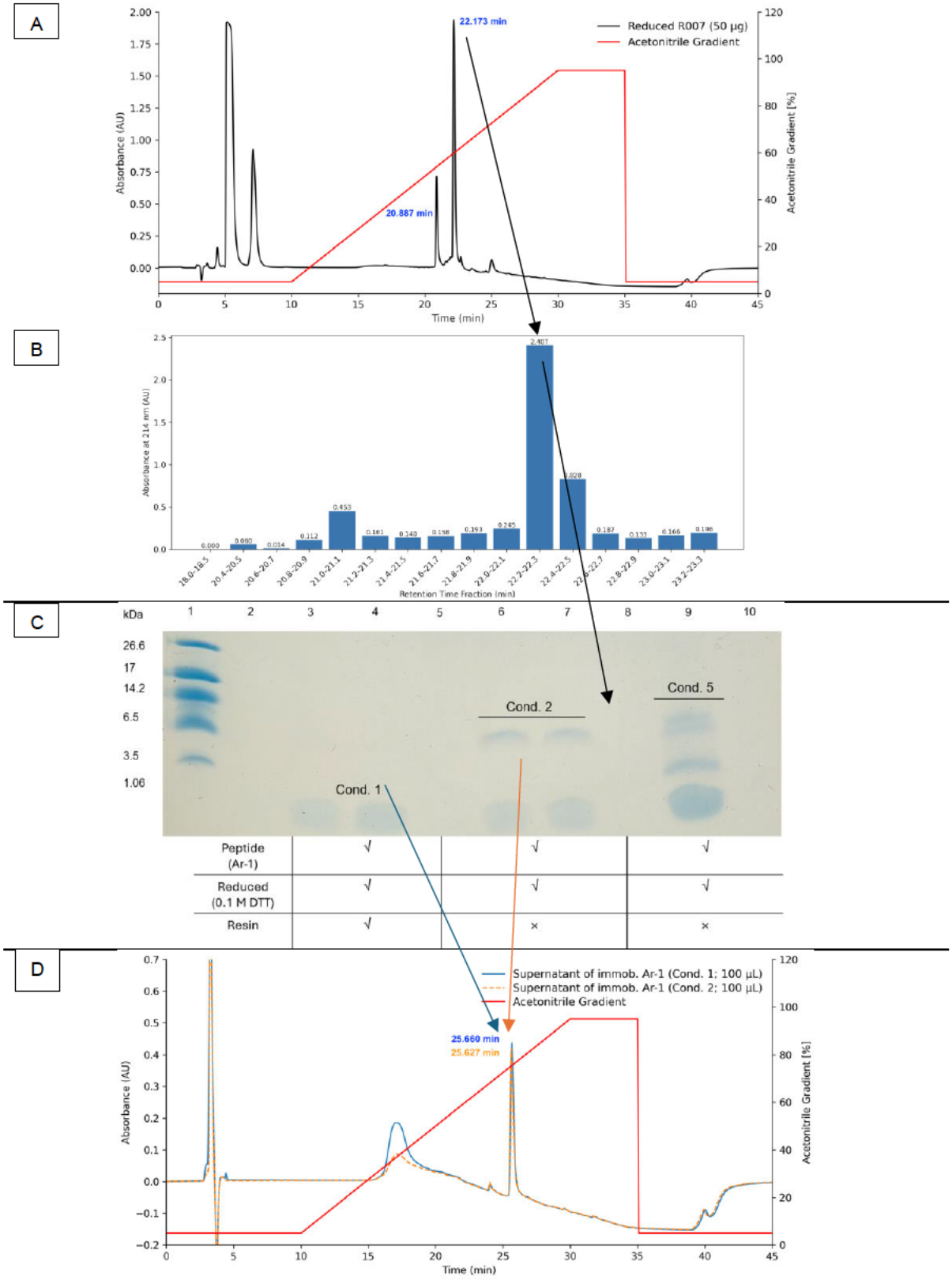

Figure 35: Immobilization of Ar-1 using Combination C. (A) RP-HPLC separation of Ar-1 and DTT. **(B)** Absorbance of the reduced Ar-1 fraction collected from 20.4 to 23.3 min. **(C)** SDS-PAGE of the peptide treated under conditions 1,2 and 5. **(D)** RP-HPLC chromatogram of the peptide treated under conditions 1 and 2. The black arrow represents the peptide treated under condition 5, from which the fractions were collected, measured for absorbance and applied to the SDS-PAGE gel. The blue and yellow arrows represent peptides treated under conditions 1 and, respectively.

4.3.4 Combination D – Peptides with Linkers and Additional Trypsin Digestion Analysis

In this chapter, the results of peptide immobilization using Combination D are presented. Figures 36A and 36B show SDS-PAGE results of the peptides ALK-33C and N33-ALK, which were treated under Conditions 1, 2, and 5. It can be observed that the supernatant of immobilized peptides treated under Condition 1 (gel lanes 3 and 4) showed less intense bands compared to the non-immobilized peptides in gel lanes 5–10.

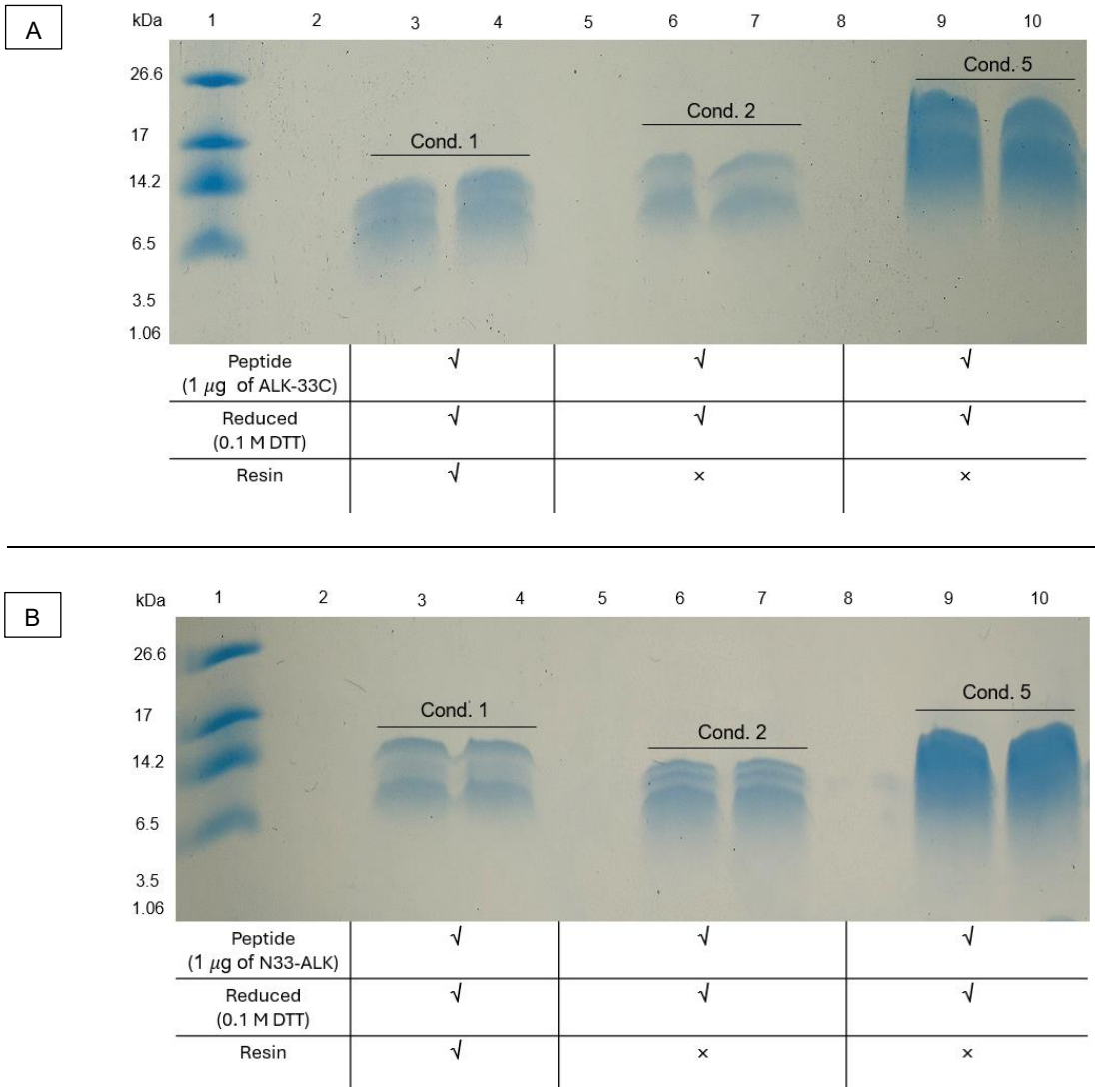

Figure 36: SDS-PAGE results of (A) ALK-33C and (B) N33-ALK. The peptides were treated under conditions 1, 2 and 5. Per gel pocket, 1 μg of peptide mass was loaded. Each sample was applied to the gel in duplicate. Samples were treated with Conditions 1,2 and 5 as described in Table 30.

Figures 37A, 37B, and 37C show the results of SDS-PAGE analysis of trypsin digestion of the supernatants obtained from pellets of immobilized ALK-33C and N33-ALK. The peptides were immobilized with incubation times of 2 and 24 h. According to the manufacturer's specifications, the trypsin used has a molecular weight of 23.3 kDa. In all gels, trypsin bands at approximately 23.3 kDa were detected. Very faint bands were observed in the supernatants of the peptide pellets in gel lanes 4–6 and 8–10 (Figures 37B and 37C), whereas almost no

bands were detected in the supernatants of immobilized peptide pellets that were not treated with trypsin digestion, shown in gel lanes 3 and 7 (Figures 37B and 37C). Overall, the results indicate that the difference in incubation time had no effect on peptide immobilization. On the other hand, trypsin digestion led to fragmentation of the immobilized peptide.

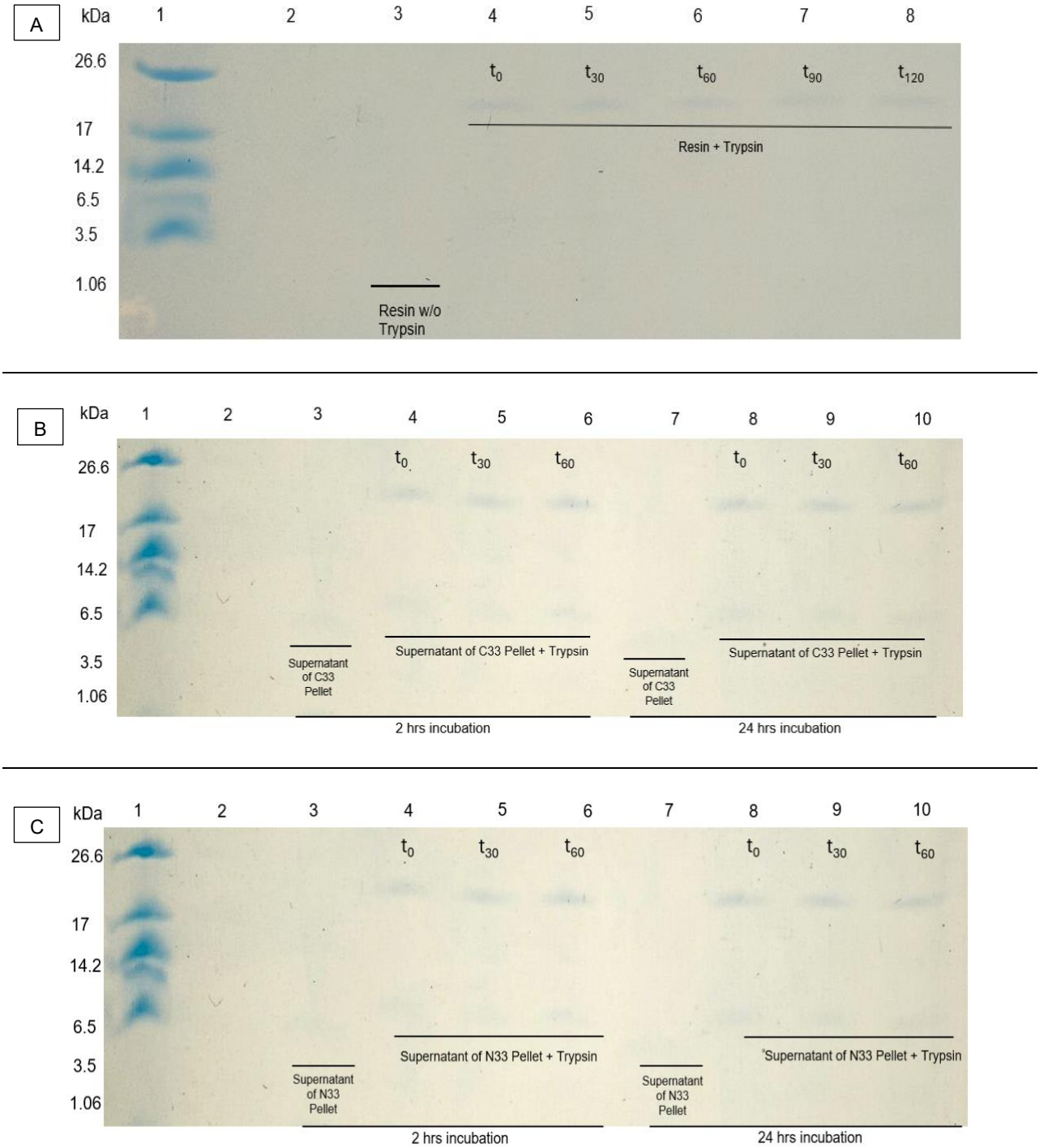

Figure 37: SDS-PAGE results of trypsin digestion of the supernatant from immobilized ALK-C33 and N33-ALK. (A) Resin with trypsin was tested as a negative control. **(B)** and **(C)** Supernatants of immobilized ALK-C33 & N33-ALK were loaded into the gel lanes in without trypsin (lane 3) and with trypsin (lanes 4-6 and lanes 8-10). For trypsin digestion, all samples were treated equally, and samples were collected over a time range from t_0 to t_{120}. The peptide-to-trypsin ratio applied was 50:1.

Figure 38B shows the RP-HPLC chromatogram of the supernatant from immobilized ALK-C33 obtained from the pellet after trypsin digestion. Figure 38A is provided to illustrate the ghost peak that should be ignored, as it resulted from clogging in the chromatographic column. In Figure 38B, the chromatogram of the supernatant from the pellet of immobilized ALK-C33 that was not treated with trypsin digestion (blue line) shows no peaks between 16 and 19 min, whereas three peaks were detected in the supernatant of the pellet of immobilized ALK-C33 after trypsin digestion (indicated by black arrows in Figure 38B). Therefore, it can be assumed that trypsin digestion led to fragmentation of the peptide in the pellet of immobilized ALK-C33, thereby confirming the presence of immobilized peptide in the pellet.

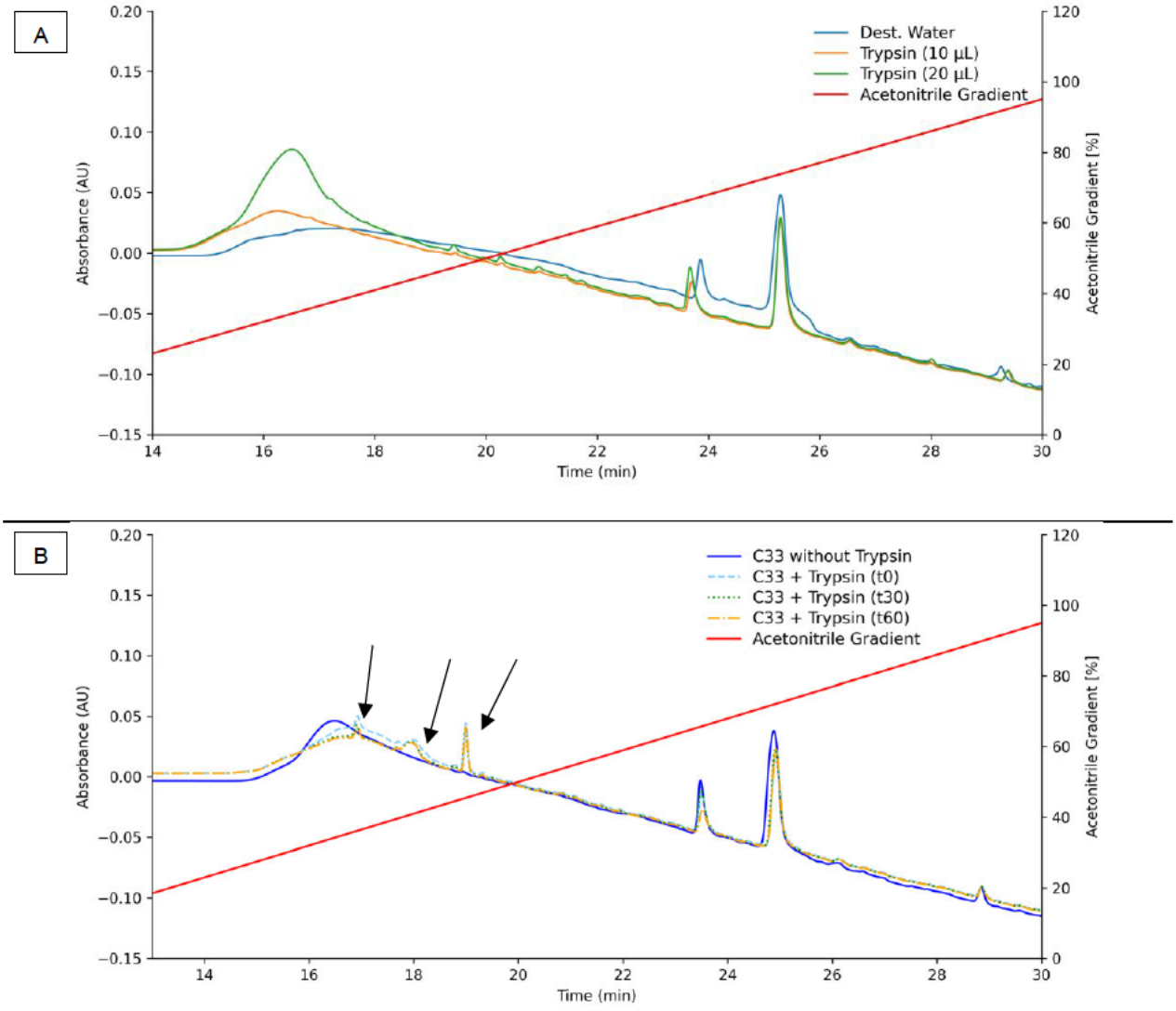

Figure 38: RP-HPLC chromatograms of (A) blank water and trypsin as negative controls and (B) supernatant of immobilized ALK-C33 obtained from the pellet after trypsin digestion. The ALK-C33 solution had a concentration of 0.2 mg/mL, and 10 μL was injected for each run. Black arrows indicate peptide fragments. After trypsin digestion, additional fractions appeared that were not present in the undigested ALK-33C. The red line represents the acetonitrile gradient.

5. Discussion

In this chapter, the results of the experiments are discussed in detail.

5.1 Suitability of the Applied Analytical Methods

Optimization of SDS-PAGE

The comparison of the reducing agents in Figure 20 showed that DTT has a stronger reducing effect than TCEP. At a concentration of 0.1 M, DTT exhibited a stronger reducing effect compared to 0.2 M and 0.4 M TCEP and was therefore more effective.

Figure 21 shows the results of the comparison between fixative solutions containing boric acid and sodium carbonate. The results indicate that the gel fixed with sodium carbonate produced clearer and more intense bands than the gel fixed with boric acid. Furthermore, considering safety aspects based on the Globally Harmonized System (GHS), boric acid is classified as harmful to health (GHS08), whereas sodium carbonate is classified as irritating but not harmful (GHS07). Therefore, sodium carbonate is safer to use in the laboratory than boric acid.

Preparation and Conditioning of RP-HPLC

The four-step method was successfully applied to condition the new column, as shown by the results in Figure 22. The chromatograms in Figure 22 show no deviation from the expected results. For example, a flat baseline was obtained after injection of demineralized water as a blank sample. Moreover, Figure 22B shows that injection of the RP-HPLC standard mixture resulted in five clearly distinguishable peaks, which corresponds to the theoretical number of peaks specified by the manufacturer. Furthermore, no ghost peaks were detected in any of the chromatograms, indicating the absence of impurities and confirming that the detected peaks originate solely from the injected samples.

The method for storing the column under idle conditions was also successfully established. The column showed reproducible results before and after an idle period of 3.5 weeks, as shown in Figure 23A, B, and C. A shift was observed in Figure 23B, where a peak eluting at approximately 18 min in Figure 23A was no longer detected, and a new peak at a retention time of 3.1 min appeared. This chromatogram represents the first run after the idle period with an injection volume of 20 μL. However, after the second run, in which 40 μL of the peptide mixture was injected (Figure 23C), the chromatogram matched the results obtained before the idle period (Figure 23A).

Investigation of Peptide-to-Trypsin Ratio

Based on the results shown in Figure 24, the 50:1 peptide-to-trypsin ratio showed the most pronounced peptide fractionation. For example, in lane 4, three distinct bands from fractions of peptide ALK-33C were detected (Figure 24A). Similar results were also observed in Figure 24B, where approximately three bands were detected from fractions of peptide N33-ALK.

In contrast, the 100:1 and 500:1 peptide-to-trypsin ratios shown in Figure 24C and Figure 24D resulted in less visible peptide bands in lane 4. Across almost all ratios, a less intense band was detected after a digestion time of 30 seconds, and no additional bands were observed after digestion times exceeding 60 seconds.

Advantages and Limitations of the Applied Analytical Methods

Based on the results of this experiment, SDS-PAGE gels and RP-HPLC chromatograms represent a complementary combination of analytical methods. Bands detected by SDS-PAGE under both unreduced and reduced conditions can be further verified using RP-HPLC chromatograms. In addition, RP-HPLC enables high-throughput analysis, as multiple samples can be injected automatically using the HPLC system. It is also a relatively simple technique and can be considered beginner friendly.

Several issues were observed for SDS-PAGE, such as strong artefacts visible in the gel, for example in Figure 21A. There are several causes that can lead to artefact formation, including premature termination of the SDS-PAGE run, incomplete denaturation of the samples, the presence of insoluble aggregates, or high salt concentrations in the samples *(Zhang et al., 2019)*. Several approaches can be applied to reduce artefacts in the gel, such as reducing the peptide mass, centrifuging the samples before loading them onto the gel, and ensuring proper heating of the samples *(Zhang et al., 2019)*. As an additional measure, dialysis can be performed if the samples contain high salt concentrations *(Zhang et al., 2019)*. Furthermore, another disadvantage of SDS-PAGE is the long preparation time required for gel casting, the extended running time, and the need for training to correctly handle and load samples.

For RP-HPLC, one disadvantage is the sensitivity of the column to clogging. Ghost peaks may occur as a result of clogging caused by sample impurities. Samples such as peptide solutions mixed with agarose resin beads can lead to blockage of the chromatographic column. Therefore, careful sample preparation is required, for example by centrifuging samples containing agarose beads for 10 minutes at 12.100 x g and transferring only the upper part of the supernatant to minimize agarose bead carryover.

Furthermore, a shift in retention time was detected in the chromatograms shown in Figures 29F and 31E, although the same samples were injected at increasing volumes. Such a shift can be expected, as peptides with higher injected mass tend to elute slightly earlier than peptides with lower mass. However, under ideal conditions the peaks should overlap as observed in other chromatograms. The observed retention time shift may also be attributed to differences between the peptide solvent and the elution solvent. The peptides were dissolved in 0.01% TFA, whereas the elution started with 0.1% TFA, which has a 100-fold higher concentration and therefore a higher acid strength. This difference affects ion-pair formation and can result in shifts in retention times.

5.2 Peptide Characterization

In total, seven peptides were successfully characterized using SDS-PAGE and RP-HPLC and the results are discussed in this chapter.

NK-2 and Derivatives

NK-2 was successfully characterized, as shown in Figure 25. Reduction of NK-2 with DTT led to a conformational change due to cleavage of disulfide bonds upon addition of the reducing agent. As a result, NK-2 changed its oligomeric state from dimer to monomer. The RP-HPLC results further verified the SDS-PAGE findings, as the peak at 25.5 min shifted to an earlier retention time of 22.3 min. In addition, in Figure 25F, the second peak, which was suspected to correspond to the dimer was no longer detected, while the first peak showed an increased absorbance.

The characterization results of NK27, as shown in Figure 26, demonstrate that substitution of the non-functional cysteine (C) residue with serine (S) at position 7, which was intended to reduce the peptide's sensitivity to oxidation by eliminating disulfide bond formation (Andrä *et al.*, 2007), was confirmed experimentally. Figures 26A and 26B show that reduction with 0.1 M DTT caused the bands of reduced NK27 to shift to a lower molecular weight range of approximately 1.06 to 3 kDa, indicating that no disulfide bond–mediated oligomerization occurs in the peptide structure. Comparison of Figures 25B and 26B shows that reduced NK27 exhibits bands at a lower molecular weight range than NK-2, indicating reduced oligomerization and improved monomeric behavior due to the absence of disulfide bond formation. In terms of hydrophobicity, NK27 showed slightly higher hydrophobicity than NK-2, as indicated by its later retention time, as shown in Figures 25E, 25F, 26E, and 26F. Interestingly, the RP-HPLC chromatograms of N33-ALK and ALK-33C shown in Figures 27B, 27C, 28B, and 28C showed different elution times, with N33-ALK eluting approximately 40 seconds earlier than ALK-33C in all chromatographic runs (see Tables 33 and 34). Therefore, N33-ALK can be considered less hydrophobic than ALK-33C, despite both peptides having the same GRAVY value of −0.2 (see Table 5). The difference in linker position between N33-ALK and ALK-33C appears to contribute to these differing characteristics of the two peptides.

Ar-1 and Derivatives

Ar-1 and R/K-Ar-1 showed similar SDS-PAGE and chromatographic profiles. Based on their structure, both peptides are cyclic and therefore sensitive to oxidative reactions. In contrast, C/S-Ar-1 showed reduced sensitivity to oxidation, as the SDS-PAGE and RP-HPLC profiles of unreduced and reduced C/S-Ar-1 were comparable. The claim by Jörg Andrä *et al.* that linear peptides appear more hydrophobic on RP-HPLC columns than cyclic peptides was confirmed in this experiment. Comparison of the elution times of unreduced Ar-1 (Figure 29C), C/S-Ar-1 (Figure 30C), and R/K-Ar-1 (Figure 31C) showed that the linear peptide C/S-Ar-1 eluted approximately one minute later than both cyclic peptides (Andrä *et al.*, 2009). A slight shift in the chromatograms was observed for the reduced peptides (Figures 29D, 30D, and 31D). Although the SDS-PAGE results showed similar bands at approximately 3.5 kDa, the retention times of the reduced peptides differed slightly. The reason to that is as described in previous Chapter – "Advantages and Limitations of the Applied Analytical Methods" in the last paragraph.

5.3 Peptide Immobilization

The results of peptide immobilization using Combinations A, B, C, and D are discussed in detail in this chapter. The terms Combinations A, B, C, and D are defined in Table 29, and the sample treatment Conditions used for immobilization are described in Table 30.

Immobilization Results of Combinations A, B, C and D

Table 41 summarizes the immobilization results for Combinations A, B, C and D.

Table 41: Overview of the results of the peptide immobilization.

Combination	Immobilization Successful?	Results		
		SDS-PAGE	**RP-HPLC**	**Trypsin Digestion**
A	No	No difference between immobilized and not-immobilized peptide. Both results show an intense bands.	Not performed	Not performed
B	No	No difference between immobilized and not-immobilized peptide. Both results show an intense bands	Not performed	Not performed
C	Yes	Immobilized peptide shows less intense bands compared to not-immobilized peptide	No difference between peaks of immobilized and not-immobilized peptide	Not performed
D	Yes	Immobilized peptide shows less intense bands compared to not-immobilized peptide	Peaks of peptide fraction were detected after trypsin digestion (see Figure 38B)	Peptide bands of the peptide fractions were detected in SDS-PAGE after trypsin digestion of the pellet supernatant (Figure 37)

For Combinations A and B (Figures 32 and 33), in which the peptides were reduced with TCEP or DTT and directly immobilized onto the resin, no indication of successful immobilization was observed. For samples treated under condition 1, where the peptide was reduced and immobilized onto the resin, weak or no bands were expected. However, in Figures 32 and 33, strong bands were still observed. No difference was detected for samples treated under condition 2, in which the resin was replaced by coupling buffer and no peptide immobilization was expected. Furthermore, when compared to samples treated under conditions 3 and 4, which served as negative controls because the peptides were not reduced and therefore could not be immobilized, the band intensities of samples treated under condition 1 showed no differences. Overall, the band intensities were comparable across conditions. In Figure 32B, no bands were detected in lanes 9 and 10 due to an error during sample preparation, which resulted in missing samples in the gel.

Figures 34 and 35 show the results of Combination C, in which an additional RP-HPLC separation step between DTT and the peptide was applied. DTT was separated because it contains two free thiol (–SH) groups that can compete with cysteine residues of the peptide for reactive groups on the resin. This hypothesis is supported by the results from Combinations A and B (Figures 32 and 33), where no immobilization occurred due to interference from the reducing agents. After RP-HPLC separation, different results were obtained for peptide

immobilization. In Figures 34C and 35C, peptide fractions were applied to the gel. Notably, for peptide samples treated under condition 1, the bands showed reduced intensity in Figure 34C and were barely detectable or absent in Figure 35C, compared to samples treated under condition 2 and condition 5. Condition 2 involved substitution of the resin with coupling buffer, while condition 5 represented peptide fractions applied directly without undergoing immobilization. Analysis of the peptide supernatants after immobilization, as shown in Figures 34D and 35D, revealed no differences in the RP-HPLC chromatograms between conditions 1 and 2, despite differences observed in the SDS-PAGE results (Figures 34C and 35C). This indicated that the peptide was successfully immobilized onto the resin.

For Combination D, successful immobilization of the peptide onto the resin was achieved. Samples treated under condition 1, representing the immobilized peptide bound to the resin, showed weaker bands compared to samples treated under condition 5, which represent the non-immobilized peptide fraction (Figure 36). The success of immobilization was further verified by trypsin digestion of the pellet containing the immobilized peptide. In Figure 37A, the negative control is shown, where trypsin was detected at approximately 23 kDa, while no band was observed in lane 3 for the negative control consisting only of resin and buffer. In Figures 37B and 37C, very faint bands were detected in lanes 4–6 and 8–10, indicating peptide fragmentation as a result of trypsin digestion. In contrast, lanes 3 and 7, which contained the undigested supernatant, showed no or barely visible bands. Increasing the incubation time from 2 to 24 hours did not appear to influence peptide immobilization. The limited effect of prolonged incubation time has also been reported in the Master's thesis of Marina Lesniewski, who observed unsuccessful immobilization despite overnight incubation. Furthermore, Figure 38B shows that trypsin digestion resulted in additional peptide fractions that were not observed in C33 without trypsin treatment, further confirming that the bands detected in Figures 37B and 37C (lanes 4–6 and 8–10) correspond to peptide fragments resulted by trypsin digestion.

Comparison of Experimental Findings with Literature and Previous Studies

Soyhan *et al.* successfully immobilized antimicrobial peptides (AMPs) on silicone catheter surfaces using reactions such as amidation, click chemistry, and nucleophilic 1,4-Michael addition reactions. The peptides used in their study were modified with an additional cysteine residue at either terminus (C-PEP or PEP-C), which played a crucial role in the immobilization process (Soyhan *et al.*, 2024). Similarly, in the present thesis, immobilization using Combination D was performed for the peptides ALK-33C and N33-ALK, both of which were equipped with terminal linker sequences. In ALK-33C, the linker (PEP-GSGSG-C) is located at the C-terminus, whereas in N33-ALK, the linker (C-GSGSG-PEP) is positioned at the N-terminus. The design of both AMPs, incorporating an additional cysteine residue at the terminal end, resulted in improved immobilization compared to the parent peptide NK-2.

Furthermore, Marina Lesniewski reported in her Master's thesis that overnight incubation did not improve AMP immobilization onto resin. This observation was confirmed in the present thesis, as increasing the immobilization incubation time from 2 hours to 24 hours did not result in a significant difference (Figure 36).

For safety reasons, immobilization of AMPs onto AminoLink beads was not performed in this thesis, as the procedure requires the use of sodium cyanoborohydride ($NaCNBH_3$), which is not permitted in the organic chemistry and biochemistry (OCB) - laboratory at HAW Hamburg. However, an alternative immobilization strategy has been described by Lapetina *et al.* from Bar-Ilan University, who demonstrated immobilization of the protein Pyk2 onto AminoLink beads via protein–protein binding interactions. In this approach, one protein acts as a bait immobilized on the beads, while the second protein (the prey, Pyk2) remains in solution (Lapetina and Gil-Henn, 2017). This strategy could represent an alternative to the SulfoLink®-based immobilization method used in this thesis.

Another alternative and interesting approach for peptide immobilization is described in a study by Wadhwani *et al.* They prepared and characterized novel peptide-functionalized gold nanoparticles that are water soluble, bear conformationally flexible peptides, are antimicrobially active, and are proteolytically stable toward trypsin (Wadhwani *et al.*, 2017).

6. Conclusion and Outlook

In summary, the peptides NK-2, Arenicin, and their derivatives were successfully characterized using the analytical methods applied in this thesis. Some limitations were observed for the applied analytical techniques, particularly RP-HPLC, which is highly sensitive to agarose beads and shows a strong tendency toward column clogging when supernatants from immobilized peptides are injected into the HPLC system. Therefore, bead carryover needs to be significantly reduced through centrifugation, and only the clarified supernatant should be injected into the RP-HPLC system. Furthermore, regarding the observed shifts in retention times, where peaks corresponding to different peptide masses did not overlap, the peptide solvent could be further optimized by using the same solvent composition as the initial elution solvent. This would ensure a consistent acid strength between the peptide solvent and the starting mobile phase composition, thereby minimizing retention time shifts. On the other hand, SDS-PAGE reliably enabled analysis of peptide bands and molecular weights as expected.

In the future, additional analytical methods such as Fourier-transform infrared (FT-IR) spectroscopy could be applied to investigate peptide secondary structure, chemical bonds, and conformational changes induced by pH of the buffer. This approach could also allow detection of bond formation between peptides and the resin (Soyhan *et al.*, 2024). Furthermore, circular dichroism (CD) spectroscopy may be used to study peptide conformational changes of the peptide's secondary structure in different buffer environments as well as in membrane-mimicking environments (Wadhwani *et al.*, 2017).

Regarding peptide immobilization, further development and optimization of Combinations C and D are recommended, as these approaches showed progressive results compared to previous Thesis conducted by Sara Jashari and Marina Lesniewski. Optimization of the immobilization strategy may be supported by detailed analysis of peptide conformational changes using FT-IR or CD spectroscopy, as suggested above. In addition, microdilution assays to determine minimum inhibitory concentration (MIC) values, as well as activity studies of the peptides before and after immobilization, should be conducted to further confirm the effectiveness of peptide immobilization using Combinations C and D. Furthermore, it is suggested to investigate peptide immobilization using AminoLink® beads via Schiff base formation, as well as immobilization onto gold surfaces through covalent bonding, as demonstrated in studies by Soyhan *et al.* and Wadhwani *et al*.

7. References

Andrä, J. *et al.* (2008) "Structure and mode of action of the antimicrobial peptide arenicin," *Biochemical Journal*, 410(1), pp. 113–122. Available at: https://doi.org/10.1042/BJ20071051.

Andrä, J. *et al.* (2009) "Significance of the cyclic structure and of arginine residues for the antibacterial activity of arenicin-1 and its interaction with phospholipid and lipopolysaccharide model membranes," *bchm*, 390(4), pp. 337–349. Available at: https://doi.org/10.1515/BC.2009.039.

Andrä, J. *et al.* (2024) "Structural analysis of the NK-lysin-derived peptide NK-2 upon interaction with bacterial membrane mimetics consisting of phosphatidylethanolamine and phosphatidylglycerol," *Biochimica et Biophysica Acta (BBA) - Biomembranes*, 1866(3), p. 184267. Available at: https://doi.org/10.1016/j.bbamem.2023.184267.

Andraö, J. *et al.* (2007) "Rationale for the Design of Shortened Derivatives of the NK-lysin-derived Antimicrobial Peptide NK-2 with Improved Activity against Gram-negative Pathogens," *Journal of Biological Chemistry*, 282(20), pp. 14719–14728. Available at: https://doi.org/10.1074/jbc.M608920200.

Bagheri, M., Beyermann, M. and Dathe, M. (2009) "Immobilization Reduces the Activity of Surface-Bound Cationic Antimicrobial Peptides with No Influence upon the Activity Spectrum," *Antimicrobial Agents and Chemotherapy*, 53(3), pp. 1132–1141. Available at: https://doi.org/10.1128/AAC.01254-08.

Bucataru, C. and Ciobanasu, C. (2024) "Antimicrobial peptides: Opportunities and challenges in overcoming resistance," *Microbiological Research*, 286, p. 127822. Available at: https://doi.org/10.1016/j.micres.2024.127822.

Chinnadurai, R.K. *et al.* (2023) "Current research status of anti-cancer peptides: Mechanism of action, production, and clinical applications," *Biomedicine & Pharmacotherapy*, 164, p. 114996. Available at: https://doi.org/10.1016/j.biopha.2023.114996.

Costa, B. *et al.* (2021) "Antimicrobial Peptides in the Battle against Orthopedic Implant-Related Infections: A Review," *Pharmaceutics*, 13(11), p. 1918. Available at: https://doi.org/10.3390/pharmaceutics13111918.

Costa, F. *et al.* (2011) "Covalent immobilization of antimicrobial peptides (AMPs) onto biomaterial surfaces," *Acta Biomaterialia*, 7(4), pp. 1431–1440. Available at: https://doi.org/10.1016/j.actbio.2010.11.005.

Costerton, J.W., Montanaro, L. and Arciola, C.R. (2005) "Biofilm in Implant Infections: Its Production and Regulation," *The International Journal of Artificial Organs*, 28(11), pp. 1062–1068. Available at: https://doi.org/10.1177/039139880502801103.

Decker, A.P., Mechesso, A.F. and Wang, G. (2022) "Expanding the Landscape of Amino Acid-Rich Antimicrobial Peptides: Definition, Deployment in Nature, Implications for Peptide Design and Therapeutic Potential," *International Journal of Molecular Sciences*, 23(21), p. 12874. Available at: https://doi.org/10.3390/ijms232112874.

Fernández De Ullivarri, M. *et al.* (2020) "Antifungal Peptides as Therapeutic Agents," *Frontiers in Cellular and Infection Microbiology*, 10, p. 105. Available at: https://doi.org/10.3389/fcimb.2020.00105.

Gabriel, M. *et al.* (2006) "Direct grafting of RGD-motif-containing peptide on the surface of polycaprolactone films," *Journal of Biomaterials Science, Polymer Edition*, 17(5), pp. 567–577. Available at: https://doi.org/10.1163/156856206776986288.

Glinel, K. *et al.* (2012) "Antibacterial surfaces developed from bio-inspired approaches," *Acta Biomaterialia*, 8(5), pp. 1670–1684. Available at: https://doi.org/10.1016/j.actbio.2012.01.011.

Haney, E.F. and Hancock, R.E.W. (2013) “Peptide design for antimicrobial and immunomodulatory applications,” *Peptide Science*, 100(6), pp. 572–583. Available at: https://doi.org/10.1002/bip.22250.

Hasan, A. *et al.* (2020) “Surface Design for Immobilization of an Antimicrobial Peptide Mimic for Efficient Anti-Biofouling,” *Chemistry – A European Journal*, 26(26), pp. 5789–5793. Available at: https://doi.org/10.1002/chem.202000746.

Huan, Y. *et al.* (2020) “Antimicrobial Peptides: Classification, Design, Application and Research Progress in Multiple Fields,” *Frontiers in Microbiology*, 11, p. 582779. Available at: https://doi.org/10.3389/fmicb.2020.582779.

Humblot, V. *et al.* (2009) “The antibacterial activity of Magainin I immobilized onto mixed thiols Self-Assembled Monolayers,” *Biomaterials*, 30(21), pp. 3503–3512. Available at: https://doi.org/10.1016/j.biomaterials.2009.03.025.

Koehbach, J. and Craik, D.J. (2019) “The Vast Structural Diversity of Antimicrobial Peptides,” *Trends in Pharmacological Sciences*, 40(7), pp. 517–528. Available at: https://doi.org/10.1016/j.tips.2019.04.012.

Kyvik, A.R. *et al.* (2023) “Antibiofilm surfaces based on the immobilization of a novel recombinant antimicrobial multidomain protein using self-assembled monolayers,” *Materials Advances*, 4(10), pp. 2354–2364. Available at: https://doi.org/10.1039/D2MA00978A.

Lapetina, S. and Gil-Henn, H. (2017) “A guide to simple, direct, and quantitative in vitro binding assays,” *Journal of Biological Methods*, 4(1), p. 1. Available at: https://doi.org/10.14440/jbm.2017.161.

Laskay, Ü.A. *et al.* (2013) “Proteome Digestion Specificity Analysis for Rational Design of Extended Bottom-up and Middle-down Proteomics Experiments,” *Journal of Proteome Research*, 12(12), pp. 5558–5569. Available at: https://doi.org/10.1021/pr400522h.

Le, C.-F., Fang, C.-M. and Sekaran, S.D. (2017) “Intracellular Targeting Mechanisms by Antimicrobial Peptides,” *Antimicrobial Agents and Chemotherapy*, 61(4), pp. e02340-16. Available at: https://doi.org/10.1128/AAC.02340-16.

Lee, T.D. (2011) “Introduction to Modern Liquid Chromatography, Third Edition,” *Journal of the American Society for Mass Spectrometry*, 22(1), pp. 196–196. Available at: https://doi.org/10.1007/s13361-010-0021-8.

Lei, J. *et al.* (no date) “The antimicrobial peptides and their potential clinical applications,” *Antimicrobial peptides* [Preprint].

Li, H.-L. *et al.* (2023) “Identification, Screening and Antibacterial Mechanism Analysis of Novel Antimicrobial Peptides from Sturgeon (Acipenser ruthenus) Spermary,” *Marine Drugs*, 21(7), p. 386. Available at: https://doi.org/10.3390/md21070386.

Li, J. *et al.* (2017) “Membrane Active Antimicrobial Peptides: Translating Mechanistic Insights to Design,” *Frontiers in Neuroscience*, 11. Available at: https://doi.org/10.3389/fnins.2017.00073.

Liang, C., Qiao, J. and Lian, H. (2017) “Determination of reversed-phase high performance liquid chromatography based octanol-water partition coefficients for neutral and ionizable compounds: Methodology evaluation,” *Journal of Chromatography A*, 1528, pp. 25–34. Available at: https://doi.org/10.1016/j.chroma.2017.10.064.

Lima, A.M. *et al.* (2022) “Plant antimicrobial peptides: An overview about classification, toxicity and clinical applications,” *International Journal of Biological Macromolecules*, 214, pp. 10–21. Available at: https://doi.org/10.1016/j.ijbiomac.2022.06.043.

Liu, R. *et al.* (2022) “Bomidin: An Optimized Antimicrobial Peptide With Broad Antiviral Activity Against Enveloped Viruses,” *Frontiers in Immunology*, 13, p. 851642. Available at: https://doi.org/10.3389/fimmu.2022.851642.

Luo, Y. and Song, Y. (2021) “Mechanism of Antimicrobial Peptides: Antimicrobial, Anti-Inflammatory and Antibiofilm Activities,” *International Journal of Molecular Sciences*, 22(21), p. 11401. Available at: https://doi.org/10.3390/ijms222111401.

Mansuri, M.S. *et al.* (2024) “Optimal conditions for carrying out trypsin digestions on complex proteomes: From bulk samples to single cells,” *Journal of Proteomics*, 297, p. 105109. Available at: https://doi.org/10.1016/j.jprot.2024.105109.

“Marina Lesniewski_Masterthesis” (2022).

Min, K.H. *et al.* (2024) “Antimicrobial Peptides and Their Biomedical Applications: A Review,” *Antibiotics*, 13(9), p. 794. Available at: https://doi.org/10.3390/antibiotics13090794.

Murray, C.J.L. *et al.* (2022) “Global burden of bacterial antimicrobial resistance in 2019: a systematic analysis,” *The Lancet*, 399(10325), pp. 629–655. Available at: https://doi.org/10.1016/S0140-6736(21)02724-0.

Nicolas, M. *et al.* (2021) “Strategies for Antimicrobial Peptides Immobilization on Surfaces to Prevent Biofilm Growth on Biomedical Devices,” *Antibiotics*, 11(1), p. 13. Available at: https://doi.org/10.3390/antibiotics11010013.

Pellissari, C.V.G. *et al.* (2021) “Statherin-derived peptides as antifungal strategy against Candida albicans,” *Archives of Oral Biology*, 125, p. 105106. Available at: https://doi.org/10.1016/j.archoralbio.2021.105106.

Prabhakar, T. *et al.* (2025) “Covalent immobilization: A review from an enzyme perspective,” *Chemical Engineering Journal*, 503, p. 158054. Available at: https://doi.org/10.1016/j.cej.2024.158054.

Raheem, N. and Straus, S.K. (2019) “Mechanisms of Action for Antimicrobial Peptides With Antibacterial and Antibiofilm Functions,” *Frontiers in Microbiology*, 10, p. 2866. Available at: https://doi.org/10.3389/fmicb.2019.02866.

Riool, M. *et al.* (2017) “Antimicrobial Peptides in Biomedical Device Manufacturing,” *Frontiers in Chemistry*, 5, p. 63. Available at: https://doi.org/10.3389/fchem.2017.00063.

Sancho-Vaello, E. *et al.* (2020) “The structure of the antimicrobial human cathelicidin LL-37 shows oligomerization and channel formation in the presence of membrane mimics,” *Scientific Reports*, 10(1), p. 17356. Available at: https://doi.org/10.1038/s41598-020-74401-5.

“SaraJashari_BA_Untersuchungen_Immobilisierung_cysteinhaltigen_Peptidantibiotika_CK33” (2024).

Schägger, H. and Von Jagow, G. (1987) “Tricine-sodium dodecyl sulfate-polyacrylamide gel electrophoresis for the separation of proteins in the range from 1 to 100 kDa,” *Analytical Biochemistry*, 166(2), pp. 368–379. Available at: https://doi.org/10.1016/0003-2697(87)90587-2.

Schromm, A.B. *et al.* (2021) “Cathelicidin and PMB neutralize endotoxins by multifactorial mechanisms including LPS interaction and targeting of host cell membranes,” *Proceedings of the National Academy of Sciences*, 118(27), p. e2101721118. Available at: https://doi.org/10.1073/pnas.2101721118.

Scocchi, M. *et al.* (2015) “Non-Membrane Permeabilizing Modes of Action of Antimicrobial Peptides on Bacteria,” *Current Topics in Medicinal Chemistry*, 16(1), pp. 76–88. Available at: https://doi.org/10.2174/1568026615666150703121009.

Sharma, D., Misba, L. and Khan, A.U. (2019) “Antibiotics versus biofilm: an emerging battleground in microbial communities,” *Antimicrobial Resistance & Infection Control*, 8(1), p. 76. Available at: https://doi.org/10.1186/s13756-019-0533-3.

Simm, S. *et al.* (2016) “50 years of amino acid hydrophobicity scales: revisiting the capacity for peptide classification,” *Biological Research*, 49(1), p. 31. Available at: https://doi.org/10.1186/s40659-016-0092-5.

Skerlavaj, B. and Boix-Lemonche, G. (2023) “The Potential of Surface-Immobilized Antimicrobial Peptides for the Enhancement of Orthopaedic Medical Devices: A Review,” *Antibiotics*, 12(2), p. 211. Available at: https://doi.org/10.3390/antibiotics12020211.

Soyhan, I. *et al.* (2024) “Effective Immobilization of Novel Antimicrobial Peptides via Conjugation onto Activated Silicon Catheter Surfaces,” *Pharmaceutics*, 16(8), p. 1045. Available at: https://doi.org/10.3390/pharmaceutics16081045.

Vilas Boas, L.C.P. *et al.* (2019) “Antiviral peptides as promising therapeutic drugs,” *Cellular and Molecular Life Sciences*, 76(18), pp. 3525–3542. Available at: https://doi.org/10.1007/s00018-019-03138-w.

Wadhwani, P. *et al.* (2017) “Antibiotic gold: tethering of antimicrobial peptides to gold nanoparticles maintains conformational flexibility of peptides and improves trypsin susceptibility,” *Biomaterials Science*, 5(4), pp. 817–827. Available at: https://doi.org/10.1039/C7BM00069C.

Wang, G. *et al.* (2022) “The evolution of the antimicrobial peptide database over 18 years: Milestones and new features,” *Protein Science*, 31(1), pp. 92–106. Available at: https://doi.org/10.1002/pro.4185.

Yasir, M. *et al.* (2020) “Mechanism of Action of Surface Immobilized Antimicrobial Peptides Against Pseudomonas aeruginosa,” *Frontiers in Microbiology*, 10, p. 3053. Available at: https://doi.org/10.3389/fmicb.2019.03053.

Zare, M. *et al.* (2025) “Immobilization of KR-12 on a Titanium Alloy Surface Using Linking Arms Improves Antimicrobial Activity and Supports Osteoblast Cytocompatibility,” *ACS Applied Bio Materials*, 8(4), pp. 2899–2915. Available at: https://doi.org/10.1021/acsabm.4c01731.

Zasloff, M. (2002) “Antimicrobial peptides of multicellular organisms,” *Nature*, 415(6870), pp. 389–395. Available at: https://doi.org/10.1038/415389a.

Zhang, Q.-Y. *et al.* (2021) “Antimicrobial peptides: mechanism of action, activity and clinical potential,” *Military Medical Research*, 8(1), p. 48. Available at: https://doi.org/10.1186/s40779-021-00343-2.

Zhang, Yuan; Wang, Ying; Li, Yifeng . (2019). *Major cause of antibody artifact bands on non-reducing SDS-PAGE and methods for minimizing artifacts. Protein Expression and Purification, 164(), 105459–*. doi: 10.1016/j.pep.2019.105459

8. Annexes

I. List of Figures

II. List of Tables

III. Python Code

The following Python code was developed to generate RP-HPLC chromatogram plots. Since the code is designed to read data in PDF format, data obtained as .txt-files from the experiment results must first be converted to PDF format.

Single Chromatogram

```
# RP-HPLC chromatogram: Unreduced NK-2 (5 µg)
# Style: thesis-final version

import re
import numpy as np
import pandas as pd
import matplotlib.pyplot as plt
from matplotlib.ticker import MultipleLocator
import pdfplumber

def extract_chromatogram_from_pdf(pdf_path: str) -> pd.DataFrame:
    """
    Extracts 'time; absorbance;' pairs (German decimal comma) from PDF.
    Returns DataFrame with Time (min) and Absorbance (AU).
    """
    rows = []
    pattern = re.compile(r'([0-9]+,[0-9]+)\s*;\s*([-]?[0-9]+,[0-9]+)\s*;')

    with pdfplumber.open(pdf_path) as pdf:
        for page in pdf.pages:
            text = page.extract_text() or ""
            for m in pattern.finditer(text):
                t = float(m.group(1).replace(",", "."))
                a = float(m.group(2).replace(",", "."))
                rows.append((t, a))

    df = pd.DataFrame(rows, columns=["Time (min)", "Absorbance (AU)"])
    return df.drop_duplicates().sort_values("Time (min)").reset_index(drop=True)


def acn_gradient_profile():
    """
    ACN gradient:
      0–10 min: 5 %
      10–30 min: linear 5 → 95 %
      30–35 min: hold 95 %
      35–45 min: 5 %
    """
    t = np.linspace(0, 45, 451)
    acn = np.zeros_like(t)

    for i, x in enumerate(t):
        if x <= 10:
            acn[i] = 5
        elif x <= 30:
            acn[i] = 5 + (95 - 5) * ((x - 10.01) / (30 - 10.01))
        elif x <= 35:
            acn[i] = 95
        else:
            acn[i] = 5

    return t, acn

# ----------------------------
# INPUT
# ----------------------------
pdf_path = "unreduced_NK2_5mikrogram_DATA.pdf"

# ----------------------------
# DATA
# ----------------------------
df = extract_chromatogram_from_pdf(pdf_path)
t_grad, acn = acn_gradient_profile()

# ----------------------------
# PLOT
# ----------------------------
```

```
plt.figure(figsize=(10, 4.8))
ax = plt.gca()

# Absorbance trace
ax.plot(
    df["Time (min)"],
    df["Absorbance (AU)"],
    color="black",
    linewidth=1.3,
    label="Unreduced NK-2 (5 µg)"
)

ax.set_xlim(0, 45)
ax.set_ylim(-0.2, 0.5)
ax.set_xlabel("Time (min)")
ax.set_ylabel("Absorbance (AU)")
ax.spines["top"].set_visible(False)

# ACN gradient (right axis)
ax2 = ax.twinx()
ax2.plot(
    t_grad,
    acn,
    color="red",
    linewidth=1.4,
    label="Acetonitrile Gradient"
)
ax2.set_ylim(0, 120)
ax2.set_ylabel("Acetonitrile Gradient [%]")
ax2.yaxis.set_major_locator(MultipleLocator(20))
ax2.spines["top"].set_visible(False)

# Legend
h1, l1 = ax.get_legend_handles_labels()
h2, l2 = ax2.get_legend_handles_labels()
ax.legend(
    h1 + h2,
    l1 + l2,
    loc="upper right",
    frameon=False,
    fontsize=11,
    labelspacing=0.3,
    handlelength=2.0
)

plt.tight_layout()

# ----------------------------
# SAVE
# ----------------------------
plt.savefig(
    "RP-HPLC_unreduced_NK2_5ug_y-0.2_0.5_black_legend11.tiff",
    dpi=300,
    bbox_inches="tight"
)
plt.savefig(
    "RP-HPLC_unreduced_NK2_5ug_y-0.2_0.5_black_legend11.png",
    dpi=300,
    bbox_inches="tight"
)

plt.show()
```

Multiple Plots in Single Chromatogram

```python
# RP-HPLC overlay (Unreduced NK-2: 1 µg, 3 µg, 5 µg)
# Window: 20–30 min
# No ACN (right y-axis removed)
# Y-axis (Absorbance): -0.2 to 0.3

import re
import pandas as pd
import matplotlib.pyplot as plt
import pdfplumber
```

```
def extract_chromatogram_from_pdf(pdf_path: str) -> pd.DataFrame:
    """
    Extracts 'time; absorbance;' pairs (German decimal comma) from PDF.
    Returns DataFrame with Time (min) and Absorbance (AU).
    """
    rows = []
    pattern = re.compile(r'([0-9]+,[0-9]+)\s*;\s*([-]?[0-9]+,[0-9]+)\s*;')

    with pdfplumber.open(pdf_path) as pdf:
        for page in pdf.pages:
            text = page.extract_text() or ""
            for m in pattern.finditer(text):
                t = float(m.group(1).replace(",", "."))
                a = float(m.group(2).replace(",", "."))
                rows.append((t, a))

    df = pd.DataFrame(rows, columns=["Time (min)", "Absorbance (AU)"])
    return df.drop_duplicates().sort_values("Time (min)").reset_index(drop=True)


# ----------------------------
# INPUT (PDF paths)
# ----------------------------
pdf_1ug = "unreduced_NK2_1mikrogram_DATA.pdf"
pdf_3ug = "unreduced_NK2_3mikrogram_DATA.pdf"
pdf_5ug = "unreduced_NK2_5mikrogram_DATA.pdf"

# ----------------------------
# DATA
# ----------------------------
df1 = extract_chromatogram_from_pdf(pdf_1ug)
df3 = extract_chromatogram_from_pdf(pdf_3ug)
df5 = extract_chromatogram_from_pdf(pdf_5ug)

# restrict to 20–30 min
df1_w = df1[(df1["Time (min)"] >= 20) & (df1["Time (min)"] <= 30)]
df3_w = df3[(df3["Time (min)"] >= 20) & (df3["Time (min)"] <= 30)]
df5_w = df5[(df5["Time (min)"] >= 20) & (df5["Time (min)"] <= 30)]

# ----------------------------
# PLOT
# ----------------------------
plt.figure(figsize=(9, 4.5))
ax = plt.gca()

ax.plot(df1_w["Time (min)"], df1_w["Absorbance (AU)"], linewidth=1.4, label="Unreduced
NK-2 (1 µg)")
ax.plot(df3_w["Time (min)"], df3_w["Absorbance (AU)"], linewidth=1.4, label="Unreduced
NK-2 (3 µg)")
ax.plot(df5_w["Time (min)"], df5_w["Absorbance (AU)"], linewidth=1.4, label="Unreduced
NK-2 (5 µg)")

ax.set_xlim(20, 30)
ax.set_ylim(-0.2, 0.3)
ax.set_xlabel("Time (min)")
ax.set_ylabel("Absorbance (AU)")
ax.spines["top"].set_visible(False)
ax.spines["right"].set_visible(False)

ax.legend(frameon=False, fontsize=11, loc="upper right")

plt.tight_layout()

# ----------------------------
# SAVE
# ----------------------------
plt.savefig("RP-HPLC_unreduced_NK2_1ug_3ug_5ug_20-30min_ymax0.3.tiff", dpi=300,
bbox_inches="tight")
plt.savefig("RP-HPLC_unreduced_NK2_1ug_3ug_5ug_20-30min_ymax0.3.png",
dpi=300, bbox_inches="tight")

plt.show()
```

Eidesstattliche Erklärung

Hiermit versichere ich, dass ich die vorliegende Masterarbeit mit dem Titel “Investigations into The Characterization and Thioether-Based Immobilization of Antimicrobial Peptides NK-2, Arenicin and Their Derivatives” ohne fremde Hilfe selbständig verfasst und nur die angegebenen Quellen und Hilfsmittel, einschließlich elektronischer Quellen verwendet habe. Alle Stellen der Arbeit, die ich anderen Werken dem Wortlaut oder dem Sinn nach entnommen habe, sind kenntlich gemacht. Dies gilt auch für Zeichnungen, Skizzen, bildlichen Darstellungen und dergleichen. Die Arbeit ist von mir in gleicher oder ähnlicher Form noch nicht eingereicht worden.

Hamburg, 06. Februar 2026

_____

Theonardho Ryvan